Theoretical Study on Novel Phenomena in Multi-Component Superconductors

Zhao Huang

February 2016

Theoretical Study on Novel Phenomena in Multi-Component Superconductors

Zhao Huang
Doctoral Program in Materials Science and Engineering

Submitted to the Graduate School of
Pure and Applied Sciences
in Partial Fulfillment of the Requirements
for the Degree of Doctor of Philosophy in
Engineering

at the
University of Tsukuba

Graduate School of Pure and Applied Sciences

Theoretical Study on Novel Phenomena in Multi-Component Superconductors

Zhao Huang

Doctoral Program in Materials Science and Engineering
Student ID: 201330159
Doctor of Philosophy in Engineering
Advised by: Prof. Xiao Hu
Signature

Abstract

Superconductors are a class of materials containing superconducting quantum condensates with exactly zero electrical resistance and expulsion of magnetic fields when cooled below a critical temperature [1]. According to Bardeen-Cooper-Schrieffer (BCS) theory, electrons near Fermi surface form Cooper pairs due to electron-phonon interaction and condense into a superconducting quantum state along with opening of a band gap [2]. In some materials, there are several Fermi surfaces originated from different bands. It is possible to have multiple superconducting gaps arising from these Fermi surfaces. The superconducting condensate is composed of several components and thus we call such materials as multi-component superconductors.

Multi-component superconductivity was first discussed in transition metals with a two-band BCS model more than fifty years ago [3]. Soon after that Kondo pointed out that superconducting critical temperature should be increased by Josephson-like interband couplings [4]. The degree of freedom of relative phase difference in a two-component superconductor was first discussed by Leggett [5]. The interest to multi-component superconductivity is recovered due to the discovery of superconductivity in MgB_2 with pronounced evidences for two superconducting gaps in 2001 [6] and the discovery of iron-based superconductors with more than two superconducting gaps in 2008 [7].

In superconductors with three or more components, time-reversal symmetry (TRS) may be broken in the presence of repulsive interband couplings, resulting in a pair of degenerate states characterized by opposite chiralities [8–10]. A hopeful candidate to realize this TRS broken (TRSB) state is the iron-based superconductor with at most five gaps originating from the five Fe 3d orbitals. Repulsive interband couplings are suggested by some experiments [11–13].

In this thesis, we mainly focus on novel phenomena of the TRSB state. Asymmetric critical currents are revealed in a Josephson junction between a three-component superconductor with broken TRS and a single-component superconductor [14]. Fractional flux plateaus are found in the magnetization curve for a superconductor loop with two halves occupied by the degenerate states with opposite chiralities [15]. Magnetic field penetrates a constriction connecting two bulks occupied by TRSB states with opposite chiralities and takes a ribbon-shaped distribution [16]. At last we study the magnetic response of two-component superconductors and find a first-order phase transition associated with vortex penetration [17].

At first, we focus on the Josephson effect of the TRSB state. We consider a Josephson junction between a three-component TRSB superconductor with gap functions $\{\Delta_1, \Delta_2, \Delta_3\}$ and a single-component superconductor with gap function Δ_0, as shown in Fig. 1(a). The phase of Δ_j are defined as φ_j with $j = 0, 1, 2, 3$. Since the intercomponent phase differences are locked in the TRSB state, we can study the supercurrent as a function of phase $\varphi = \varphi_1 - \varphi_0$. By adopting Bogoliubov-de Gennes equations, we obtain Andreev spectra and the current-phase relation as shown in Fig. 1(b). It is interesting to find that critical currents are unequal in the two opposite directions. The asymmetry of critical current is a clear manifestation of broken TRS.

It is intriguing to notice that asymmetric critical currents have been observed in a hybrid junction between a single-band superconductor PbIn and an iron-based superconductor $BaFe_{2-x}Co_xAs_2$ [18].

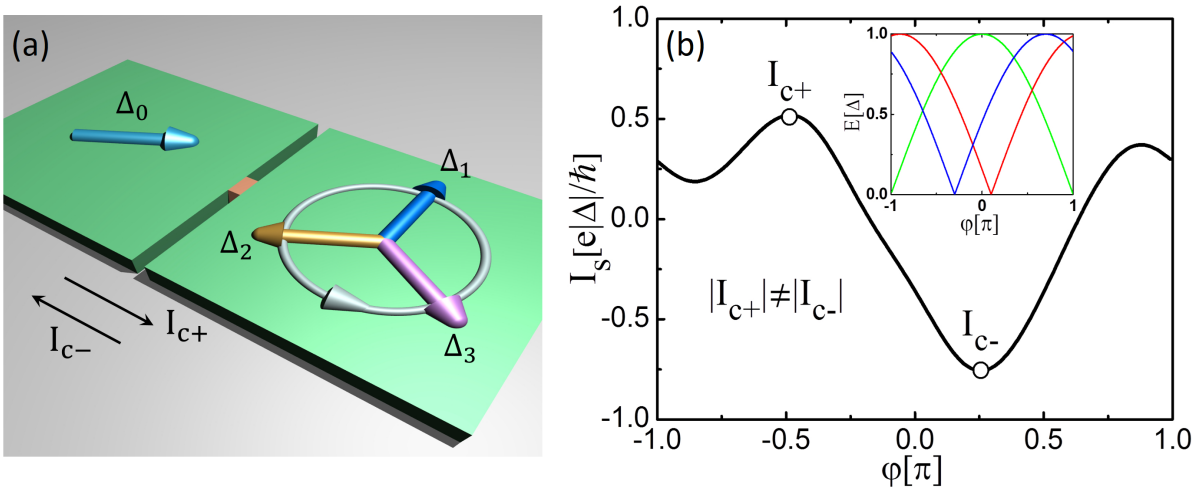

FIG. 1. (a) Schematics of point contact junction between single-band superconductor and three-band TRSB superconductor. Arrows indicate phases of gap functions and white circle with rotating direction represents the chirality referring to the mutual phases blue → yellow → purple among three condensates. (b) Current-phase relation of ballistic point-contact junction between single-band and three-band superconductor for parameters $\varphi_2 - \varphi_1 = 0.9\pi$, $\varphi_3 - \varphi_1 = 1.3\pi$ and temperature $T = 0.2|\Delta|/k_B$ with k_B the Boltzmann constant. For simplicity, all gap functions are assigned with the same amplitude $|\Delta|$. Inset: Andreev spectra for the same parameter set.

The difference between two critical currents is well beyond the experimental precision. In the light of our theoretical work, TRSB states have already been realized in iron-based superconductors.

Next, we consider a loop of a multi-component superconductor where the two halves are occupied by two TRSB states carrying on opposite chiralities, accompanied by two domain walls associated with inter-component phase kinks. We define the phase kink between component-i and j as D_{ij} with $i \neq j$ and $i, j = 1, 2, 3$. The situation is interesting when the two domain walls accommodate different phase kinks, such as D_{12} and D_{23} in domain wall I and II respectively shown in Fig. 2(a). By inspection one sees that ψ_2 rotates $4\pi/3$ anticlockwise over the two domain walls, while ψ_1 and ψ_3 rotate $-2\pi/3$. When the external magnetic field provides the additional phase rotation of $2\pi/3$ in all condensates, a state with 2π phase winding in ψ_2 and 0 in both ψ_1 and ψ_3 is stabilized. This yields a fractional flux $\eta\Phi_0$ in the loop. The state with a fractional flux trapped in this loop is stable in a certain range of external magnetic field, which leads to a fractional flux plateau in magnetization curve shown schematically in Fig. 2(b).

The above discussion can be elucidated by the integration of magnetic flux over the superconducting loop using Ginzburg-Landau (GL) formalism where the supercurrent is given by [1, 19]

$$\mathbf{J} = \sum_{j=1,2,3} \frac{2e}{m_j} |\psi_j|^2 \hbar \left(\nabla \varphi_j - \frac{2\pi}{\Phi_0} \mathbf{A} \right), \tag{1}$$

with m_j and φ_j the effective mass and phase of component-j. For a thick loop, supercurrent is zero deep inside the superconductor. In this case the magnetic flux trapped in the loop is given by the line integration of phase differences as can be seen from Eq. (1)

$$\Phi = \frac{\Phi_0}{2\pi} \left[\oint_C \frac{p_1 \nabla\varphi_1 + p_2 \nabla\varphi_2 + p_3 \nabla\varphi_3}{p_1 + p_2 + p_3} dl \right] = \frac{\Phi_0}{2\pi} \left[\oint_C \nabla\varphi_1 dl + \int_{\mathrm{DW}} \frac{p_2 \nabla\varphi_{12} + p_3 \nabla\varphi_{13}}{p_1 + p_2 + p_3} dl \right], \tag{2}$$

with $p_j = |\psi_j|^2/m_j^*$ and $\varphi_{ij} = \varphi_i - \varphi_j$ for $i, j = 1, 2, 3$, where "C" is taken as the middle line of the loop with zero supercurrent everywhere, and the "DW" stands for domain-wall regimes (grey parts in Fig. 2) with phase kinks. At the right side, we divide the integrand into two terms, indicating two contributions to the total magnetic flux. The first contribution should be an integer multiple of 2π due to the single-valued wave function in the loop. The integrand in the second contribution is nonzero only on domain walls. This contribution is nonzero when two different phase kinks are realized at domain wall I and II, with the value depending on the quantities p_j.

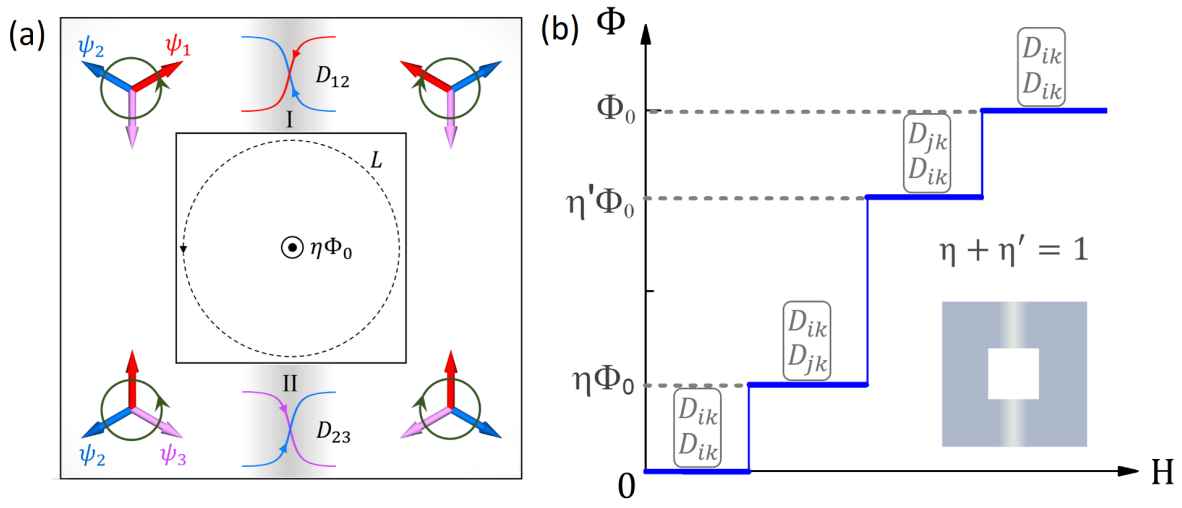

FIG. 2. (a) Schematic setup with a loop of TRSB superconductor, where the two halves are occupied by the two degenerate states with opposite chiralities. The three arrows denote the phases of order parameters and the green circle indicates the chirality. Between the two halves of the loop there are two domain wall I and II accommodating inter-component phase kinks. Phase kinks between two different pairs of components can trap fractional flux ($0 < \eta < 1$). The dashed circle denotes the direction for counting phase winding in the loop. (b) Schematic magnetization curve with fractional flux plateaus displayed together with gauge-invariant phase kinks denoted by [D_{ik}/D_{jk}] in the order of domain wall I and II.

Presuming the same length of domain walls I and II, the two configurations [D_{ik}/D_{jk}] and [D_{jk}/D_{ik}] at the domain walls [I/II] take the same free energy. However, integrating phase differences for these two configurations along the closed path in the anticlockwise way [see Fig. 2(a)] results in opposite fractional values of 2π in the second term in Eq. (2). Therefore, these two configurations give two fractional fluxes Φ_1 and Φ_2 related by $\Phi_1 + \Phi_2 = \Phi_0$. Although fractional fluxes individually take arbitrary values depending on material parameters and temperature, they form pairs related by the flux quantum Φ_0, which is a unique signature of TRSB state. Fractional flux plateaus with corresponding configurations of phase kinks are schematically shown in Fig. 2(b). This phenomenon is a clear evidence of TRSB superconductivity, and in a general point of view it provides a novel chance to explore relative phase difference, phase kink and soliton in ubiquitous multi-component superconductivity such as that in iron pnicitides.

In this thesis we also study vortex states on a domain wall at a constriction connecting two bulk superconductors with degenerate TRSB states, as shown in Fig. 3(a). With GL approach we find that vortices in different components dissociate from each other, resulting in a ribbon-shaped distribution of magnetic field at the domain wall as shown in Fig. 3(b) [16].

At last, we explore the magnetic response of two-component superconductors in terms of GL theory. We find that, in a certain parameter regime, a vortex lattice is thermodynamically stable, which is characterized by the following features: (1) the vortex-lattice constant is finite and determined by the parameters of GL free-energy functional, (2) the superconducting order parameters do not recover to the bulk values, and (3) the magnetic field is only partially screened. At a threshold field H_{c1}, many vortices enter simultaneously to form such a lattice in the whole sample, yielding a discontinuous jump in magnetization and thus a first-order phase transition [17]. As a sharp contrast, in single-component superconductors vortices penetrate into the sample at H_{c1} associated with a continuous phase transition corresponding to infinite separation among vortices. This phenomenon can be observed even when both components are categorized into type II in absence of intercomponent coupling.

To summarize, we have explored several novel phenomena in multi-component superconductors, which can be used to identify the TRSB state. The present work highlights the unique properties of multi-component superconductors and provide deeper understandings on multi-component supercon-

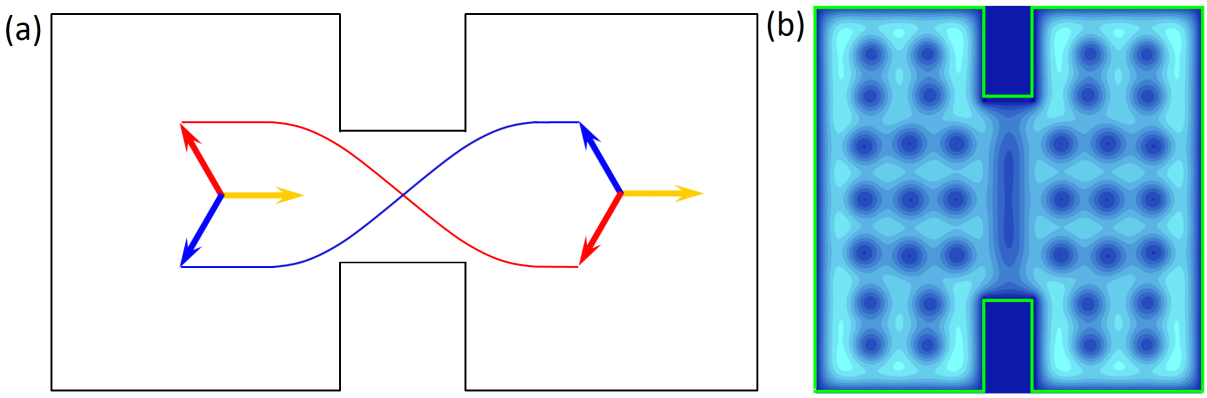

FIG. 3. (a) Schematics of constriction junction between two bulks occupied by TRSB states with opposite chiralities. A domain wall forms on the constriction where the red and blue order parameters form a phase kink. (b) Ribbon-shaped distribution of magnetic field on constriction.

ductivity.

[1] M. Tinkham, *Introduction to Superconductivity* (McGraw-Hill, Inc., New York, 1996).
[2] J. Bardeen, L. N. Cooper, and J. R. Schrieffer, Phys. Rev. **108**, 1175 (1057).
[3] H. Suhl, B. T. Matthias, and L. R. Walker, Phys. Rev. Lett. **12**, 552 (1959).
[4] J. Kondo, Prog. Theor. Phys. **29**, 1 (1963).
[5] A. J. Leggett, Prog. Theor. Phys. **36**, 1 (1966).
[6] J. Nagamatsu, N. Nakagawa, T. Muranaka, Y. Zenitani, and J. Akimitsu, Nature **410**, 63 (2001).
[7] Y. Kamihara, T. Watanabe, M. Hirano, and H. Hosono, J. Am. Chem. Soc. **130**, 3296 (2008).
[8] D. F. Agterberg, V. Barzykin, and L. P. Gor'kov, Phys. Rev. B **60**, 14868 (1999).
[9] V. Stanev and Z. Tešanović, Phys. Rev. B **81**, 134522 (2010).
[10] X. Hu and Z. Wang Phys. Rev. B **85**, 064516 (2012).
[11] K. Nakayama, T. Sato, P. Richard, Y. M. Xu, Y. Sekiba, S. Souma, G. F. Chen, J. L. Luo, N. L. Wang, H. Ding, and T. Takahashi, Europhys. Lett. **87**, 173003 (2009).
[12] K. Okazaki, Y. Ota, Y. Kotani, Y. Ishida, T. Shimojima, T. Kiss, S. Watanabe, C. T. Chen, C. H. Lee, H. Eisaki, T. Saito, H. Fukazawa, Y. Kohori, K. Hashimoto, T. Shibauchi, Y. Matsuda, H. Ikeda, H. Miyahara, R. Arita, A. Chainani, and S. Shin, Science **337**, 1314 (2012).
[13] S. Maiti, M. M. Korshunov, and A. V. Chubukov, Phys. Rev. B **85**, 014511 (2012).
[14] Z. Huang and X. Hu, Appl. Phys. Lett. **104**, 162602 (2014).
[15] Z. Huang and X. Hu, Phys. Rev. B **92**, 214516 (2015).
[16] Z. Huang and X. Hu, J. Supercond. Nov. Magn. (in press, arXiv:1510.05890).
[17] Z. Huang and X. Hu, in preparation.
[18] S. Schmidt, S. Döring, F. Schmidl, V. Grosse, and P. Seidel, Appl. Phys. Lett. **97**, 172504 (2010).
[19] A. Gurevich, Physica C **456**, 160 (2007).

Contents

Acknowledgements

I have completed my PhD work with uncountable support, excellent guidance and encouragement. I would like to express my acknowledgement on this occasion.

First and foremost, I want to express my greatest gratitude to Professor Xiao Hu for his continuous guide during the last five years, from initial advices in my master course, through ongoing discussions and inspiration to this day. His expertise, innovation, passion and seriousness in scientific research have deeply affected me and greatly encouraged me during my PhD study. In addition, Professor Hu has offered many tips on raising effective communication and building interpersonal relationships. His advices will continue guiding me in my future career and life.

I am sincerely grateful to Dr. Kawakami, Prof. Zhi Wang, Dr. Shizeng Lin, Prof. Qifeng Liang, Prof. Rui Yu, Prof. Bin Xi, Prof. Xueyuan Hu, Dr. Madhav Ghimire Dr. Yuki Takahashi, Dr. Feng Liu and Mr. Longhua Wu for their sincere help and fruitful discussions during my last five years.

I also like to give my sincere thanks to my family, father Bangjun Huang, mother Enxiang Tian and elder sister Xiaocong Huang for their supports and heartfelt consideration during my doctoral study.

This work was performed in Nano-System Theoretical Physics Unit, International Center for Materials Nanoarchitectonics (WPI-MANA), National Institute for Materials Science and Graduate School of Pure and Applied Sciences of University of Tsukuba. I greatly appreciate the financial support from NIMS (Junior Research Assistantship) during my last five years.

Abbreviations

ARPES	**A**ngle **R**esolved **P**hotoemission **S**pectroscopy
BCS	**B**ardeen-**C**ooper-**S**chrieffer
BdG	**B**ogoliubov-**d**e **G**ennes
CPR	**C**urrent-**P**hase **R**elation
GL	**G**inzburg **L**andau
SNS	**S**uperconductor-**N**ormal-**S**uperconductor
SIS	**S**uperconductor-**I**nsulator-**S**uperconductor
SQUID	**S**uperconducting-**QU**antum **I**nterference **D**evice
TDGL	**T**ime **D**ependent **G**inzburg **L**andau
TRSB	**T**ime-**R**eversal-**S**ymmetry-**B**roken
TRSR	**T**ime-**R**eversal-**S**ymmetry-**R**eserved

Chapter 1

Introduction

1.1 Basics of Superconductivity

In 1908 a Dutch physics Heike Kamerlingh Onnes successfully liquefied helium which gave him a refrigeration technique to reach $4.2K$, and then he started to study the electric conductivity of metals around this temperature. Three years later in mercury he observed an extraordinary phenomenon: the electrical resistance dropped abruptly to zero at $4.2K$, which opens the gate of superconductivity . Since then in the last one hundred years, superconductivity has remained as a fascinating field in condensed matter physics with continuing surprises.

Flux quantization

Soon after the Bohr's model was established, de Broglie proposed the matter wave and pointed out the correspondence between its phase-winding numbers and the discrete electron orbitals in the Hydrogen atom. Since then, the phase winding becomes a fundamental property of quantum mechanics and serves as a guidance to find quantized observables in the quantum states discovered later on. In superconductors, the phase winding of superconducting wave leads to the flux quantization, which is firstly recognized by F. London [1]. He introduced the concept "macroscopic quantum state" to describe superconductivity and indicate the ground state of superconductors in the form of $\psi = \sqrt{n_s}\exp(i\varphi)$, where $n_s = \psi^*\psi$ represent the density of superconducting charges and φ is the phase of the wave function. From the quantum mechanics, the current density is

$$\mathbf{J} = \frac{q}{2m}\left[\psi^*\left(-i\hbar\nabla - \frac{q}{c}\mathbf{A}\right)\psi + \psi\left(-i\hbar\nabla - \frac{q}{c}\mathbf{A}\right)\psi^*\right] = \frac{2en_s}{m}\left(\hbar\nabla\varphi - \frac{2e}{c}\mathbf{A}\right), \tag{1.1}$$

where $\mathbf{A}$ is the vector potential and $q = 2e$ (Cooper-pair) is the unit charge in supercurrent which becomes known after the advent of BCS theory [2]. By integrating the phase gradient from a location "a" to a location "b", we obtain the phase shift between "a" and "b" as

$$\Delta\varphi = \frac{1}{\hbar}\int_a^b \left(\frac{m}{2en_s}\mathbf{J} + \frac{2e}{c}\mathbf{A}\right)\cdot d\mathbf{l} \tag{1.2}$$

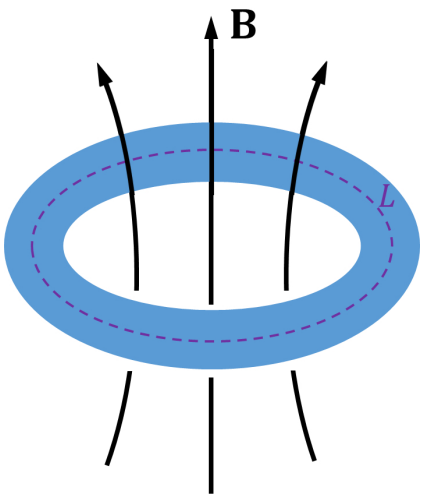

FIGURE 1.1: Schematics of superconducting ring with trapped quantized flux. L is a path deep inside superconductor where supercurrent is zero everywhere.

Now we consider a superconducting ring with a closed path L deep inside the sample with $J = 0$ as shown in Fig. 3.1, where the phase shift around the closed path is given by

$$\Delta\varphi = \frac{2e}{\hbar c}\oint_L \mathbf{A}\cdot d\mathbf{l} = \frac{2e}{\hbar c}\Phi. \tag{1.3}$$

Combined with the condition of single-value wave function $\Delta\varphi = 2\pi n$ with n an integer, Eq. (1.3) gives

$$\Phi = n\frac{hc}{2e} = n\Phi_0, \tag{1.4}$$

where $\Phi_0 = 2.07\times 10^{-15} Wb$ is called the magnetic flux quantum. This has been shown experimentally with measurements of the flux trapped in a thick hollow cylinder which screens the supercurrent to zero [3, 4].

Meissner effect

It is interesting to take a curl on left and right side of Eq. (1.1), where we obtain

$$\nabla\times\mathbf{J} = -\frac{4e^2 n_s}{mc}\mathbf{B}, \tag{1.5}$$

which is the second London equation. Together with the Maxwell equations

$$\nabla\times\mathbf{B} = \frac{4\pi}{c}\mathbf{J}, \quad \nabla\cdot\mathbf{B} = 0, \tag{1.6}$$

we obtain

$$\nabla^2\mathbf{B} = \frac{1}{\lambda^2}\mathbf{B}, \tag{1.7}$$

where

$$\lambda = \sqrt{\frac{mc^2}{16e^2\pi n_s}}. \tag{1.8}$$

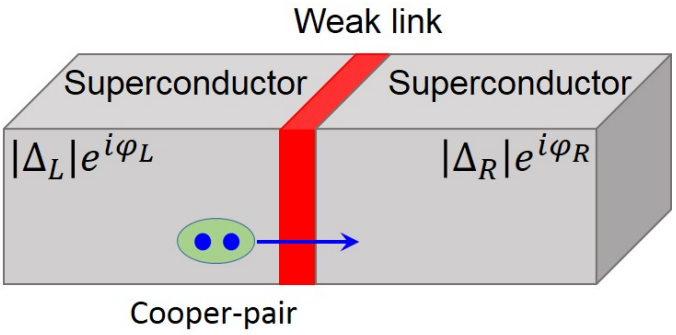

FIGURE 1.2: Schematics of superconducting ring with trapped quantized flux. L is a path deep inside superconductor where supercurrent is zero everywhere.

If we consider a superconducting medium occupying the half space $x > 0$ and an external magnetic field at $x \leq 0$, solution of Eq. (1.7) is given by

$$B(x) = B_0 \exp\left(-\frac{x}{\lambda}\right), \tag{1.9}$$

which indicates the Meissner effect and λ is the London penetration length which characterizes the distance to which a magnetic field penetrates into a superconductor.

Josephson effect

In 1962, B. D. Josephson [5] studied a device, known as the Josephson junction, consisted with two superconductors separated by a thin insulating film and predicted two following phenomena:(1) a current flows across the junction with zero-voltage drop in presence of phase difference between two superconductors, which is called the DC Josephson effect, and (2) the supercurrent changes periodically with a frequency $\nu = 2eV/h$ in presence of a voltage V between two sides of the junction, which is called the AC Josephson effect. The DC Josephson effect was soon observed experimentally by Anderson and Rowell in 1963 [6], and the AC Josephson effect was observed by Yanson et al. in 1965 [7]. Later on Josephson effect was also found in other junctions where the insulator was replaced by normal metal, semiconductor or superconducting constriction with size smaller than the superconducting coherence length [8]. In general, Josephson effect takes place in a junction where two superconducting bulks connected and coupled by a weak link.

Here we use the Schrodinger equation to derive the supercurrent as function of the phase shift across the junction. This method was provided by Feynman [9], which is rough however has a clear physics picture. The quantum mechanical wavefunctions of two superconducting states are given by

$$\psi_j = \sqrt{n_{sj}} e^{i\varphi_j} \tag{1.10}$$

where φ_j and n_{sj} are phase and density of Cooper-pairs with $j = 1, 2$. The dynamics of the wavefunctions is determined by the following coupled wave equations

$$\begin{aligned} i\hbar \frac{\partial \psi_1}{\partial t} &= \mu_1 \psi_1 + k\psi_2 \\ i\hbar \frac{\partial \psi_2}{\partial t} &= \mu_2 \psi_2 + k\psi_1 \end{aligned} \tag{1.11}$$

where k is the coupling coefficient which characterizes the coupling strength across the weak link and μ_1 and μ_2 represent the chemical potentials in the two bulks. Substituting Eq. (1.11) into Eq. (1.10) gives

$$\frac{\partial n_{s1}}{\partial t} = -\frac{\partial n_{s2}}{\partial t} = \frac{2k}{\hbar}\sqrt{n_{s1}n_{s2}}\sin(\varphi_2 - \varphi_1) \tag{1.12}$$

$$-\frac{\partial}{\partial t}(\varphi_2 - \varphi_1) = \mu_2 - \mu_1 \tag{1.13}$$

The first equation describes a charge transportation and thus we get the Josephson current

$$j = 2e\frac{\partial n_{s1}}{\partial t} = \frac{4ek}{\hbar}\sqrt{n_{s1}n_{s2}}\sin(\varphi_2 - \varphi_1). \tag{1.14}$$

When a voltage V is applied across the junction, the energy levels shifts to $\mu_1 - \mu_2 = 2eV$. Writing $j_c = 4ek\sqrt{n_{s1}n_{s2}}/\hbar$ and $\Delta\varphi = \varphi_2 - \varphi_1$, we obtain

$$j = j_c \sin\Delta\varphi \tag{1.15}$$

$$\frac{\partial\Delta\varphi}{\partial t} = \frac{2eV}{\hbar} \tag{1.16}$$

which represent the DC and AC Josephson effect. From Eq. (1.16), we obtain that a DC voltage $1\mu V$ produce a AC current with frequency $\omega = 863.6$MHz. When Cooper-pairs pass through the potential barrier at the junction, photons with energy $\hbar\omega = 2eV$ will be released or absorbed. With this effect, precise value of $e/\hbar$ can be obtained by measuring V and ω [10].

For simplicity, we carry out the above discussion in terms of the phase difference δ. Since δ is not gauge invariant, in general it cannot determine the Josephson current which is a gauge-invariant physical quantity. This problem is solved by introducing the gauge-invariant phase difference

$$\theta = \Delta\varphi - \frac{2\pi}{\Phi_0}\int \mathbf{A}\cdot d\mathbf{l}, \tag{1.17}$$

where the integration is from one side of the junction to the other, so the general expression of current-phase relation is

$$j_s = j_c \sin\theta. \tag{1.18}$$

When gauge $A = 0$ is adopted, which is reasonable in absence of magnetic flux, Eq. (1.18) is reduced to Eq. (1.15).

Quantum interference

When we connect two superconductors with two Josephson junctions to form a superconducting circuit as shown in Fig. 1.3, phase differences across the two junctions are related, which leads to quantum interference phenomena. Since the two junctions are very short compared with the whole circle, the trapped flux in "L" is given by

$$\Phi = \oint_L \mathbf{A}\cdot d\mathbf{l} = \int_b^c \mathbf{A}\cdot d\mathbf{l} + \int_d^a \mathbf{A}\cdot d\mathbf{l}. \tag{1.19}$$

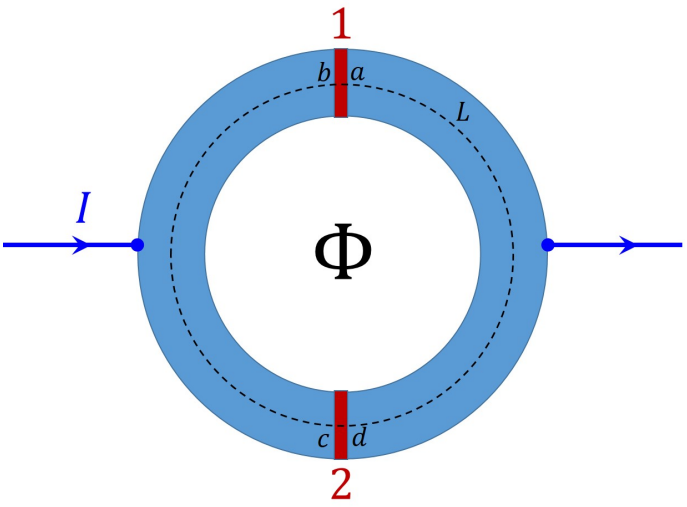

FIGURE 1.3: Schematics of a superconducting quantum interference device (SQUID) with two Josephson junctions. "L" is a closed path where the supercurrent is zero on its path in the superconducting region, i.e. from b to c and d to a.

Considering that $J = 0$ on the parts of "L" in the superconductor, according to Eq. (1.2) we have the phase differences

$$\varphi_c - \varphi_b = \frac{2\pi}{\Phi_0}\int_b^c \mathbf{A}\cdot d\mathbf{l}, \quad \varphi_a - \varphi_d = \frac{2\pi}{\Phi_0}\int_d^a \mathbf{A}\cdot d\mathbf{l}, \tag{1.20}$$

which leads to

$$(\varphi_c - \varphi_b) + (\varphi_a - \varphi_d) = \frac{2\pi}{\Phi_0}\Phi. \tag{1.21}$$

The condition of single-valued wave function requires

$$(\varphi_c - \varphi_b) + (\varphi_b - \varphi_a) + (\varphi_a - \varphi_d) + (\varphi_d - \varphi_c) = 2\pi n. \tag{1.22}$$

By combining above two equations, we obtain the relation between the phase shift across junction-1 $\Delta\varphi_1 = \varphi_a - \varphi_b$ and the phase shift across junction-2 $\Delta\varphi_2 = \varphi_d - \varphi_c$ as

$$\Delta\varphi_2 - \Delta\varphi_1 = 2\pi n - \frac{2\pi}{\Phi_0}\Phi. \tag{1.23}$$

Here we consider a simple case that two junctions have the same critical current I_c and the total supercurrent is thus given by

$$\begin{aligned} I &= I_c \sin\Delta\varphi_1 + I_c \sin\Delta\varphi_2 \\ &= I_c \sin(\Delta\varphi_2 + 2\pi\Phi/\Phi_0) + I_c \sin\Delta\varphi_2 \\ &= 2I_c \cos(\pi\Phi/\Phi_0)\sin(\Delta\varphi_2 + \pi\Phi/\Phi_0), \end{aligned} \tag{1.24}$$

and thus the maximum supercurrent as

$$I_m = 2I_c|\cos(\pi\Phi/\Phi_0)|, \tag{1.25}$$

which is shown in Fig. 1.4. There are two special cases of trapped flux: (1) when $\Phi = n\Phi_0$, the two phase shifts can simultaneously take the value $\pi/2$ and give the greatest total supercurrent $2I_c$, which is a constructive

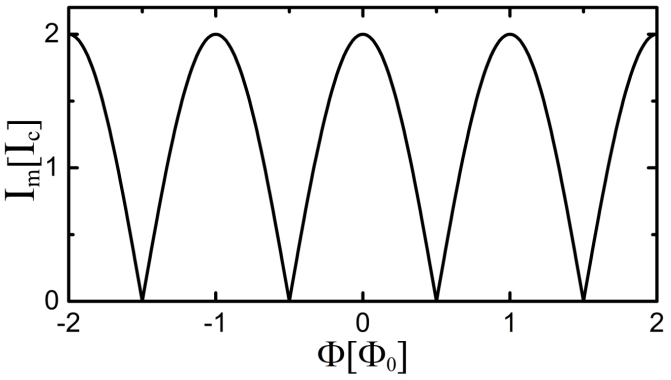

FIGURE 1.4: Schematics of a superconducting quantum interference device (SQUID) with two Josephson junctions. "L" is a closed path where the supercurrent is zero on its path in the superconducting region, i.e. from b to c and d to a.

interference and (2) when $\Phi = n\Phi_0 + \Phi_0/2$, the two phase shifts always have a difference of π, where Josephson current in junctions cancel each other, which indicates a destructive interference.

1.2 Microscopic Theory of Superconductivity

1.2.1 Bardeen-Cooper-Schrieffer Theory

Although phenomenological theories give a good description of the electrodynamic properties of superconductors, the microscopic picture of the superconductivity still remains unknown for forty years after the discovery of superconductivty, which becomes an urgent problem in the community of solid state physics. From 1950, experimental discoveries such as isotope effect and observation of superconducting gap provides clues to answers of these questions, which finally lead to advent of BCS theory in 1957.

The first evidence of an energy gap between the superconducing ground state and the excited state is from measurements of electronic contribution of specific heat [11], which reveals an exponential form of temperature dependence as

$$c_{es} \propto e^{-bT_c/T}. \tag{1.26}$$

Since the number of particles above an energy gap E_g is proportional to $\exp\{-E_g/2k_BT\}$ at temperature T, the measurements of specific heat suggests existence of superconducting gap

$$E_g = 2bk_BT_c. \tag{1.27}$$

With $b \approx 1.5$ from the measurements, the energy gap is given by

$$E_g \approx 3k_BT_c. \tag{1.28}$$

The gap was later directly observed by irradiating electromagnetic waves on the superconductor, where the waves were absorbed strongly when photon energy was larger than E_g [12]. In conventional superconductors, the energy gap is at the order of $10^{-4}eV$.

In 1950, Maxwell [13] and Reynolds [14] independently found the relevance between critical temperature T_c and the mass of the isotope M: $T_c M^{\beta} = constant$ with $\beta \approx 0.5$. It is well known that the mass of ions in crystal lattices is associated with the vibration properties on crystal lattice, therefore phonon-electron interactions should be considered seriously in the mechanism of superconductivity.

Soon Frohlich proposed that the phonon-electron interaction possibly induces an attraction among electrons [15]. The microscopic picture is given in the following way. When an electron goes through a positive ionic crystal cell, the lattice around is distorted due to the Coulomb interaction, which increases the local density of positive charges, and thus another electron should approach this site. In presence of the ionic crystal lattice, an effective attraction forms between two electrons. A reasonable condition for the attraction is that the moving frequency of electrons should be smaller than the frequency of phonons, otherwise the distortion cannot be induced by the moving electron. However it is still not clear whether this attraction is related to emergence of superconductivity or not.

In 1956, Cooper obtained a bound state formed by a pair of electrons in presence of an attraction between them [16], as the dawn of advent of BCS theory. In his model, he put two additional electrons into a metal at $0K$ and considered unchanged Fermi surface, which forces the two electrons to occupy the states above the Fermi surface due to Pauli principle, and thus the many-body problem is reduced to a simple two-body problem. Then he assumed an attraction between the electrons and solve the energy spectrum. He obtained a bound state below the Fermi surface, where indeed has no space for additional electrons. Therefore, the Fermi sea becomes unstable with the formation of the bound state and a reorganization of Fermi surface is inevitable. The Cooper-pairing effect provides a basis for understanding of superconductivity. The pairs form a Bose condensate which is the origin of all quantum phenomena in superconductors.

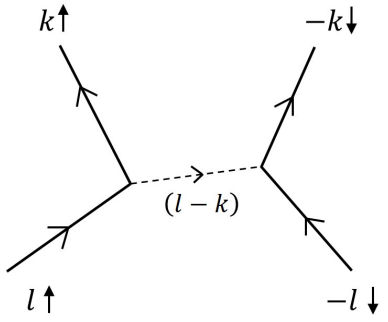

FIGURE 1.5: Schematics of phonon-electron interaction in the BCS model. Electron with momentum l emits a phonon with momentum $(l-k)$ which is absorbed by another electron with moment $-l$. The Cooper pair $(l\uparrow, -l\downarrow)$ is scattered to the state $(k\uparrow, -k\downarrow)$.

Only one year later, Bardeen, Cooper and Schrieffer proposed the great BCS theory which is the first microscopic theory of superconductivity since the discovery of superconductivity. In BCS theory, we have the paring Hamiltonian

$$\mathcal{H} = \sum_{k\sigma} \varepsilon_k c^{\dagger}_{k,\sigma} c_{k\sigma} + \sum_{k,l} V c^{\dagger}_{k\uparrow} c^{\dagger}_{-k\downarrow} c_{-l\downarrow} c_{l\uparrow} \tag{1.29}$$

where ε is the single-particle energy relative to the Fermi energy, k, l are momentum, σ is spin and V is the pairing interaction. BCS took the ground state as

$$|\psi_G\rangle = \prod_k (u_k + v_k c^\dagger_{k\uparrow} c^\dagger_{-k\downarrow})|\phi_0\rangle, \tag{1.30}$$

where $|u_k|^2 + |v_k|^2 = 1$. $|u_k|^2$ and $|v_k|^2$ are the probabilities of the Cooper pair being unoccupied and occupied. Here for simplicity, we take u_k and v_k as real. To obtain the energy minimum, we set

$$\delta\langle\psi_G|\mathcal{H}|\psi_G\rangle = 0, \tag{1.31}$$

where

$$\langle\psi_G|\mathcal{H}|\psi_G\rangle = 2\varepsilon_k v_k^2 + \sum_{k,l} V_{kl} u_k v_k u_l v_l. \tag{1.32}$$

It is convenient to use

$$u_k = \sin\theta_k \quad \textit{and} \quad v_k = \cos\theta_k, \tag{1.33}$$

and the right side of Eq. (1.32) changes to

$$\sum_k \varepsilon_k(1 + \cos 2\theta_k) + \frac{1}{4}\sum_{k,l} V_{kl} \sin 2\theta_k \sin 2\theta_l. \tag{1.34}$$

We minimize the energy by taking the derivative with respect to θ_k as zero, which gives

$$-2\varepsilon_k \sin 2\theta_k + \sum_l V_{kl} \cos 2\theta_k \sin 2\theta_l = 0, \tag{1.35}$$

and we obtain

$$\tan 2\theta_k = \frac{1}{2\varepsilon_k}\sum_l V_{kl} \sin 2\theta_l. \tag{1.36}$$

By defining quantities

$$\Delta_k = -\sum_l V_{kl} u_l v_l = -\frac{1}{2}\sum_l V_{kl} \sin 2\theta_l, \quad E_k = \sqrt{\Delta_k^2 + \varepsilon_k^2}, \tag{1.37}$$

Eq. (1.36) becomes

$$\tan 2\theta = -\frac{\Delta_k}{\varepsilon_k}, \tag{1.38}$$

and thus we have

$$2u_k v_k = \sin 2\theta_k = \frac{\Delta_k}{E_k} \tag{1.39}$$

and

$$v_k^2 - u_k^2 = \cos 2\theta_k = -\frac{\varepsilon_k}{E_k}. \tag{1.40}$$

Here we put the minus sign for $\cos 2\theta_k$ to make $v_k \to 0$ as $\varepsilon_k \to \infty$, which is based on the consideration that the pairing should take place around Fermi surface. From Eq. (1.36), (1.38) and (1.39), we get

$$\Delta_k = -\frac{1}{2}\sum_l \frac{\Delta_l}{\sqrt{\Delta_l^2 + \varepsilon_l^2}} V_{kl}. \tag{1.41}$$

BCS made an assumption that

$$V_{kl} = \begin{cases} -V & |\varepsilon_k|, |\varepsilon_l| \le \hbar\omega_c, \\ 0 & |\varepsilon_k|, |\varepsilon_l| > \hbar\omega_c, \end{cases} \tag{1.42}$$

where V is a positive constant. Δ_k becomes an constant Δ independent of k, which reduces Eq. (1.41) to

$$1 = \frac{V}{2}\sum_k \frac{1}{\sqrt{\Delta_k^2 + \varepsilon_k^2}}. \tag{1.43}$$

The summation above can be replaced by an integration, and thus Eq. (1.43) is rewritten as

$$1 = \frac{N(0)V}{2}\int_{-\hbar\omega}^{\hbar\omega} \frac{d\varepsilon}{\sqrt{\Delta^2 + \varepsilon^2}} = N(0)V \sinh^{-1}\frac{\hbar\omega_c}{\Delta}, \tag{1.44}$$

where the density of states from $-\hbar\omega_c$ to $\hbar\omega_c$ is taken as the density at Fermi surface $N(0)$ approximately. In the weak coupling limit $N(0)V \ll 1$, we obtain

$$\Delta \approx 2\hbar\omega_c e^{-1/N(0)V}. \tag{1.45}$$

In BCS theory, the attraction between electrons are taken as the electron-phonon interaction. Therefore we can have a cut-off frequency ω_c which is the largest frequency of phonons in the materials. Since $\hbar\omega_c$ for isotopes of the same element is proportional to $M^{-0.5}$, the proportionality between Δ and $\hbar\omega_c$ is consistent with the isotope effect.

1.2.2 Bogoliubov-de Gennes Equations

According to the picture of Cooper-pairs, excitation above the superconducting gap are particles and holes. Here we assume the wavefunctions of electrons at coordinate $\mathbf{r}$ as linear combinations of the quasiparticle states

$$\begin{aligned}
\Psi^\dagger(\mathbf{r}\uparrow) &= \sum_n \left[\gamma_{n\uparrow}^\dagger u_n^*(\mathbf{r}) - \gamma_{n\downarrow} v_n(\mathbf{r}))\right], \\
\Psi^\dagger(\mathbf{r}\downarrow) &= \sum_n \left[\gamma_{n\downarrow}^\dagger u_n^*(\mathbf{r}) + \gamma_{n\uparrow} v_n(\mathbf{r}))\right], \\
\Psi(\mathbf{r}\uparrow) &= \sum_n \left[\gamma_{n\uparrow} u_n(\mathbf{r}) - \gamma_{n\downarrow}^\dagger v_n^*(\mathbf{r}))\right], \\
\Psi(\mathbf{r}\downarrow) &= \sum_n \left[\gamma_{n\downarrow} u_n(\mathbf{r}) + \gamma_{n\uparrow}^\dagger v_n(\mathbf{r}))\right],
\end{aligned} \tag{1.46}$$

where $\gamma_{n\uparrow}$ create a quasiparticle of spin up in the state n and $\gamma_{n\downarrow}$ annihilates a quasiparticle with spin down. The electron operators follow the Fermi communication relations

$$\Psi(\mathbf{r},\alpha)\Psi(\mathbf{r}',\beta) + \Psi(\mathbf{r}',\beta)\Psi(\mathbf{r},\alpha) = 0, \tag{1.47}$$

$$\Psi^{\dagger}(\mathbf{r},\alpha)\Psi^{\dagger}(\mathbf{r}',\beta) + \Psi^{\dagger}(\mathbf{r}',\beta)\Psi^{\dagger}(\mathbf{r},\alpha) = 0, \tag{1.48}$$

$$\Psi^{\dagger}(\mathbf{r},\alpha)\Psi(\mathbf{r}',\beta) + \Psi(\mathbf{r}',\beta)\Psi^{\dagger}(\mathbf{r},\alpha) = \delta_{\alpha\beta}\delta(\mathbf{r}-\mathbf{r}'), \tag{1.49}$$

where α and β are spin indexes. The quasiparticle operators should also follow the Fermi commutation relations

$$\gamma_{n,\alpha}\gamma_{m,\beta} + \gamma_{m,\beta}\gamma_{n,\alpha} = 0, \tag{1.50}$$

$$\gamma^{\dagger}_{n,\alpha}\gamma^{\dagger}_{m,\beta} + \gamma^{\dagger}_{m,\beta}\gamma^{\dagger}_{n,\alpha} = 0, \tag{1.51}$$

$$\gamma^{\dagger}_{n,\alpha}\gamma_{m,\beta} + \gamma_{m,\beta}\gamma^{\dagger}_{n,\alpha} = \delta_{\alpha\beta}\delta_{mn}. \tag{1.52}$$

The BCS Hamiltonian in the real space is

$$\mathcal{H} = \sum_{\alpha}\int \Psi^{\dagger}(\mathbf{r},\alpha)\hat{H}_0\Psi(\mathbf{r},\alpha)d^3r - \frac{V}{2}\sum_{\alpha,\beta}\int \Psi^{\dagger}(\mathbf{r},\alpha)\Psi^{\dagger}(\mathbf{r},\beta)\Psi(\mathbf{r},\beta)\Psi(\mathbf{r},\alpha)d^3r, \tag{1.53}$$

where $V > 0$. De Gennes simplified this Hamiltonian to an effective mean-field Hamiltonian which is the second order of Ψ:

$$\begin{aligned} H_{eff} = \sum_{\alpha}\int \Big[\Psi^{\dagger}(\mathbf{r},\alpha)\hat{H}_0\Psi(\mathbf{r},\alpha) + U(\mathbf{r})\Psi^{\dagger}(\mathbf{r},\alpha)\Psi(\mathbf{r},\alpha)\Big]d^3r \\ + \int \Big[\Delta\Psi^{\dagger}(\mathbf{r},\uparrow)\Psi^{\dagger}(\mathbf{r},\downarrow) + \Delta^{*}\Psi(\mathbf{r},\downarrow)\Psi(\mathbf{r},\uparrow))\Big]d^3r, \end{aligned} \tag{1.54}$$

which contains a real effective field

$$U(\mathbf{r}) = -V\langle\Psi^{\dagger}(\mathbf{r},\downarrow)\Psi(\mathbf{r},\downarrow)\rangle = -V\langle\Psi^{\dagger}(\mathbf{r},\uparrow)\Psi(\mathbf{r},\uparrow)\rangle, \tag{1.55}$$

and a complex effective field

$$\Delta(\mathbf{r}) = -V\langle\Psi(\downarrow)\Psi(\mathbf{r}\uparrow)\rangle = V\langle\Psi(\uparrow)\Psi(\mathbf{r}\downarrow)\rangle. \tag{1.56}$$

This Hamiltonian should be diagonal in the quasiparticle operators $\gamma_{n,\alpha}$ and $\gamma^{\dagger}_{n,\alpha}$ as

$$H_{eff} = E_g + \sum_{n,\alpha}\epsilon_n\gamma^{\dagger}_{n,\alpha}\gamma_{n,\alpha}, \tag{1.57}$$

where E_g is the energy of the ground state and ϵ_n is the energy of excited state $|n\rangle$. From Eq. (1.54), we have the commutators

$$[H_{eff},\Psi(\mathbf{r},\uparrow)] = -[H_0 + U(\mathbf{r})]\Psi(\mathbf{r},\uparrow) - \Delta(\mathbf{r})\Psi^{\dagger}(\mathbf{r},\downarrow), \tag{1.58}$$

$$[H_{eff},\Psi(\mathbf{r},\downarrow)] = -[H_0 + U(\mathbf{r})]\Psi(\mathbf{r},\downarrow) + \Delta(\mathbf{r})\Psi^{\dagger}(\mathbf{r},\uparrow). \tag{1.59}$$

we also have the commutator from Eq. (1.57) as

$$[H_{eff}, \gamma_{n,\alpha}] = -\epsilon_n \gamma_{n,\alpha}, \tag{1.60}$$

$$[H_{eff}, \gamma^{\dagger}_{n,\alpha}] = \epsilon_n \gamma^{\dagger}_{n,\alpha}. \tag{1.61}$$

Since Eq. (1.58) and (1.59) should be equivalent to Eq. (1.60) and (1.61), we express Ψ with γ by using Eq. (1.46) and compare the terms with γ and $\gamma^{\dagger}$. We find that Eq. (1.60) and (1.61) hold when u and v satisfy the Bogoliubov de-Gennes (BdG) equations

$$[H_0 + U]u + \Delta v = \epsilon u, \tag{1.62}$$

$$-[H_0^* + U]v + \Delta^* u = \epsilon v. \tag{1.63}$$

1.3 Ginzburg-Landau Theory

In the introduction of microscopic picture of superconductivity, we obtain the ground state, excited state and energy gap from the BCS theory, which also successfully explains phenomena such as zero resistance, Meissner effect and isotope effect. Nevertheless, it is inconvenient to study a sample with inhomogeneous superconductivity based on BCS theory. Similarly, the London theory does not consider the suppression of density of Cooper pairs under magnetic field and also has no discussion on the spacial variation of the density. Therefore both theories have difficulty in dealing with spatial inhomogeneity, which unfortunately is a common occasion when superconductors are under external electromagnetic field. In such cases, the Ginzburg-Landau (GL) theory are proved to be a valuable tool [17].

In 1950 Ginzburg and Landau established a phenomenological theory based on Landau theory of second-order phase transition [18]. Based on this Ginzburg-Landau (GL) theory in 1957 Abrikosov predicted a vortex structure where supercurrent flows around a normal core, which appears in type-II superconductors [19]. Later in 1959, Gor'kov derived the GL theory from BCS theory near the phase transition point, where the superconducting order parameters are small and changes slowly in space [20]. This derivation yielded a microscopic interpretation of all the parameters and allows a calculation of coefficients in GL theory. After the develop in this decade, GL theory was fully understood and widely accepted as a powerful tool in research of superconductors. In this Chapter, I will briefly introduce the GL theory as a basis for the further study.

1.3.1 Ginzburg-Landau Free Energy Functional

The GL theory is based on the Landau theory of second-order phase transitions, where a crucial point is the expansion of the free energy in powers of an order parameter which distinguishes the symmetry of the two phases. This order parameter is nonzero below the critical temperature and zero above it. When temperature is close to the superconducting phase transition temperature T_c, the value and spatial gradient of the superconducting order parameter are small, which allows the expansion of free energy in the form

$$f = f_n + \alpha |\Psi(r)|^2 + \frac{\beta}{2} |\Psi(r)|^4 + \frac{\hbar^2}{2m} |\nabla \Psi(r)|^2, \tag{1.64}$$

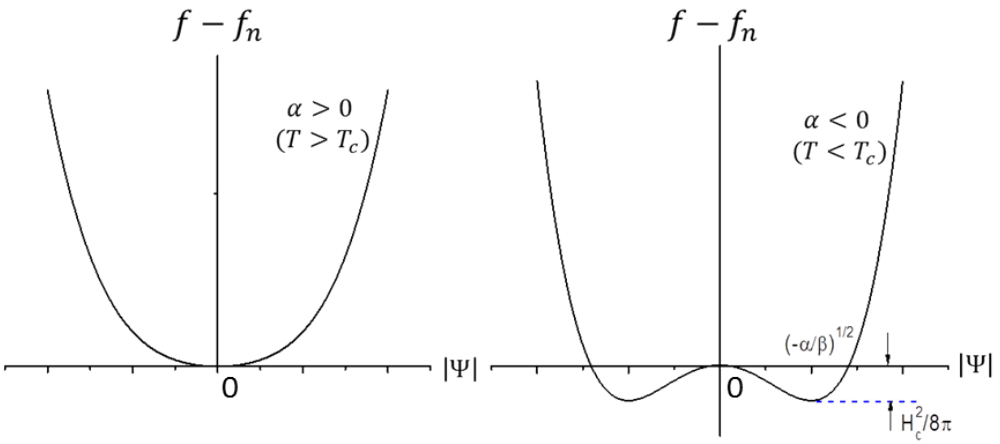

FIGURE 1.6: GL free energy for $T > T_c$ and $T < T_c$.

where f_n is the free energy of the normal state, $\Psi(r)$ is a complex order parameter with $|\Psi(r)|^2$ representing the local density of Cooper-pairs, and the gradient term corresponds to quantum mechanical kinetic energy of a Cooper-pair. Coefficients of $|\Psi|^2$ and $|\Psi|^4$ are temperature dependent, but at temperature neat T_c only the leading term is kept, and thus we have

$$\alpha = \alpha_0 \left(1 - \frac{T}{T_c}\right) \qquad \alpha_0 < 0 \tag{1.65}$$

and β is a positive constant.

In absence of external fields, the equilibrium state is uniform where the order parameter is homogeneous and can be obtained by minimizing the free energy without the gradient term, which leads to

$$\begin{aligned} T < T_c: &\quad \alpha < 0, \quad |\Psi|^2 = |\Psi_\infty|^2 = -\alpha/\beta, \\ T > T_c: &\quad \alpha > 0, \quad \Psi = 0. \end{aligned} \tag{1.66}$$

In this thesis, we denote the order parameter at the uniform state as the bulk order parameter Ψ_∞ and its value is called the bulk value. A corresponding curve showing the free energy as a function of the order parameter is given in Fig. 1.6. At $T < T_c$, we have

$$f - f_n = -\frac{\alpha^2}{2\beta} = -\frac{H_{tc}^2}{8\pi}, \tag{1.67}$$

where we obtain the thermodynamic critical field H_{tc} as

$$H_{tc} = \sqrt{\frac{4\pi\alpha^2}{\beta}}. \tag{1.68}$$

Now let us consider the behavior in presence of a magnetic field. We need to add the term of energy density of magnetic field $\mathbf{B}^2/8\pi$ and replace $\nabla\Psi$ with $[\nabla - i(2e/\hbar c)\mathbf{A}]\Psi$ to restore the gauge invariance. The final

expression of the free energy thus takes the form

$$f = f_n + \alpha |\Psi(r)|^2 + \frac{\beta}{2}|\Psi(r)|^4 + \frac{1}{2m}\left|\left(\frac{\hbar}{i}\nabla - \frac{2e}{c}\mathbf{A}\right)\Psi(r)\right|^2 + \frac{(\nabla\times\mathbf{A})^2}{8\pi}. \tag{1.69}$$

We can check this free energy is gauge invariant under the following gauge transformation

$$\mathbf{A} \to \mathbf{A} + \frac{2e}{\hbar c}\nabla\chi, \quad \Psi \to \Psi e^{i\chi}. \tag{1.70}$$

By varying the free energy with respect to $\mathbf{A}$ and Ψ^*, one can obtain the GL equations as

$$\alpha\Psi + \beta|\Psi|^2\Psi + \frac{1}{2m}\left(\frac{\hbar}{i}\nabla - \frac{2e}{c}\mathbf{A}\right)^2\Psi = 0, \tag{1.71}$$

$$\mathbf{J_s} = \frac{c}{4\pi}\nabla\times\nabla\times\mathbf{A} = \frac{2e}{m}|\Psi|^2\left(\hbar\nabla\varphi - \frac{2e}{c}\mathbf{A}\right), \tag{1.72}$$

where J_s is the supercurrent and φ is the phase of the order parameter.

The general boundary condition for superconductors are provided by de Gennes [21], which assures that no supercurrent passes through the boundary. The formula of boundary condition is given by

$$\mathbf{n}\cdot\left(\frac{\hbar}{i}\nabla + \frac{2e}{c}\mathbf{A}\right)\Psi = \frac{i\hbar}{b}\Psi, \tag{1.73}$$

where $\mathbf{n}$ is the unitary vector perpendicular to the boundary and b is a real constant. The value of b depends on the nature of the material which the boundary attaches to and generally there are three cases: (1) $b \to \infty$ indicates a superconductor/insulator boundary, (2) $b > 0$ describes a superconductor/normal metal interface, (3) $b = 0$ when the superconductor is attached to a ferromagnet which require $\Psi = 0$ at the boundary.

In presence of external field, the free energy continuous at phase transition point is the Gibbs free energy

$$G = f - \frac{\mathbf{H}\cdot\mathbf{B}}{4\pi}. \tag{1.74}$$

At H_{tc}, both the bulk superconducting state and the normal state have the same Gibbs free energy as

$$G_{s0} = -\frac{H_{tc}^2}{8\pi}. \tag{1.75}$$

London penetration length

Here we derive the London penetration length from the second GL equation. In London gauge where $|\Psi|$ is a constant, we put a curl operation on both sides of Eq. (1.72) and get

$$\frac{c}{4\pi}\nabla\times\nabla\times\mathbf{B} = \frac{4e^2|\Psi|^2}{mc}\mathbf{B}, \tag{1.76}$$

which leads to

$$\nabla^2\mathbf{B} = -\frac{16\pi e^2\alpha}{m\beta c^2}\mathbf{B}, \tag{1.77}$$

after substituting the order parameter of the equilibrium state. If we consider a superconducting medium occupying the half space $x > 0$ and an external magnetic field at $x \leq 0$, solution of Eq. (1.77) is given by

$$B(x) = B_0 \exp\left(-\frac{x}{\lambda}\right), \tag{1.78}$$

where we get the penetration length λ as

$$\lambda = \sqrt{-\frac{m\beta c^2}{16\pi e^2 \alpha}}. \tag{1.79}$$

Coherence length

When a disturbance of superconducting order parameter from the bulk value takes place somewhere in a superconducutor in absence of external field, the order parameter should recover to the bulk value far away. The characteristic length to describe this recovery is the GL coherence length. Here we set $\Psi = \Psi_\infty + g(x)$ where Ψ is the bulk order parameter and $g(x)$ is the deviation, and Eq. (5.2) becomes

$$\alpha(\Psi_\infty + g) + \beta(\Psi_\infty + g)^3 - \frac{\hbar^2}{2m}\nabla^2(\Psi_\infty + g) = 0, \tag{1.80}$$

where we use the gauge $A = 0$ and take Ψ as real for simplicity. By considering a small deviation that $g \ll \Psi_\infty$, we have, to the first order in g,

$$\alpha(\Psi_\infty + g) + \beta(\Psi_\infty^3 + 3\Psi_\infty^2 g) - \frac{\hbar^2}{2m}\nabla^2 g = 0. \tag{1.81}$$

After substituting the value of Ψ_b, we get

$$\nabla^2 g = \left(\frac{2}{\xi^2}\right) g, \tag{1.82}$$

where ξ is the coherence length and given by

$$\xi = \sqrt{-\frac{\hbar^2}{2m\alpha}}. \tag{1.83}$$

The solution of Eq. (1.82) is

$$g(x) = g(0) \exp\left(\frac{-\sqrt{2}x}{\xi}\right), \tag{1.84}$$

which shows that the deviation decays in a length of order ξ.

Now we can introduce the famous dimensionless Ginzburg-Landau parameter κ, which is defined as

$$\kappa = \frac{\lambda}{\xi} = \sqrt{\frac{m^2\beta c^2}{8\pi e^2 \hbar^2}}. \tag{1.85}$$

As will be discussed later in details, $\kappa = 1/\sqrt{2}$ separates superconductor of type-I and type-II.

Nucleation field

When the magnetic field is initially very high, the superconductivity of a sample is completely broken. When we decrease the magnetic field, there is a critical field where the superconductivity begins to appear in the

interior of a bulk sample; we call this critical field as the nucleation field H_n. At nucleation field, the order parameter is extremely small and thus we only keep the first of Ψ in Eq. (5.2), which leads to the linearized GL equation

$$\alpha\Psi + \frac{1}{2m}\left(\frac{\hbar}{i}\nabla - \frac{2e}{c}\mathbf{A}\right)^2 \Psi = 0. \tag{1.86}$$

We consider a bulk sample in a field $\mathbf{H}$ along the z direction and the vector potential is taken as

$$A_y = Hx. \tag{1.87}$$

In this condition, Eq. (1.86) becomes

$$\left[-\nabla^2 + i\frac{4\pi Hx}{\Phi_0}\frac{\partial}{\partial y} + \left(\frac{2\pi H}{\Phi_0}\right)^2 x^2\right]\Psi = \frac{1}{\xi^2}\Psi. \tag{1.88}$$

We search for a solution in the form

$$\Psi = f(x)e^{i(k_y y + k_z z)} \tag{1.89}$$

because the effective potential is a function of x. Substituting Eq. (1.89) into Eq. (1.88), we get

$$-\nabla^2 f + \left(\frac{2\pi H}{\Phi_0}\right)^2 \left(x - \frac{k_y \Phi_0}{2\pi H}\right)^2 f = Ef, \tag{1.90}$$

where

$$E = \left(\frac{1}{\xi^2} - k_z^2\right). \tag{1.91}$$

We notice that k_y only shifts the the location of potential minimum which is unimportant for the present discussion. Eq. (1.90) is a Schrodinger equation for a particle in a harmonic oscillator potential, where the resulting eigenvalues are

$$E = E_n = \left(n + \frac{1}{2}\right)\hbar\left(\frac{2eH}{mc}\right) \tag{1.92}$$

with an integer n. From above two equations, we obtain

$$H = \frac{\Phi_0}{2\pi(2n+1)}\left(\frac{1}{\xi^2} - k_z^2\right). \tag{1.93}$$

Clearly the highest magnetic field is reached at $k_z = 0$ which means that there is no energy wasted at the z direction and $n = 0$ which indicates the lowest Landau level. This field is the nucleation field which has the formula

$$H_n = \frac{\Phi_0}{2\pi\xi^2}, \tag{1.94}$$

and the corresponding eigenfunction is

$$f(x) = \exp\left(-\frac{x^2}{2\xi^2}\right) = \exp\left(-\frac{\pi H_n x^2}{\Phi_0}\right). \tag{1.95}$$

Here it is interesting to write the thermodynamic critical field in Eq. (1.68) in another way as

$$H_{tc} = \frac{\Phi_0}{2\sqrt{2}\pi\xi\lambda}. \tag{1.96}$$

By comparing Eq. (1.94) and Eq. (1.96), we get a relation

$$H_n = \sqrt{2}\kappa H_{tc}. \tag{1.97}$$

1.3.2 Classification of Superconductivity

We now introduce the interface between the normal state and superconducting state, where the interface energy changes sign at $\kappa = 1/\sqrt{2}$, leading to different magnetic response. We consider an infinite one-dimensional superconductor along x axis where order parameter is only a function of x and the magnetic field is along z axis but changes only with the coordinate x. The boundary conditions are

$$\begin{aligned} x \to -\infty: &\quad \Psi = \Psi_\infty \ \ \& \ \ \mathbf{B} = \mathbf{0}, \\ x \to +\infty: &\quad \Psi = 0 \ \ \& \ \ \mathbf{B} = \mathbf{H_{tc}}. \end{aligned} \tag{1.98}$$

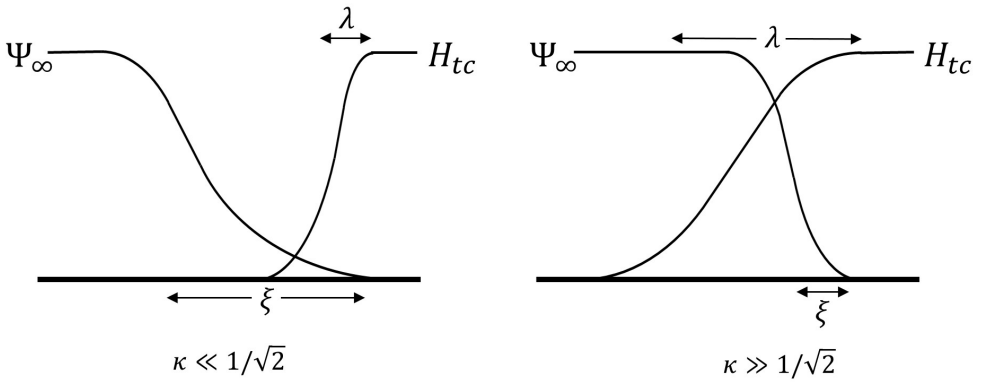

FIGURE 1.7: Schematics of variation of order parameter and magnetic at interface. The case $\kappa \ll 1/\sqrt{2}$ indicates a type-I superconductor with positive interface energy; the case $\kappa \gg 1/\sqrt{2}$ indicates a type-II superconductor with negative interface energy.

Since the external field is fixed at H_{tc}, the appropriate free energy to consider is the Gibbs free energy. We have mentioned that the Gibbs free energy of bulk superconducting state and normal state have the same value G_{s0} as given in Eq. (1.75). Here we see the excess Gibbs free energy over G_{s0}, which is written as

$$\begin{aligned} \rho &= \int_{-\infty}^{\infty} (G + \frac{H_{tc}^2}{8\pi}) dx \\ &= \int_{-\infty}^{\infty} \left[\alpha |\Psi(r)|^2 + \frac{\beta}{2} |\Psi(r)|^4 + \frac{1}{2m} \left| \left(\frac{\hbar}{i}\nabla - \frac{2e}{c}\mathbf{A} \right) \Psi(r) \right|^2 + \frac{(B - H_{tc})^2}{8\pi} \right] dx. \end{aligned} \tag{1.99}$$

If we multiply the first GL equation Eq. 5.2 by Ψ^* and integrate over all x, we get

$$\int_{-\infty}^{\infty}\left[\alpha\left|\Psi\left(r\right)\right|^2+\beta\left|\Psi(r)\right|^4+\frac{1}{2m}\left|\left(\frac{\hbar}{i}\nabla-\frac{2e}{c}\mathbf{A}\right)\Psi(r)\right|^2\right]dx=0, \tag{1.100}$$

which can simplifies the excess Gibbs free energy to

$$\rho=\frac{H_{tc}^2}{8\pi}\int_{-\infty}^{\infty}\left[\left(1-\frac{h}{H_{tc}}\right)^2-\left(\frac{\Psi}{\Psi_\infty}\right)^4\right]dx. \tag{1.101}$$

This form clearly displays a positive diamagnetic energy and a negative condensation energy, which together decides the sign of ρ. When the penetration length is much smaller than the coherence length as shown in Fig. 1.7(a), the diamagnetic effect is strong and order parameter recovers slowly, which makes the diamagnetic energy dominant, thus leading to positive interface energy. On the other hand when the penetration length is much larger than the coherence length as shown in Fig. 1.7(b), the condensation energy is dominant which gives negative interface energy. For both cases, the exact results [22] have been obtained as

$$\begin{aligned}\kappa\ll\frac{1}{\sqrt{2}}:&\quad\rho'=\frac{4\sqrt{2}\xi}{3}>0,\\ \kappa\gg\frac{1}{\sqrt{2}}:&\quad\rho'=-\frac{8(\sqrt{2}-1)\lambda}{3}<0,\end{aligned} \tag{1.102}$$

where ρ' is the value of integration in Eq. (1.101). The crossover point of zero interface energy is found at

$$\kappa=\frac{1}{\sqrt{2}} \tag{1.103}$$

by Ginzburg and Landau with numerical integration. We also have $H_n = H_{tc}$ at this crossover point according to Eq. (1.97). In Abrikosov's path-breaking paper in 1957, he anticipated a distinct behaviors of superconductors with negative interface energy under magnetic fields: magnetic flux penetrating through the sample is subdivided until each flux becomes a flux quantum Φ_0, which is carried by a vortex where supercurrent rotates around a normal core. Since then, superconductors with $\kappa < 1/\sqrt{2}$ and $\kappa > 1/\sqrt{2}$ are categorized as type-I and type-II superconductors. Type-I superconductivity is usually exhibited by pure metals such as aluminium, indium and mercury. There are many type-II superconductors including cuprate superconductors, MgB_2 and iron-based superconductors.

1.3.3 Vortex Matter in Type-II Superconductors

In the previous introduction, we have shown that phase coherence allows 2π phase winding and trapped flux quantum Φ_0. Abrikosov pointed out that a vortex with 2π phase winding around a normal core can penetrate into a superconductor in type-II superconductors due to the negative interface energy. Here we introduce the structure of this vortex in the GL frame.

From the second GL equation Eq. (1.72), we get the phase gradient as

$$\nabla\varphi=\frac{2e}{\hbar c}\mathbf{A}+\frac{m\mathbf{J_s}}{2e\hbar|\Psi|^2}. \tag{1.104}$$

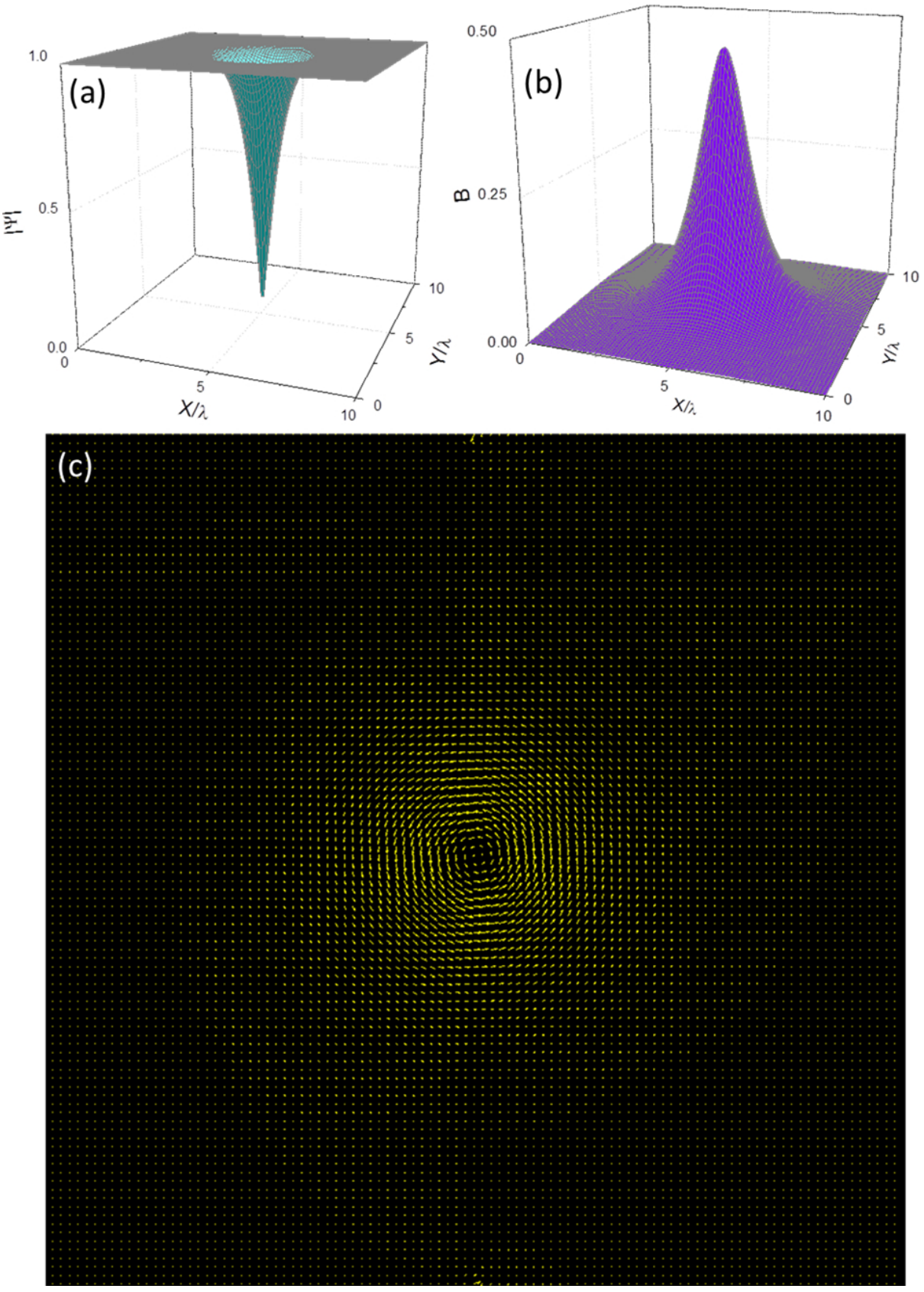

FIGURE 1.8: (a) Distribution of order parameter in a vortex. (b) Distribution of magnetic field in a vortex (c) Supercurrent flowing around the normal core.

By integrating the phase gradient along a closed path "c", the single-valued order parameter requires

$$\oint_c \left(\frac{2e}{\hbar c}\mathbf{A} + \frac{m\mathbf{J_s}}{2e\hbar|\Psi|^2} \right) dl = N2\pi, \tag{1.105}$$

which further leads to

$$\oint_c \left(\mathbf{A} + \frac{cm\mathbf{J_s}}{4e^2|\Psi|^2} \right) dl = N\Phi_0, \tag{1.106}$$

which defines a vortex for $N = 1$.

To illustrate the structure of a vortex, I display Fig. 1.8 which is a numerical result of one vortex in a sample with size $(10\lambda \times 10\lambda)$. At the core of the vortex, the magnetic field is largest and the order parameter is suppressed to zero. Outside the normal core, the magnetic field and supercurrents decay at the length scale of λ and order parameter increases at the length scale of ξ. Far from the core we can find a closed path where magnetic field and supercurrents are zero everywhere, and thus the flux inside is Φ_0.

There is an interface connecting the normal core and the bulk superconducing state far away. In type-II superconductors, this interface energy is negative which makes the entry of vortices energetically favored. In stead of joining together, vortices separated from each other to achieve maximum area of interface in total, which leads to the formation of triangle vortex lattices.

1.3.4 Time-Dependent Ginzburg-Landau Approach

In order to give a better understanding and description of the dynamics of various superconducting transitions, Gorkov and Eliashberg derived the time-dependent Ginzburg-Landau (TDGL) equations as [23, 24]

$$\frac{\hbar^2}{2m^*D}\left(\partial_t + i\frac{e^*}{\hbar}\Phi_E \right)\Psi = -\frac{\delta f}{\delta \Psi^*}, \tag{1.107}$$

$$\frac{\sigma}{c}\left(\frac{1}{c}\partial_t \mathbf{A} + \nabla\Phi_E \right) = -\frac{\delta f}{\delta \mathbf{A}}, \tag{1.108}$$

where f is the GL free energy. The constant D is the phenomenogical diffusion coefficient, σ the electrical conductivity and Φ_E the electric scalar potental. The gauge invariant quantities are the magnetic field, $\mathbf{B} = \nabla \times \mathbf{A}$; current density, $\mathbf{J} = \sigma\mathbf{E} + \mathbf{J_s}$; density of Cooper pairs, $n_s = |\Psi|^2$ and the electric field, $\mathbf{E} = -(1/c)\partial\mathbf{A}/\partial t - \nabla\Phi_E$. In a dimensionless form [24], TDGL equations are simplified to

$$\left(\frac{\partial}{\partial t} + i\kappa\Phi_E \right)\Psi = -\frac{\delta f}{\delta \Psi^*}, \tag{1.109}$$

$$\sigma\left(\frac{\partial \mathbf{A}}{\partial t} + \nabla\Phi_E \right) = -\frac{1}{2}\frac{\delta f}{\delta \mathbf{A}} \tag{1.110}$$

with the GL free energy

$$f = -|\Psi|^2 + \frac{1}{2}|\Psi|^4 + \left| \left(\frac{1}{i\kappa}\nabla - \mathbf{A} \right)\Psi \right|^2 + (\nabla \times \mathbf{A})^2. \tag{1.111}$$

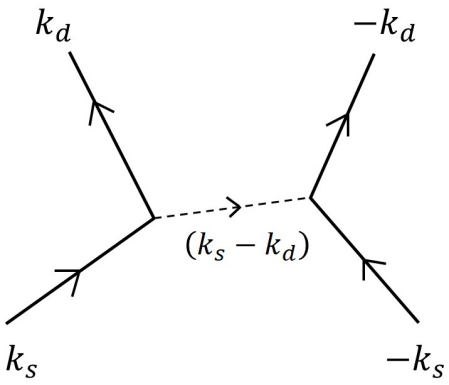

FIGURE 1.9: Schematic of phonon-electron interaction which transfer a Cooper pair in s-band to d-band.

TDGL equations are gauge invariant under the following transformation:

$$\Psi' = \Psi e^{i\kappa\chi},\ \mathbf{A}' = \mathbf{A} + \nabla\chi,\ \Phi' = \Phi - \frac{\partial\chi}{\partial t}. \tag{1.112}$$

To give a better understanding of TDGL equations, we choose the gauge Φ_E=0. The first TDGL equation Eq. (1.109) becomes

$$\frac{\partial\Psi}{\partial t} = -\frac{\delta f}{\delta\Psi^*} \tag{1.113}$$

This is just the Langevin equation without random forces. The minus sign at the right side guarantees the evolution direction to the energy minimum. As we have

$$\frac{\partial\mathbf{A}}{\partial t} = -\mathbf{E},\ -\frac{1}{2}\frac{\delta f}{\delta\mathbf{A}} = J_s - \nabla\times\nabla\times\mathbf{A} \tag{1.114}$$

Eq. (1.110) is rewritten as

$$\nabla\times\nabla\times\mathbf{A} = \mathbf{J_s} + \sigma\mathbf{E} \tag{1.115}$$

which is the Ampere's Law. In this sense, TDGL equations describe the dynamics of cooper pairs in an electromagnetic field. Since the TDGL equations are nonlinear differential equations of complex variables, it is difficult to solve them analytically. Within this thesis, I use the numerical method provided by Gropp et al. [24] to study various superconducting systems.

1.4 Time-Reversal-Symmetry-Broken (TRSB) State in Multi-Component Superconductors

1.4.1 Multi-Component Superconductivity

The original BCS theory was a simplified model considering a single isotropic superconducting gap, which has lots of room for refinement. Two years after its establishment, Suhl, Matthias and Walker studied the two-band extention [25], with the motivation to explain the superconductivity in transition metals. In BCS theory, a pair of electrons ($k\uparrow, -k\downarrow$) is excited to the state ($k'\uparrow, -k'\downarrow$) through a virtual process of emission and reabsorption

of a phonon. As an extention in two-band superconductivity, this electron-phonon interaction may take place between two bands if an interband scattering process is available. Therefore an extra term describing interband coupling should be included in the hamiltonian as

$$\begin{aligned} H = &\sum_{k\sigma} \xi_{ks} c^{\dagger}_{k\sigma} c_{k\sigma} + \sum_{k\sigma} \xi_{kd} d^{\dagger}_{k\sigma} d_{k\sigma} - \sum_{kk'} V_{ss} c^{\dagger}_{k\uparrow} c^{\dagger}_{-k\downarrow} c_{-k'\downarrow} c_{k'\uparrow} - \sum_{kk'} V_{dd} d^{\dagger}_{k\uparrow} d^{\dagger}_{-k\downarrow} d_{-k'\downarrow} d_{k'\uparrow} \\ &- \sum_{kk'} V_{sd} \left(c^{\dagger}_{k\uparrow} c^{\dagger}_{-k\downarrow} d_{-k'\downarrow} d_{k'\uparrow} + d^{\dagger}_{k\uparrow} d^{\dagger}_{-k\downarrow} c_{-k'\downarrow} c_{k'\uparrow} \right) \end{aligned} \tag{1.116}$$

where ξ_{ks}, ξ_{kd} are kinetic energy of single particles in $s-$ and $d-$band. $c^{\dagger}$, c and $d^{\dagger}$, d are the corresponding creation and annihilation operators. V_{ss}, V_{dd} and V_{sd} are the averaged electron-phonon interaction energy from $s-s$, $d-d$ and $s-d$ process which is shown in Fig. (1.9). They found only one critical temperature in presence of interband coupling, no matter how small it is. Another consequence of interband coupling is that the interband coupling itself can induce superconductivity even when $V_{ss} = 0$ and $V_{dd} = 0$. Then J. Kondo developed this theory by pointing out that superconducting transition temperature is always raised over that of a single band when the interband coupling V_{sd} is introduced [26]. It means that even a repulsive coupling can lower the energy of system, after introducing a minus sign between two gap functions.

After Kondo's study, this topic slept for almost 40 years until the discovery of MgB_2 [27] in 2001. MgB_2 has two superconducting gaps of the π and σ bands of electrons, which are 7.1meV and 2.2meV respectively [28]. And the two gaps are weakly coupled. Concerning the two gap structure of MgB2, the studies of multi-component superconductivity were still limited to two-component superconductivity. Then in 2008, multi-band iron-based superconductivity was discovered [29]. In principle, iron pnictides may have at most five gaps because of five Fermi sheets mainly originating from five-fold degenerated Fe $3d$ orbitals [30, 31]. In support, some angle resolved photoemission spectroscopy (ARPES) experiments observed as many as four different gaps [32, 33]. Some tight-binding calculations show that one electron and two hole-like bands are most strongly coupled in the pair scattering channel [34, 35]. All these make the study of multi-component superconductivity with interband couplings quite urgent. In this thesis, I mainly focus on the superconductors with three or more components with broken time-reversal symmetry.

1.4.2 Time-Reversal Symmetry

Before starting the introduction of TRSB state, let me first explain the time-reversal symmetry (TRS). Actually this term *time reversal* is a misnomer, which reminds us of science fiction. The time-reversal process is what happens when seeing a movie backwards. After the time-reversal operation, the time still flow forward but the motion reversed following the original trajectory as shown in Fig. 1.10.

In the original motion, we set the acceleration at time t_0 as $a(t_0)$. After reversal of motion, the acceleration $a_R(t_0)$ is given by

$$a_R(t_0) = \frac{v_R(t_0 + dt) - v_R(t_0)}{dt} = \frac{-v(t_0 - dt) + v(t_0)}{dt} = a(t_0), \tag{1.117}$$

which shows that the acceleration does not change under time-reversal operation.

Now we discuss whether the reversed motion is real or not, in other words, whether it obeys the physical law. We first consider a falling ball in the gravitational field with an accelerated speed g. Its reversed motion is

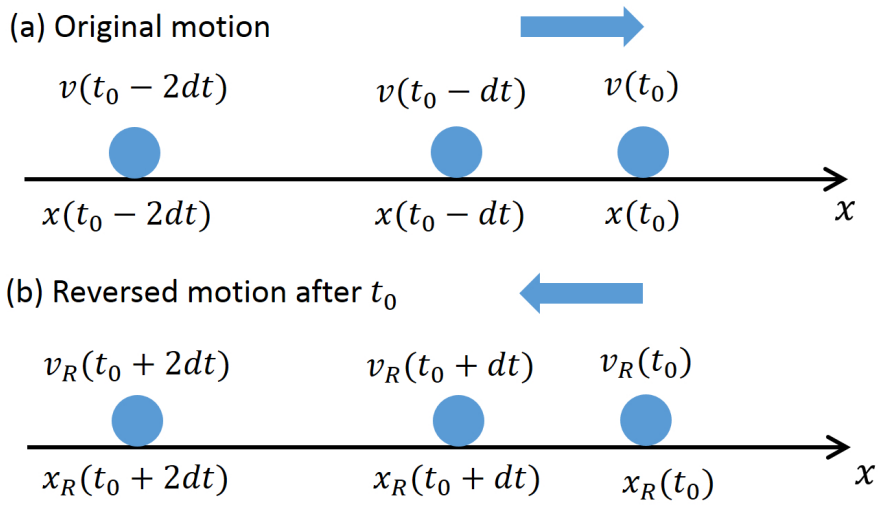

FIGURE 1.10: Schematics of reversed motion after the time-reversal operation at time t_0. Speed at every site reverses relative to the original motion. x and v refer to the coordinate and speed of the original motion, and x_R and v_R refer to coordinate and speed of the reversed motion. Time-reversal requires $x_R(t_0) = x(t_0)$, $x_R(t_0 + dt) = x(t_0 - dt)$, $x_R(t_0 + 2dt) = x(to - 2dt)$, $v_R(t_0) = -v_(t_0)$, $v_R(t_0 + dt) = -v(t_0 - dt)$, $v_R(t_0 + 2dt) = -v(t_0 - 2dt)$.

the ball going up with the speed decreasing at acceleration g, which follows the Newton's law and thus a real movement. In this case, we say the dynamics of the ball here has the time-reversal symmetry.

The situation differs when we consider a moving electron under a magnetic field $\mathbf{B}$, where the electron feels the Lorentz force $F = e\mathbf{v}\times\mathbf{B}$ which depends on the speed $\mathbf{v}$, as shown in Fig. 1.11. The reversal of motion changes the direction of Lorentz force and further leads to reversal of acceleration, contradictory to Eq. (1.117). The electron can not follow the original trajectory back due to the Lorentz force. This means that the motion of the electron after time-reversal operation is not real, in other words, conflicting with the physical law. In this case, we say that the electron's dynamics here has no time-reversal symmetry.

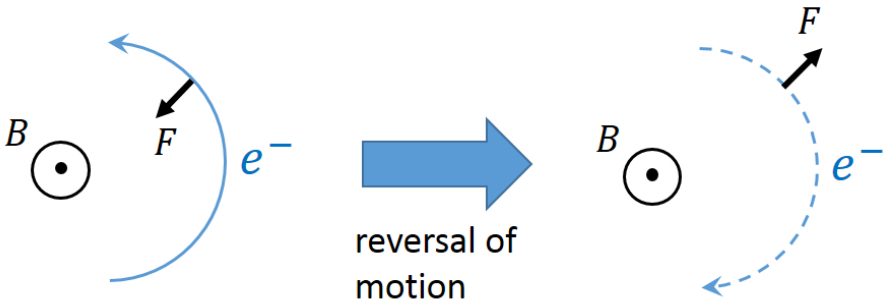

FIGURE 1.11: Unphysical motion of electron after the time-reversal operation. B is the magnetic field and F is the Lorentz force. The dashed line refers to the motion of electron under time-reversal operation, where the newton's law seems failed.

Now we introduce the time-reversal symmetry in quantum mechanics. We use Θ as the time-reversal operator, and we should have

$$\Theta\mathbf{x}\Theta^{-1} = \mathbf{x}, \quad \Theta\mathbf{p}\Theta^{-1} = -\mathbf{p} \tag{1.118}$$

where $\mathbf{x}$ and $\mathbf{p}$ is the position and momentum operator. We consider

$$|\alpha\rangle \to \Theta|\alpha\rangle, \tag{1.119}$$

as a time reversal operation and $\Theta|\alpha\rangle$ is the time-reversed state, or motion-reversed state. We now derive the basis properties of Θ by studying the time evolution of the time-reversed state. We consider a system at a quantum state α at $t = 0$. At a slightly later time $t = dt$, the state becomes

$$|\alpha; t = dt\rangle = \left(1 - \frac{iH}{\hbar}dt\right)|\alpha\rangle, \tag{1.120}$$

where H is the Hamiltonian of the system. Now we first apply Θ on the state at $t = 0$, and let the system evolve under the dynamics of H. The state at $t = dt$ is

$$\left(1 - \frac{iH}{\hbar}dt\right)\Theta|\alpha\rangle. \tag{1.121}$$

If the motion reserves the time-reversal symmetry, the above state should be the same as

$$\Theta|\alpha; t = -dt\rangle = \Theta\left(1 + \frac{iH}{\hbar}dt\right)|\alpha\rangle, \tag{1.122}$$

and thus we obtain

$$\left(1 - \frac{iH}{\hbar}dt\right)\Theta|\alpha\rangle = \Theta\left(1 + \frac{iH}{\hbar}dt\right)|\alpha\rangle, \tag{1.123}$$

which is reduced to

$$-iH\Theta|\alpha\rangle = \Theta iH|\alpha\rangle. \tag{1.124}$$

If Θ is a unitary operator, we have

$$-H\Theta = \Theta H, \tag{1.125}$$

which makes

$$H\Theta|n\rangle = -\Theta H|n\rangle = -E_n\Theta|n\rangle, \tag{1.126}$$

where $|n\rangle$ is an eigenstate with energy eigenvalue E_n. Eq. (1.125) also implies

$$\Theta^{-1}\frac{\mathbf{p}^2}{2m}\Theta = -\frac{\mathbf{p}^2}{2m} \tag{1.127}$$

Both Eq. (1.126) and (1.127) indicate that Θ makes the energy of state negative, which is nonsensical because no state has energy lower than a particle at rest.

The above arguments suggest that Θ should be antiunitary, and thus Eq. (1.124) leads to

$$\Theta H = H\Theta. \tag{1.128}$$

With this equation, the problems in Eq. (1.126) and (1.127) do not exist and we obtain physically sensible results. For simplicity, we use

$$\Theta = K \tag{1.129}$$

where K means taking the complex conjugate. Eq. (1.128) is the condition of time-reversal symmetry.

1.4.3 TRSB States in Three-Component Superconductors

Superconductivity in each condensate is described by a complex superconducting order parameter $\psi_j = |\psi_j| e^{i\varphi_j}$. The phase differences between order parameters are decided by the intercomponent couplings. In two-component superconductors, an attractive coupling leads to two parallel order parameters while a repulsive coupling gives opposite signs of two order parameters. The situation differs when there are three components, where a frustrated state can emerge as a compromise of three repulsive interband couplings. In this case, interband phase differences are neither 0 nor π, leading to time-reversal symmetry (TRS) breaking [36]. The TRSB state can be realized in a multi-band superconductor even with all the gap functions of s-wave symmetry, which distinguishes it from magnetic superconductors and chiral p-wave superconductors. Due to the discovery of iron-pnictide superconductors where several orbitals of Fe contribute to multi superconducting condensates, this possibility becomes realistic and attracts wide attentions [37–49]. Stanev and Tesanovic had a thorough discussion of possibility of TRSB states with BCS theory in the context of iron-based superconductors [37]. A detailed discussion on thermodynamic stability with GL theory was established by Hu and Wang, which provides a phase diagram of the TRSB sate [41].

Here we adopt the GL theory of three-component superconductors to introduce the TRSB state [38, 41, 50]. The GL free energy functional takes the following form

$$F = \sum_{j=1,2,3} \left[\alpha_j \left|\psi_j\right|^2 + \frac{\beta_j}{2} \left|\psi_j\right|^4 + \frac{1}{2m_j} \left| \left(-i\hbar\nabla - \frac{2e}{c}\mathbf{A} \right) \psi_j \right|^2 \right] - \sum_{j<k} \gamma_{jk} \left(\psi_j^* \psi_k + c.c. \right) + \frac{1}{8\pi} \left(\nabla \times \mathbf{A} \right)^2 , \quad (1.130)$$

where α_j is a temperature-dependent coefficient which is negative when $T < T_{cj}$ and positive when $T > T_{cj}$, with T_{cj} the critical point of the superconducting component-j before considering inter-band couplings, and γ_{jk} is an Josephson-like inter-component coupling taken as constant for simplicity. Other parameters are all conventionally defined. The GL equations in absence of magnetic fields are given by

$$\alpha_1\psi_1 + \beta_1 |\psi_1|^2 \psi_1 - \gamma_{12}\psi_2 - \gamma_{13}\psi_3 = 0, \quad (1.131)$$

$$\alpha_2\psi_2 + \beta_2 |\psi_2|^2 \psi_2 - \gamma_{12}\psi_1 - \gamma_{23}\psi_3 = 0, \quad (1.132)$$

$$\alpha_3\psi_3 + \beta_3 |\psi_3|^2 \psi_3 - \gamma_{13}\psi_1 - \gamma_{23}\psi_2 = 0, \quad (1.133)$$

which gives order parameters at the the equilibrium state. The status of time-reversal symmetry is decided by the phase differences of order parameters. When the phase differences are either 0 or π, all order parameters can become real after dropping a common phase, which makes the gap functions real since each GL order parameter has the same phase with the corresponding gap function. A gap function as a real number reserves the time-reversal symmetry of the Hamiltonian according to Eq. (1.128). We call this state as the time-reversal-symmetry-reserved (TRSR) state. On the other hand, when phase differences of order parameter are neither 0 or π, some of the order parameters have to be a complex number which breaks the time-reversal symmetry. We call this superconductoring state as the TRSB state. In the following, we discuss the situation of interband couplings which induces the TRSR state or the TRSB state.

Time-reversal symmetry reserved state

(1) When three inter-band couplings are all attractive ($\gamma_{jk} > 0$) (expressed as $(+,+,+)$), three order parameters have the same phase in the equilibrium state, as shown in Fig. 1.12(a)

(2) When two couplings are repulsive while the other coupling is attractive $(+,-,-)$, two order parameters have the same phase while the other one has a π phase difference from them, as shown in Fig. 1.12(b)

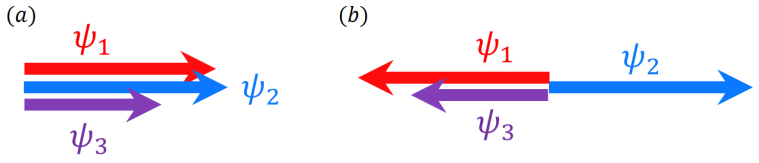

FIGURE 1.12: TRSR state with (a) three attractive couplings $(+,+,+)$, or (b) two repulsive couplings and one attractive coupling $(+,-,-)$.

Superconducting states in both cases reserve the TRS because the intercomponent phase differences are either 0 or π. We also find that the inter-component phase differences enjoy the most favorable value in compliance with the corresponding inter-component coupling. In other words, we have $\Delta\varphi_{jk} = 0$ when $\gamma_{jk} > 0$ and $\Delta\varphi_{jk} = \pi$ when $\gamma_{jk} < 0$. However we will see below that for $(+,+,-)$ and $(-,-,-)$ it is impossible to put all the inter-component phase differences at the most favorable value, which introduces frustrated intercomponent phase difference.

TRSB state

First let us discuss the cases $(+,+,-)$ and $(-,-,-)$ with intercompnent couplings distinct from each other. For $(+,+,-)$ case where the attractive couplings are much stronger than the repulsive coupling and the amplitude of three order parameters are comparable, three parallel order parameters still have the same phase. And for $(-,-,-)$ case where two repulsive couplings are much stronger than the attractive one, we still have the equilibrium state as shown in Fig. 1.12(b). However, when three components and inter-band couplings are comparable, it is possible to obtain a case that inter-component phase differences are neither 0 nor π, as shown by Fig. 1.13. In three-component superconductors, we have two degenerate TRSB states with opposite chiralities. The phase diagram of the TRSB state can be found in [41].

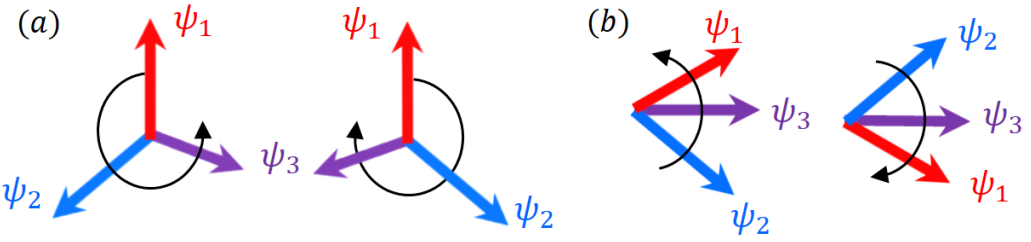

FIGURE 1.13: Two degenerate TRSB states with opposite chiralities for (a) three repulsive couplings $(-,-,-)$ and (b) one repulsive and two attractive couplings $(+,+,-)$.

A hopeful candidate to carry this TRSB state is the iron-based superconductor with at most five gaps originating from the five Fe 3d orbitals [51]. In $Ba_{0.6}K_{0.4}Fe_2As_2$, angle resolved photoemission spectroscopy (ARPES) measurements observed four different gaps at two electron-like and two hole-like Fermi pockets [33]. Sign reversals between Cooper pairing of electron pockets and hole pockets caused by spin fluctuations were discussed [52, 53]. A sign reversal between two strong hole pockets has also been suggested in KFe_2As_2 [43, 54, 55].

It has been suggested that spontaneous broken TRS is accompanied by novel phenomena such as fractional vortices [56, 57], modified phase slip [58], spontaneous supercurrent and self-induced flux[59, 60], massless

Leggett mode [42, 61], mixed phase density mode [62] and vortex clusters [47]. In this thesis, I will mainly explore the novel phenomena in the TRSB state, which helps to identify the TRSB state in possible materials.

Chapter 2

Josephson Effects in Three-Band Superconductors with Broken Time-Reversal Symmetry

The Josephson effect is a remarkable macroscopic tunneling phenomenon associated with broken gauge symmetry in a superconducting state [5]. When phase difference $\Delta\varphi$ exists between two superconductors connected by a weak link, dc supercurrent flows through the junction with zero voltage bias. The detailed form of current phase relation (CPR) depends on the materials and geometries of the weak links, while the ac Josephson relation is given by $\partial_t(\Delta\varphi) = 2eV/\hbar$.

Because the Josephson effect is due to interference between wave functions of two superconductors that are weakly linked, it carries the information of gap structures. Therefore, it is widely used as a tool to detect the pairing symmetry in an unconventional superconductor. For example, the half-flux quanta observed in the tricrystal junction in high-temperature cuprate superconductor serves as the best evidence for the d-wave pairing symmetry [59].

In this chapter, I will first introduce the Andreev reflection as the mechanism of Cooper-pair tunneling in superconductor-normal metal-superconductor (SNS) Josepshon junction. Then I will study a SNS junction connecting a single-band superconductor and a three-band TRSB superconductor. Phenomena such as asymmetric critical currents, subharmonic Shapiro steps, and symmetric Fraunhhofer patterns are revealed theoretically. Existing experimental results consistent with our proposal are discussed in terms of the present work.

2.1 Andreev Reflection

Andreev reflection is a type of particle scattering that occurs at the interface between a superconductor and a normal metal, which was first discovered by Alexander F. Andreev [63]. When an electron in the normal metal penetrates into the superconductor at energy lower than the superconducting gap, the incident electron forms a Cooper-pair with reflection of a hole of opposite spin and velocity, as shown in Fig. 2.1. The Andreev reflection

is originated from the absence of excited states within the superconducting gap, which forces the pairing of the incident electron by pulling another electron from the normal metal (i.e. reflection of a hole).

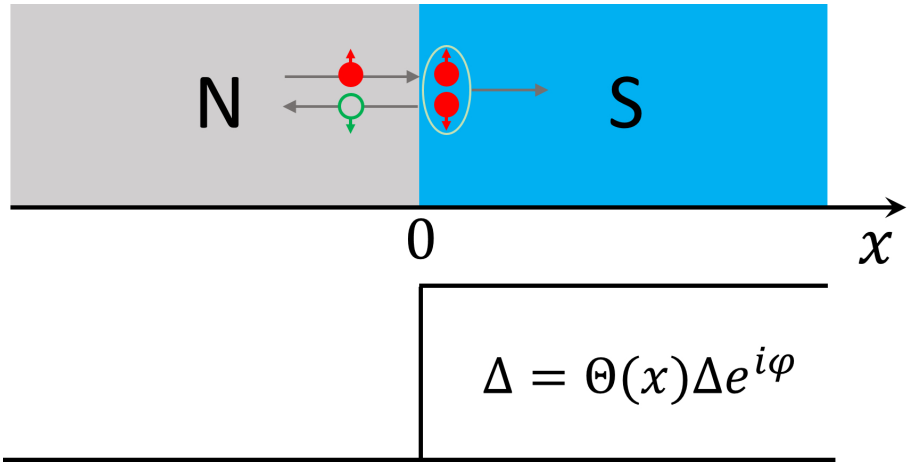

FIGURE 2.1: Schematics of a N-S junction showing the process of Andreev reflection. $\Theta(x)$ is the step function.

Let us now consider this phenomenon quantitatively with the Blonder-Tinkham-Klapwijk (BTK) model [64]. We consider an electron moving along x axis and the junction is located at $x = 0$ as shown in Fig. 2.1. We study the system with the one-dimensional BdG equation

$$\begin{pmatrix} -\hbar^2\partial_x^2/2m - E_F & \Delta\Theta(x) \\ \Delta^*\Theta(x) & \hbar^2\partial_x^2/2m + E_F \end{pmatrix}\psi = E\psi, \tag{2.1}$$

where $E_F = \hbar^2 k_F^2/2m$ and $\psi = (u_\uparrow(x), v_\downarrow(x))^T$ is the wavefunction in the Nambu spinor notation where u and v are the particle and hole part. We first obtain the wavefunction in the normal metal ($x < 0$) and the superconductor ($x > 0$) separately and then connect them with boundary conditions.

Solutions in normal metal

In the normal metal, the BdG equation is reduced to

$$\begin{pmatrix} -\hbar^2\partial_x^2/2m - E_F & 0 \\ 0 & \hbar^2\partial_x^2/2m + E_F \end{pmatrix}\begin{pmatrix} u(x) \\ v(x) \end{pmatrix} = E\begin{pmatrix} u(x) \\ v(x) \end{pmatrix}, \tag{2.2}$$

which exhibits two energy spectra: $\varepsilon = \hbar^2 k^2/2m - E_F$ for particles and $\varepsilon = -\hbar^2 k^2/2m + E_F$ for holes, as shown in Fig. 2.2. The group velocities of an electron and hole are give by

$$v_{Ne} = \frac{1}{\hbar}\frac{d\varepsilon}{dk_e} = \frac{\hbar k_e}{m}, \quad v_{Nh} = \frac{1}{\hbar}\frac{d\varepsilon}{dk_h} = -\frac{\hbar k_h}{m}. \tag{2.3}$$

For eigenenergy E, there are four solutions of eigenfunction including two particle solutions which refer to

$$(1)\ \textit{right moving electrons}:\ k = k_e,\ \psi_+^e = \begin{pmatrix} 1 \\ 0 \end{pmatrix} e^{ik_e x}, \tag{2.4}$$

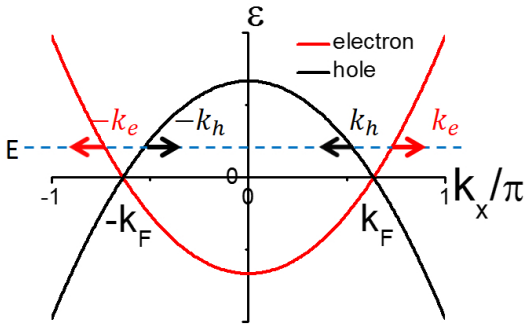

FIGURE 2.2: Energy spectra in normal metal with four solutions of BdG equations at energy level E. Red and black arrows refer to the directions of group velocity of electrons and holes.

$$(2)\ left\ moving\ electrons:\ k=-k_e,\ \psi_-^e=\begin{pmatrix}1\\0\end{pmatrix}e^{-ik_e x}, \tag{2.5}$$

where $k_e = k_F\sqrt{1+E/E_F}$, and two hole solutions which refer to

$$(1)\ left\ moving\ holes:\ k=k_h,\ \psi_+^h=\begin{pmatrix}0\\1\end{pmatrix}e^{ik_h x}, \tag{2.6}$$

$$(2)\ right\ moving\ holes:\ k=-k_h,\ \psi_-^h=\begin{pmatrix}0\\1\end{pmatrix}e^{-ik_h x}, \tag{2.7}$$

where $k_h = k_F\sqrt{1-E/E_F}$.

Solutions in superconductor

In the superconductor, the BdG equation is reduced to

$$\begin{pmatrix}-\hbar^2\partial_x^2/2m-E_F & \Delta e^{i\varphi}\\ \Delta e^{-i\varphi} & \hbar^2\partial_x^2/2m+E_F\end{pmatrix}\begin{pmatrix}u(x)\\v(x)\end{pmatrix}=E\begin{pmatrix}u(x)\\v(x)\end{pmatrix}, \tag{2.8}$$

which exhibits two energy spectra: $\varepsilon = \pm\sqrt{(\hbar^2k'^2/2m-E_F)^2+\Delta^2}$, as shown in Fig. 2.3. The group velocities of an electron-like particle and an hole-like particle are given by

$$v_{Se}=\frac{1}{\hbar}\frac{dE}{dk'_e}=\frac{\sqrt{E^2-\Delta^2}}{E}\frac{\hbar k'_e}{m},\quad v_{Sh}=\frac{1}{\hbar}\frac{dE}{dk'_h}=-\frac{\sqrt{E^2-\Delta^2}}{E}\frac{\hbar k'_h}{m}. \tag{2.9}$$

For eigenenergy $E > \Delta$, there are four solutions of eigenfunction including two particle-like solutions which refer to

$$(1)\ right\ moving\ electron-like\ quasiparticle:\ k=k'_e,\ \psi_+^e=\begin{pmatrix}u_0e^{i\varphi}\\v_0\end{pmatrix}e^{ik'_e x}, \tag{2.10}$$

$$(2)\ left\ moving\ electron-like\ quasiparticle:\ k=-k'_e,\ \psi_-^e=\begin{pmatrix}u_0e^{i\varphi}\\v_0\end{pmatrix}e^{-ik'_e x}, \tag{2.11}$$

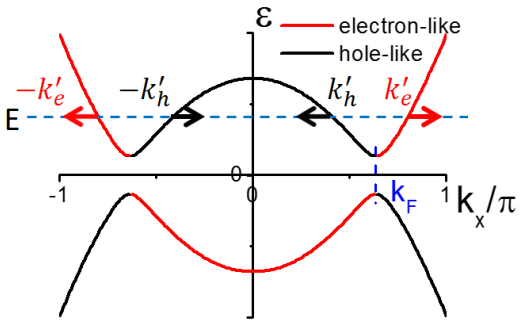

FIGURE 2.3: Energy spectra in superconductor with four solutions of BdG equations at energy level E. Red and black arrows refer to the directions of group velocity of electron-like and hole-like particles.

where

$$k_e = k_F \sqrt{1 + \sqrt{\frac{E^2 - \Delta^2}{E_F^2}}}, \tag{2.12}$$

and two hole-like solutions which refer to

$$(1)\ left\ moving\ hole-like\ quasiparticle:\ k = k'_h,\ \psi_+^h = \begin{pmatrix} v_0 e^{i\varphi} \\ u_0 \end{pmatrix} e^{ik'_h x}, \tag{2.13}$$

$$(2)\ right\ moving\ hole-like\ quasiparticle:\ k = -k'_h,\ \psi_-^h = \begin{pmatrix} v_0 e^{i\varphi} \\ u_0 \end{pmatrix} e^{-ik'_h x}, \tag{2.14}$$

where

$$k_h = k_F \sqrt{1 - \sqrt{\frac{E^2 - \Delta^2}{E_F^2}}}. \tag{2.15}$$

Here the quantities u_0 and v_0 are

$$u_0 = \sqrt{\frac{1}{2}\left(1 + \sqrt{1 - \left(\frac{\Delta}{E}\right)^2}\right)}, \quad v_0 = \sqrt{\frac{1}{2}\left(1 - \sqrt{1 - \left(\frac{\Delta}{E}\right)^2}\right)}. \tag{2.16}$$

In a superconductor, the excited quasiparticle is neither an electrons nor a hole but a combination of both. We call the quasiparticle electron-like when $|k| > k_F$ because the electron has a larger contribution in the wavefunction ($|u_0| > |v_0|$). Similarly we have the hole-like quasiparticles when $|k| < k_F$ because the hole has a larger contribution in the wavefunction ($|u_0| < |v_0|$). For $E \gg \Delta$, one can find $u_0 \to 1$ and $v_0 \to 0$ because quasiparticle cannot feel the gap which makes the exciton an electron again.

Superconductor-normal metal junction

Now we consider a junction connecting the normal metal and the superconductor. At energy level E, there are eight possible excitations as shown in Fig. (2.4)(a). The BdG equations are given by

$$\begin{pmatrix} -\hbar^2\partial_x^2/2m - E_F + V\delta(x) & \Delta e^{i\varphi}\Theta(x) \\ \Delta e^{-i\varphi}\Theta(x) & \hbar^2\partial_x^2/2m + E_F - V\delta(x) \end{pmatrix} \begin{pmatrix} u(x) \\ v(x) \end{pmatrix} = E \begin{pmatrix} u(x) \\ v(x) \end{pmatrix}. \tag{2.17}$$

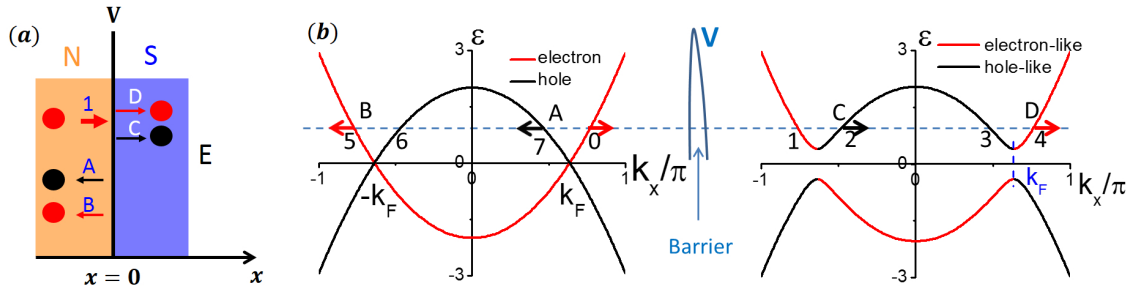

FIGURE 2.4: (a) Schematics of junction with potential barrier V connecting normal metal and superconductor. An electron is injected from the normal metal to the superconductor, has the possibilities of reflected as an hole, reflected as an electron, tunneling as a hole-like particle and tunneling as an electron-like particle with probability currents A, B, C and D. (b) Energy spectra of junction where $0 \sim 7$ are eight excited states at energy level E. Red and black arrows refer to directions of probability currents of quasiparticles.

Here we consider a case that $\Delta \ll E_f$, where we can approximately take the momentum of excited states as k_F. The group velocities of For the case of an injected electron from normal metal, the wavefunction at the side of the normal metal is

$$\psi_N = \begin{pmatrix} 1 \\ 0 \end{pmatrix} e^{ik_F x} + b \begin{pmatrix} 1 \\ 0 \end{pmatrix} e^{-ik_F x} + a \begin{pmatrix} 0 \\ 1 \end{pmatrix} e^{ik_F x}, \tag{2.18}$$

and the superconductor is

$$\psi_S = d \begin{pmatrix} u_0 e^{i\varphi} \\ v_0 \end{pmatrix} e^{ik_F x} + c \begin{pmatrix} v_0 e^{i\varphi} \\ u_0 \end{pmatrix} e^{-ik_F x}. \tag{2.19}$$

By adopting the boundary conditions

$$\psi_s(0) = \psi_N(0) = \psi(0), \quad \frac{\hbar^2}{2m}[\psi_s'(0) - \psi_N'(0)] = V\psi(0), \tag{2.20}$$

where the superscript ' means the gradient with respect to x, we obtain

$$a = \frac{u_0 v_0}{\gamma} e^{-i\varphi}, \quad b = -\frac{(u_0^2 - v_0^2)(Z^2 + iZ)}{\gamma}, \quad , c = \frac{iv_0 Z}{\gamma} e^{-i\varphi}, \quad d = \frac{u_0(1 - iZ)}{\gamma} e^{-i\varphi}, \tag{2.21}$$

where

$$Z = \frac{mV}{\hbar^2 k_F}, \quad \gamma = u_0^2 + (u_0^2 - v_0^2)Z^2. \tag{2.22}$$

Here $|a|^2$, $|b|^2$ $|c|^2$ and $|d|^2$ are the probabilities of the appearance of corresponding quasiparticles. From Eq. (2.3), we have the group velocity of particles and holes as

$$v_{Ne} = v_{NF}, \quad v_{Nh} = -v_{NF}, \tag{2.23}$$

where $v_{NF} = \hbar k_F / m$. From Eq. (2.9), we have the group velocities of electron-like particles and hole-like particles as

$$v_{Se} = \frac{\sqrt{E^2 - \Delta^2}}{E} v_{NF} = (u_0^2 - v_0^2) v_{NF}, \quad v_{Sh} = -\frac{\sqrt{E^2 - \Delta^2}}{E} v_{NF} = -(u_0^2 - v_0^2) v_{NF}. \tag{2.24}$$

We finally obtain the probability currents as

$$A = \left| \frac{|a|^2 v_{Nh}}{v_{NF}} \right| = \frac{u_0^2 v_0^2}{\gamma^2}, \tag{2.25}$$

$$B = \left| \frac{|b|^2 v_{Ne}}{v_{NF}} \right| = \frac{(u_0^2 - v_0^2) Z^2 (Z^2 + 1)}{\gamma^2}, \tag{2.26}$$

$$C = \left| \frac{|c|^2 v_{Sh}}{v_{NF}} \right| = \frac{v_0^2 (u_0^2 - v_0^2) Z^2}{\gamma^2}, \tag{2.27}$$

$$D = \left| \frac{|d|^2 v_{Se}}{v_{NF}} \right| = \frac{u_0^2 (u_0^2 - v_0^2)(1 + Z^2)}{\gamma^2}, \tag{2.28}$$

where the velocities are normalized with the velocity of the injected electron v_{NF}. One can easily verify that

$$A + B + C + D = 1, \tag{2.29}$$

which is required by the conservation of particle number.

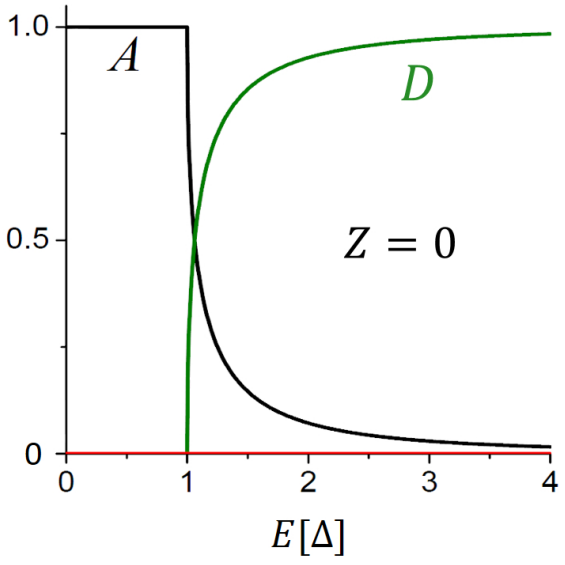

FIGURE 2.5: Probability currents of ballistic case with $Z = 0$. A and D refer to the probability to have a hole reflected and a electron transmitted. B and C are vanishing in the case.

Now we consider a simple case with $Z = 0$. We find that the B and C vanish which is due to absence of scattering center to change the wave vector from k_F to $-k_F$. The probability current of transmitted electron and reflected hole as a function of energy level is shown in Fig. (2.5). When energy of the injected electron is lower than the gap, a hole is certainly reflected. When the energy is above the gap, since the electron still feel the existence of gap, it is still possible to have a hole reflected.

2.2 Asymmetric Critical Currents

In this paper, we investigate the tunneling phenomena in a Josephson junction connecting a single-band superconductor and a three-band TRSB superconductor as shown in Fig. 2.6.

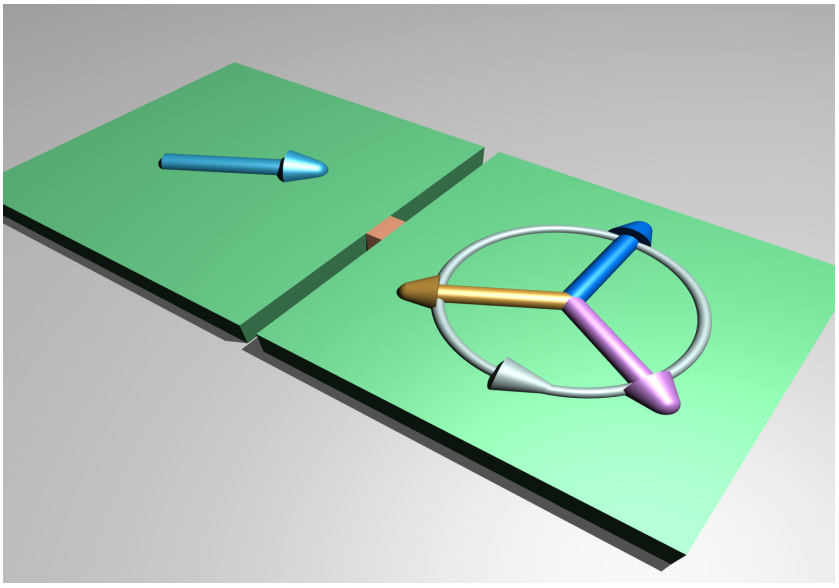

FIGURE 2.6: (color online) Schematics of point contact junction between single-band superconductor and three-band TRSB superconductor. Arrows indicate phases of gap functions and white circle with rotating direction represents the chirality.

We consider a point contact junction [65] with the size much smaller than the BCS coherence length. We model the SNS junction by a step change in the gap functions

$$\Delta(x) = \begin{cases} \Delta_0, & x < 0; \\ 0, & x = 0; \\ \{\Delta_1, \Delta_2, \Delta_3\}, & x > 0, \end{cases} \tag{2.30}$$

with the origin at the point contact in Fig. 2.6; for simplicity all gaps are taken as s-wave pairing. In the bulk on the right hand side, Δ_1, Δ_2 and Δ_3 are determined by the interband Cooper-pair scattering processes, and nontrivial phase differences exist among Δ_1, Δ_2 and Δ_3[41]. By extending previous works for two-band case [60, 66], the full BdG equations are given by

$$\begin{pmatrix} H_1 + T_{11} & T_{12} & T_{13} \\ T_{12} & H_2 + T_{22} & T_{23} \\ T_{13} & T_{23} & H_3 + T_{33} \end{pmatrix} \begin{pmatrix} \psi_1 \\ \psi_2 \\ \psi_3 \end{pmatrix} = E \begin{pmatrix} \psi_1 \\ \psi_2 \\ \psi_3 \end{pmatrix}, \tag{2.31}$$

with $T_{jk} = t_{jk}\delta(x)\sigma_z$, $\psi_j = (u_{j\uparrow}(x), v_{j\downarrow}(x))^T$ and

$$H_j = \begin{pmatrix} -\hbar^2\partial_x^2/2m - E_F & \Delta_j\Theta(x) + \Delta_0\Theta(-x) \\ \Delta_j^*\Theta(x) + \Delta_0^*\Theta(-x) & \hbar^2\partial_x^2/2m + E_F \end{pmatrix} \tag{2.32}$$

with σ_z the Pauli matrix, $\Theta(x)$ the Heaviside function and $E_F = \hbar^2 k_F^2/2m$. Here ψ_j are written in the Nambu spinor notation and T_{jk} are the intraband ($j = k$) and interband ($j \neq k$) single-particle scattering terms. The BdG equations describe the transporting process of Copper pairs through the Andreev reflections [64] in the ballistic limit.

In order to calculate the Andreev levels, we consider the right moving quasiparticles in the three-band superconductor on the right-hand side and the left moving quasiparticles in the single-band superconductor on the left-hand side [65]. The solution has the form $\psi_j = \psi_{0-}\Theta(-x) + \psi_{j+}\Theta(x)$ with

$$\begin{aligned} \psi_{0-} &= a_{j-}\begin{pmatrix} u_0 e^{i\varphi_0} \\ v_0 \end{pmatrix} e^{-ik_F x} + b_{j-}\begin{pmatrix} v_0 e^{i\varphi_0} \\ u_0 \end{pmatrix} e^{ik_F x}, \\ \psi_{j+} &= a_{j+}\begin{pmatrix} u_j e^{i\varphi_j} \\ v_j \end{pmatrix} e^{ik_F x} + b_{j+}\begin{pmatrix} v_j e^{i\varphi_j} \\ u_j \end{pmatrix} e^{-ik_F x}, \end{aligned} \tag{2.33}$$

where

$$u_j = \sqrt{\frac{1}{2}\left(1 + \sqrt{1 - \left(\frac{|\Delta_j|}{E}\right)^2}\right)}, v_j = \sqrt{\frac{1}{2}\left(1 - \sqrt{1 - \left(\frac{|\Delta_j|}{E}\right)^2}\right)} \tag{2.34}$$

with $j = 1, 2$ and 3. To obtain Eq. (2.33), we have assumed the Andreev approximation $E, \Delta_j \ll E_F$, and thus the wave vectors simply read $\pm k_F$. While Eq. (2.33) shares the same form with the two-band superconductors [66], the physics is quite different as will be revealed below due to the broken TRS.

From Eq. (2.33), the boundary conditions are given by

$$\begin{aligned} \psi_{0-}(0) &= \psi_{j+}(0), \\ \left(\frac{\partial \psi_{j+}}{\partial x} - \frac{\partial \psi_{0-}}{\partial x}\right)\Big|_{x=0} &= \frac{2m}{\hbar^2}\left[t_{jj}\psi_{j-}(0) + t_{jk}\psi_{k-}(0) + t_{jl}\psi_{l-}(0)\right]. \end{aligned} \tag{2.35}$$

Ballistic junction with equal gap

Here we first consider a simple case with $|\Delta_0| = |\Delta_j| = |\Delta|$ in the ballistic limit ($t_{jk} = 0$). From Eq. (2.35), we obtain the Andreev spectra as

$$E_j^{\pm} = \pm|\Delta|\cos(\varphi_{j0}/2) \tag{2.36}$$

with $\varphi_{j0} = \varphi_j - \varphi_0$. Supercurrent in each channel is given by [67]

$$I_j = \frac{2e}{\hbar}\frac{\partial E_j^+}{\partial \varphi_{j0}} f(E_j^+) + \frac{2e}{\hbar}\frac{\partial E_j^-}{\partial \varphi_{j0}} f(E_j^-) \tag{2.37}$$

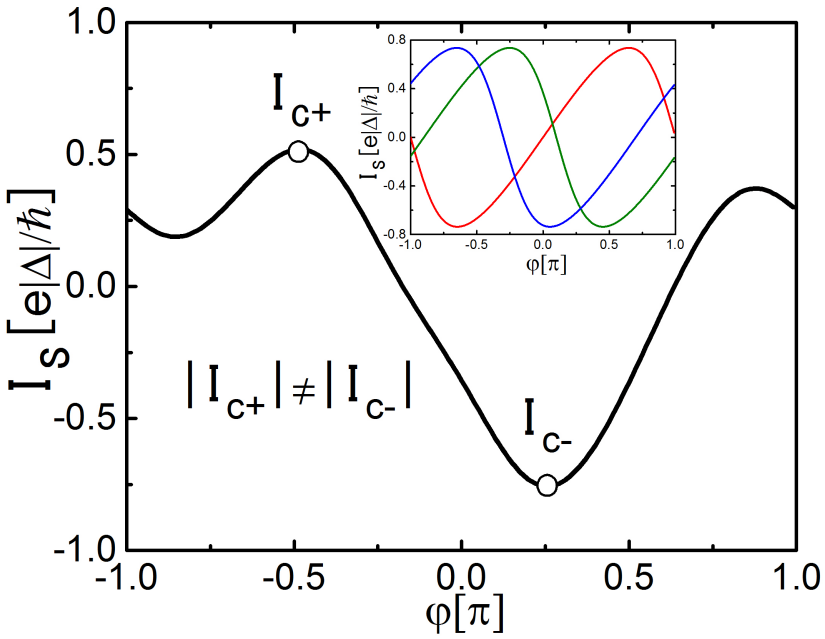

FIGURE 2.7: (color online) Current-phase relation of ballistic point-contact junction between single-band and three-band superconductor for parameters $\varphi_{21} = 0.9\pi$, $\varphi_{31} = 1.3\pi$ and $T = 0.2\Delta/k_B$. Inset: Red, green and blue curves indicate the Josephson current in condensate-1, 2 and 3.

where $f(E_j)$ is the Fermi-Dirac distribution function. Thus we obtain the total current

$$\begin{aligned} I_s(\varphi) = & \frac{e|\Delta|}{\hbar} \sin(\varphi/2) \tanh \frac{|\Delta| \cos(\varphi/2)}{2k_B T} \\ & + \frac{e|\Delta|}{\hbar} \sin[(\varphi+\varphi_{21})/2] \tanh \frac{|\Delta| \cos[(\varphi+\varphi_{21})/2]}{2k_B T} \\ & + \frac{e|\Delta|}{\hbar} \sin[(\varphi+\varphi_{31})/2] \tanh \frac{|\Delta| \cos[(\varphi+\varphi_{31})/2]}{2k_B T}, \end{aligned} \tag{2.38}$$

where $\varphi \equiv \varphi_{10}$, and φ_{21} and φ_{31} are interband phase differences for the three-band superconductor.

In a three-band superconductor with interband attractions, all gap functions take the same phase which reserves the TRS. However, when the interband couplings are repulsive, gap functions have to take different phases with nontrivial phase differences, which breaks the TRS [36–43].

To be specific, we consider a case with equal gap amplitudes albeit different interband couplings, such that $\varphi_{21} = 0.9\pi$ and $\varphi_{31} = 1.3\pi$. The current phase relation (CPR) for this system is displayed in Fig. 2.7. It is interesting to find that critical currents in the two opposite directions are unequal.

The reason for the asymmetry in the critical currents can be found from the symmetry of CPR. In a conventional time-reversal-symmetry-reserved (TRSR) superconductor (three-band: $\varphi_{jk} = 0$ or π), the same critical currents in two directions is a direct consequence of anti-reversal symmetry of CPR $I(-\varphi) = -I(\varphi)$ as can be seen in Eq. (2.38). This property is protected by TRS [68]. However in a TRSB state under concern, this anti-reversal symmetry is broken as in Eq. (2.38) since $\varphi_{21}, \varphi_{31} \neq 0, \pi$. The asymmetric critical currents can also be understood from the absence of symmetry in the Andreev spectra.

The relation between the broken TRS and asymmetric critical currents can be seen in another way. Upon the time-reversal transformation to the whole system, supercurrent reverses its direction and the superconducting state changes according to ($\varphi_j \to -\varphi_j$). In a TRSB state, the superconducting state upon TRS operation results in another state with chirality opposite to the original one. Therefore the same amount of supercurrents can only be guaranteed by two different states, which are not connected to each other. It is clearly not the case in the TRSR state.

As temperature approaches T_c, the gap function is suppressed and Eq. (2.38) is approximately reduced to

$$I_s(\varphi) = \frac{e|\Delta|^2}{4\hbar k_B T}[\sin\varphi + \sin(\varphi + \varphi_{21}) + \sin(\varphi + \varphi_{31})]. \tag{2.39}$$

A translational anti-symmetry $I_s(\varphi) = -I_s(\varphi + \pi)$ appears, which makes the two critical currents in the two opposite directions equal to each other. At low temperatures, the translational antisymmetry is destroyed by high harmonics additional to those in Eq. (2.39), which realize the asymmetric critical currents discussed above.

As shown in Fig. 2.7, zero Josephson current is obtained when $\varphi \neq 0, \pi$, indicating a φ-Josephson junction [69, 70]. However, the critical currents in the opposite directions are asymmetric in the present system, which is different from the previously discussed φ-junction.

Non-ballistic junction

Now we put a scattering center at the interface by taking $t_{jk} \neq 0$ at Eq. (2.31) and consider the possible effect of single-particle scattering among different bands. The BdG equations can only be solved numerically, and the results for a typical TRSB state are displayed in Fig. 2.8. We find that the asymmetry in critical currents remains unchanged. The gaps in Fig. 2.8(b) are caused by interband scattering which is similar to hybridization of two bands.

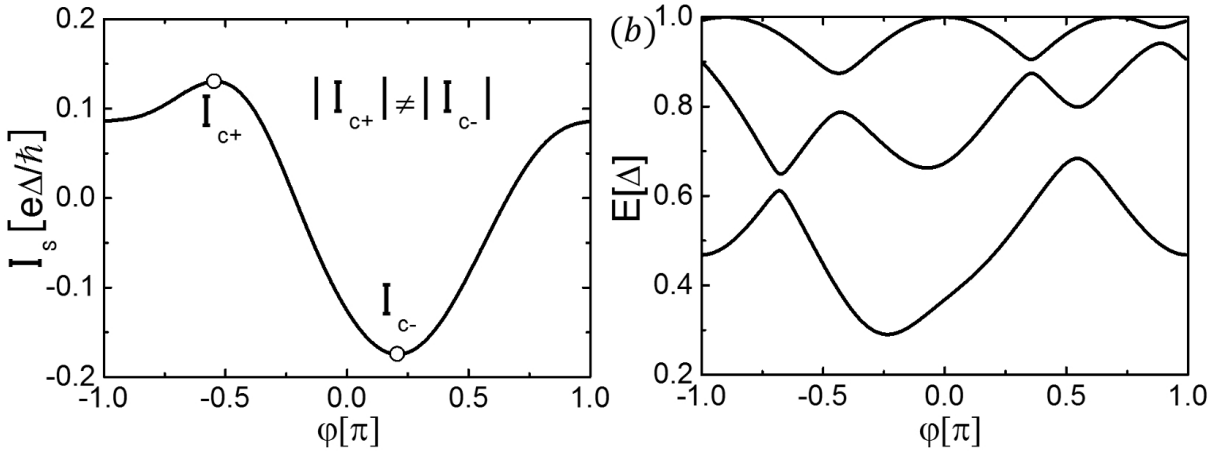

FIGURE 2.8: Current-phase relation and Andreev spectra of point-contact junction between a single-band and three-band superconductor with intraband and interband single-particle scattering. The panels (a) and (b) show the asymmetric critical currents and Andreev spectra. Here we use the same TRSB state as in Fig. 2.7(a) and (b). The hopping coefficients are $t_{11} = 1.1, t_{22} = 1.2, t_{33} = 0.8$, $t_{12} = 0.3, t_{13} = 0.1$ *and* $t_{23} = 0.5$. All t_{jk} are in unite of $2m/\hbar^2 k_F$.

Unequal gaps

In the above investigation, we have considered a special case with $|\Delta_0| = |\Delta_j|$. Now we study the general situation with $|\Delta_0| \neq |\Delta_j|$, in which Josephson current is contributed from not only discrete Andreev levels below the two gaps but also intermediate continuum levels between the two gaps with a formalism similar to the single-band system [71].

We first consider the supercurrent carried by the Andreev levels. As in the main text, the wave functions at two sides of the junction and boundary conditions are given by

$$\begin{aligned}\psi_{j-} &= a_{j-}\begin{pmatrix} u_0 e^{i\varphi_0} \\ v_0 \end{pmatrix} e^{-ik_F x} + b_{j-}\begin{pmatrix} v_0 e^{i\varphi_0} \\ u_0 \end{pmatrix} e^{ik_F x}, \\ \psi_{j+} &= a_{j+}\begin{pmatrix} u_j e^{i\varphi_j} \\ v_j \end{pmatrix} e^{ik_F x} + b_{j+}\begin{pmatrix} v_j e^{i\varphi_j} \\ u_j \end{pmatrix} e^{-ik_F x},\end{aligned} \tag{2.40}$$

and

$$\begin{aligned}\psi_{j-}(0) &= \psi_{j+}(0), \\ \left(\frac{\partial\psi_{j+}}{\partial x} - \frac{\partial\psi_{j-}}{\partial x}\right)\Big|_{x=0} &= \frac{2m}{\hbar^2}\left[t_{jj}\psi_{j-}(0) + t_{jk}\psi_{k-}(0) + t_{jl}\psi_{l-}(0)\right],\end{aligned} \tag{2.41}$$

which lead to

$$\begin{pmatrix} M_1 & C_{12} & C_{13} \\ C_{12} & M_2 & C_{23} \\ C_{13} & C_{23} & M_3 \end{pmatrix}\begin{pmatrix} D_1 \\ D_2 \\ D_3 \end{pmatrix} = 0, \tag{2.42}$$

with $D_j = (a_{j+}, b_{j+}, a_{j-}, b_{j-})^T$,

$$M_j = \begin{pmatrix} u_j e^{i\varphi_{j0}} & v_j e^{i\varphi_{j0}} & -u_0 & -v_0 \\ v_j & u_j & -v_0 & -u_0 \\ u_j e^{i\varphi_{j0}} & -v_j e^{i\varphi_{j0}} & (1-T_{jj})u_0 & -(1+T_{jj})v_0 \\ v_j & -u_j & (1-T_{jj})v_0 & -(1+T_{jj})u_0 \end{pmatrix},$$

and

$$C_{jk} = \begin{pmatrix} 0 & 0 & 0 & 0 \\ 0 & 0 & 0 & 0 \\ 0 & 0 & -T_{jk}u_0 & -T_{jk}v_0 \\ 0 & 0 & -T_{jk}v_0 & -T_{jk}u_0 \end{pmatrix}$$

with $T_{jk} = 2mt_{jk}/i\hbar^2 k_F$.

Non-zero solutions are available when the determinant of the square matrix in Eq. (2.42) is zero, which results in the Andreev spectra $E_j^{\pm}(\varphi_{j0})$. The tunneling current can be calculated with the formula

$$I_A = \sum_{j=1,2,3} \frac{2e}{\hbar}\frac{\partial E_j^+}{\partial\varphi_{j0}} f_{E_j^+} + \frac{2e}{\hbar}\frac{\partial E_j^-}{\partial\varphi_{j0}} f_{E_j^-}, \tag{2.43}$$

where $f_{E_j^+}$ and $f_{E_j^-}$ are the Fermi-Dirac distribution function.

The analytical expression of I_A is available for a ballistic junction with $t_{jk} = 0$, where the square matrix in Eq. (2.42) is reduced to three 4×4 diagonal block matrices. The Andreev spectra are obtained as

$$E_j^{\pm} = \pm \frac{|\Delta_0||\Delta_j| \sin\varphi_{j0}}{\sqrt{|\Delta_0|^2 + |\Delta_j|^2 - 2|\Delta_0||\Delta_j| \cos\varphi_{j0}}} \tag{2.44}$$

with the restriction $\cos\varphi_{j0} \leq |\Delta_0/\Delta_j|$, which carry the tunneling current

$$\begin{aligned} I_A = \sum_{j=1,2,3} \Bigg[\frac{2e}{\hbar} & \frac{|\Delta_0|^2|\Delta_j|^2 - \left(|\Delta_0|^2 + |\Delta_j|^2 - |\Delta_0||\Delta_j| \cos\varphi_{j0}\right)|\Delta_0||\Delta_j| \cos\varphi_{j0}}{\left(|\Delta_0|^2 + |\Delta_j|^2 - |\Delta_0||\Delta_j| \cos\varphi_{j0}\right)^{3/2}} \\ & \times \tanh \frac{|\Delta_0||\Delta_j| \sin\varphi_{j0}}{2k_BT\sqrt{|\Delta_0|^2 + |\Delta_j|^2 - |\Delta_0||\Delta_j| \cos\varphi_{j0}}} \Bigg]. \end{aligned} \tag{2.45}$$

Now we consider the tunneling current flowing in the energy region between the two gaps. To be specific, we take $|\Delta_0| < |\Delta_j|$. In this energy region, electron-like and hole-like quasiparticles are injected from the left single-band superconductor and transmitted into the right three-band superconductor, contributing to the tunneling current.

The wave function in the left superconductor is given by

$$\psi_{j-} = \begin{pmatrix} u_0 e^{i\varphi_0} \\ v_0 \end{pmatrix} e^{ik_F x} + a_{j-} \begin{pmatrix} u_0 e^{i\varphi_0} \\ v_0 \end{pmatrix} e^{-ik_F x} + b_{j-} \begin{pmatrix} v_0 e^{i\varphi_0} \\ u_0 \end{pmatrix} e^{ik_F x}, \tag{2.46}$$

where the first term is the incident electron-like quasiparticle which is absent in Eq. (2.40), the second term is the reflected electron-like quasiparticle and the third term is the reflected hole-like quasiparticle. The transmitted wave ψ_{j+} maintains the form

$$\psi_{j+} = a_{j+} \begin{pmatrix} u_j e^{i\varphi_j} \\ v_j \end{pmatrix} e^{ik_F x} + b_{j+} \begin{pmatrix} v_j e^{i\varphi_j} \\ u_j \end{pmatrix} e^{-ik_F x}. \tag{2.47}$$

By using the boundary conditions in Eq. (2.41), we obtain

$$\begin{pmatrix} M_1 & C_{12} & C_{13} \\ C_{12} & M_2 & C_{23} \\ C_{13} & C_{23} & M_3 \end{pmatrix} \begin{pmatrix} D_1 \\ D_2 \\ D_3 \end{pmatrix} = \begin{pmatrix} Q_1 \\ Q_2 \\ Q_3 \end{pmatrix}, \tag{2.48}$$

with $Q_j = \left(u_0, v_0, (1 + T_{jj} + T_{jk} + T_{jl})u_0, (1 + T_{jj} + T_{jk} + T_{jl})v_0\right)^T$, from where we can obtain $(a_{j+}, b_{j+}, a_{j-}, b_{j-})$. It is noted that Eq. (2.43) is not convenient for calculating the tunneling current in the present continuum energy regime. Instead we integrate the electrical current density as

$$I_I^e = \sum_{j=1,2,3} e\frac{\hbar k_F}{m} \left(\int_{|\Delta_0|}^{|\Delta_j|} + \int_{-|\Delta_j|}^{-|\Delta_0|} \right) \left(|a_{j+}|^2 - |b_{j+}|^2\right) N_{s-} f_{E_j} dE_j, \tag{2.49}$$

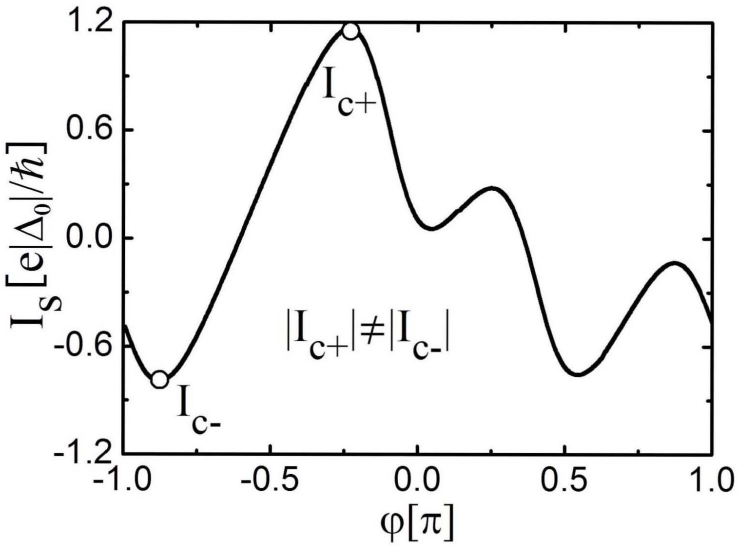

FIGURE 2.9: (color online) Current phase relation of point-contact junction between single-band and three-band TRSB superconductor with different gap amplitudes. Here we have $|\Delta_1| = 1.2|\Delta_0|$, $|\Delta_2| = 1.3|\Delta_0|$, $|\Delta_3| = 1.5|\Delta_0|$, $\varphi_{21} = 0.6\pi$, $\varphi_{31} = 1.1\pi$, $t_{11} = t_{22} = t_{33} = 0.2$ and $t_{12} = t_{13} = t_{23} = 0.1$. All t_{jk} are in unite of $2m/\hbar^2 k_F$.

where N_{s-} is the density of states for the electron-like quasiparticles in the left superconductor and f_{E_j} is the Fermi-Dirac distribution function. A similar calculation can be done for the incident hole-like quasiparticles, which contribute a current I_I^h. The total current carried by the intermediate energy region is thus given by

$$I_I = I_I^e + I_I^h. \tag{2.50}$$

The ballistic case can be solved analytically and the tunneling current is

$$I_I = \sum_{j=1,2,3} \left[\frac{2e}{h} \int_{|\Delta_0|}^{|\Delta_j|} \sqrt{1 - \left|\frac{\Delta_0}{E_j}\right|^2} \left(\frac{1}{1 - \left|\frac{\Delta_0}{E_j}\right| \cos\left[\varphi_{j0} - \cos^{-1}\left|\frac{E_j}{\Delta_j}\right|\right]} - \frac{1}{1 - \left|\frac{\Delta_0}{E_j}\right| \cos\left[\varphi_{j0} + \cos^{-1}\left|\frac{E_j}{\Delta_j}\right|\right]} \right) \tanh\frac{E_j}{2k_BT} dE_j \right]. \tag{2.51}$$

The calculation result can be extended to the $|\Delta_0| > |\Delta_j|$, by simply reversing the limits of integration.

For a non-ballistic junction with scattering centers at the interface ($t_{jk} \neq 0$), numerical calculations are required and the current phase relation is shown in Fig. 2.9. An asymmetry in critical currents is found when the three-band superconductor stays at a TRSB state where $\varphi_{21}, \varphi_{31} \neq 0, \pi$.

2.3 Subharmonic Shapiro Steps

Conventional shapiro steps

When a Josephson junction under a DC bias V_0 is irradiated by a microwave with frequency ω_1, the voltage drop across the junction is

$$V = V_0 + V_1 \cos \omega_1 t. \tag{2.52}$$

Putting it into Eq. (1.16), and integrating over time, we obtain

$$\Delta\varphi = \Delta\varphi_0 + \frac{2eV_0}{\hbar}t + \frac{2eV_1}{\hbar\omega_1} \sin \omega_1 t \tag{2.53}$$

where $\Delta\varphi_0$ is a constant of integration. The Josephson current now becomes

$$\begin{aligned} j &= j_c \sin\left(\Delta\varphi_0 + \frac{2eV_0}{\hbar}t + \frac{2eV_1}{\hbar\omega_1} \sin \omega_1 t\right) \\ &= j_c \sum (-1)^n J_n\left(\frac{2eV_1}{\hbar\omega_1}\right) \sin\left(\Delta\varphi_0 + \frac{2eV_0}{\hbar}t - n\frac{2eV_1}{\hbar}t\right) \end{aligned} \tag{2.54}$$

where J_n is the Bessel function of the first kind. The Josephson current has not only a component with frequency $\omega = 2eV_0/\hbar$ but also abundant harmonics from the microwave, which has modulating effect on the Josephson current. When we have

$$V_0 = V_n = nV_1, \tag{2.55}$$

a DC component of supercurrent is obtained. By taking into the normal current as well, in the I-V curve current steps appear with the total DC current taking any value in the range

$$V_n/R - j_c J_n\left(\frac{2eV_1}{\hbar\omega_1}\right) \leq I \leq V_n/R + j_c J_n\left(\frac{2eV_1}{\hbar\omega_1}\right), \tag{2.56}$$

where R is the normal resistance of the junction. These steps are named as Shapiro steps in the credit of its first observation by S. Shapiro in 1963 [72].

Subharmonic Shapiro steps

Now we analyze the response of the TRSB state to a microwave irradiation. For this purpose, we rewrite the CPR Eq. (2.38). In the three tunneling channels, we have $I_j(-\varphi_{j0}) = -I_j(\varphi_{j0})$ and $I_j(\varphi_{j0} + 2\pi) = I_j(\varphi_{j0})$ according to Eq. (2.37). Therefore, I_j can be expanded into a Fourier series with only sine functions, and thus the CPR can be written as

$$I_s(\varphi) = \sum_{n=1}^{+\infty} [I_{1n} \sin n\varphi + I_{2n} \sin n(\varphi + \varphi_{21}) + I_{3n} \sin n(\varphi + \varphi_{31})], \tag{2.57}$$

where

$$I_{jn} = \frac{1}{\pi} \int_{-\pi}^{\pi} \frac{e|\Delta|}{\hbar} \sin(\xi/2) \tanh \frac{|\Delta| \cos(\xi/2)}{2k_B T} \sin n\xi d\xi \tag{2.58}$$

with $j = 1, 2$ and 3. It is noticed that the supercurrents carried by the three channels may enhance and suppress each other, depending on the phase differences and the order of Fourier components. To illustrate this effect clearly, we consider an isotropic state with $|\Delta_1| = |\Delta_2| = |\Delta_3|$ and $\varphi_{21} = \varphi_{32} = 2\pi/3$ at the right-hand side of the junction. It is interesting to observe that a complete cancelation takes place for $3n + 1$ and $3n + 2$ for n=0,1,2, ... , and the CPR is reduced to

$$I_s(\varphi) = I_c \sin 3\varphi. \tag{2.59}$$

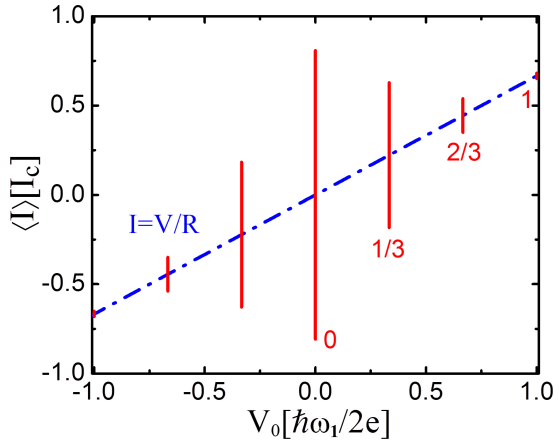

FIGURE 2.10: (color online) Subharmonic Shapiro steps of overdamped junction between single-band and three-band isotropic TRSB superconductor ($|\Delta_1| = |\Delta_2| = |\Delta_3|$ and $\varphi_{21} = \varphi_{32} = 2\pi/3$) driven by ac voltage source. The parameters are $V_1 = 0.15\hbar\omega_1/e$ and $R = 0.75\hbar\omega_1/eI_c$.

Now we take the applied voltage with the form $V = V_0 + V_1 \cos\omega_1 t$. The Josephson current is given by

$$I_s(\varphi) = I_c \sum_{m=-\infty}^{+\infty} (-1)^m J_m(\frac{6eV_1}{\hbar\omega_1}) \sin(\delta_0 + 3\omega_0 t - m\omega_1 t) \tag{2.60}$$

with J_m the Bessel function of the first kind, δ_0 an arbitrary phase and $\omega_0 = 2eV_0/\hbar$. It is easy to find that the supercurrent contains a dc component when

$$V_0 = \frac{m}{3}\frac{\hbar\omega_1}{2e}. \tag{2.61}$$

The fractional numbers $m/3$ indicate the subharmonic Shapiro steps.

We assume that junction is overdamped with a shunted resistance R, and thus the total dc current on the mth subharmonic Shapiro step can take any value in the range

$$\frac{V_0}{R} - I_c J_m(\frac{6eV_1}{\hbar\omega_1}) \leq \langle I\rangle \leq \frac{V_0}{R} + I_c J_m(\frac{6eV_1}{\hbar\omega_1}) \tag{2.62}$$

as shown in Fig. 2.10.

For general TRSB states where cancelations are not complete, $1/2$ Shapiro step appears. However, because the $1/2$ step is still suppressed and the $1/3$ step is enhanced, we expect that the $1/3$ step is comparable or even larger than the $1/2$ step.

2.4 Fraunhofer Patterns

Now let us see the Fraunhofer interference in an extended junction between a single-band superconductor and a three-band TRSB superconductor. We adopt the general expression for Josephson currents [68, 73] $I_s(\varphi)$ in

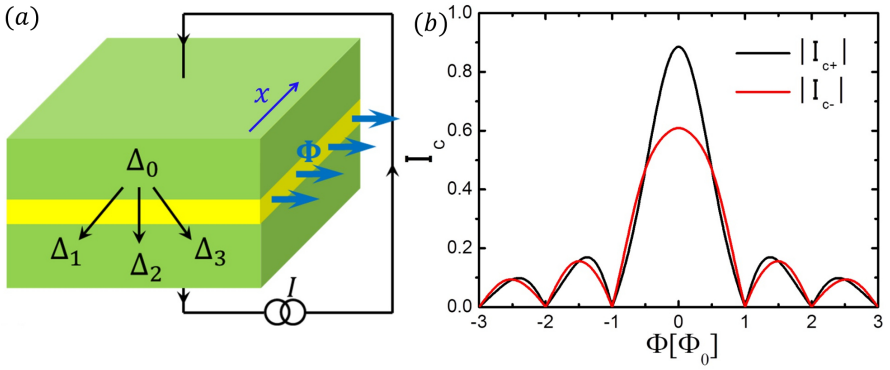

FIGURE 2.11: (a) Schematic figure of extended junction between single-band superconductor and three-band TRSB superconductors under magnetic fields, (b) Symmetric Fraunhofer pattern under changing magnetic fields. We use the CPR in the form of Fourier series with the coefficient $I_{11} = I_{21} = I_{31} = 1.0, I_{12} = I_{22} = I_{32} = 0.1$.

Eq. (2.57). In the presence of a flux Φ penetrating into the junction, the Josephson current is given

$$I_\Phi(\varphi) = \frac{1}{L}\int_0^L I_s(\varphi + \frac{2\pi\Phi}{\Phi_0}\frac{x}{L})dx = \sum_n \frac{\sin(n\pi\Phi/\Phi_0)}{n\pi\Phi/\Phi_0} \times [I_{1n}\sin n\varphi + I_{2n}\sin n(\varphi+\varphi_{21}) + I_{3n}\sin n(\varphi+\varphi_{31})]. \tag{2.63}$$

We find that the supercurrent is symmetric with respect to the direction of magnetic flux, which indicates that TRSB states do not couple with magnetic fields.

2.5 Discussions and Conclusions

Although we have focused on point-contact junction in the above investigations, it is clear that the main results remain valid for junctions with extensions since the most essential ingredient is the existence of TRSB state characterized by nontrivial phase differences among condensates, in which the high harmonics in Josephson current become more prominent.

There is a special case where component-2 and component-3 are equivalent, which results in $\varphi_{21} = -\varphi_{31}$, and the critical currents in opposite directions are equal according to Eq. (2.38), albeit the broken TRS. We notice that the case $\varphi_{21} = -\varphi_{31}$ generated by two equivalent components is accidental without symmetry protection. When temperature changes, gap amplitudes and/or interband couplings become different for the two components, for which asymmetric critical currents appear. In the case that component-2 coincides with component-3, we may distinguish the TRSB state from TRSR state by using the Shapiro steps. For TRSB state, 1/3-step is larger than or comparable to 1/2-step (Fig. 3 is an extreme case where 1/2-step is suppressed to zero since the three components are equivalent), while in the TRSR state 1/2-step is expected larger than 1/3-step.

It is intriguing to notice that asymmetric critical currents have been observed in a hybrid junction between a single-band superconductor PbIn and an iron-based superconductor $BaFe_{2-x}Co_xAs_2$ [74, 75]. The difference between two critical currents is well beyond the experimental precision. Subharmonic Shapiro steps were also detected in the same setup, indicating the importance of high-order harmonics in the Josephson current. While

the asymmetric critical currents was explained by presuming vortices accidentally trapped in one of the two superconductors [76], we wish to point out the two phenomena observed in the experiments can be understood in terms of the existence of a TRSB state as discussed in the present work. Further careful investigations are highly anticipated to make the situation clear. For example, the Fraunhofer pattern is to be measured, which should be asymmetric with respect to the flux direction if some vortices are trapped in one of the two superconductors [77], while the TRSB state corresponds to a symmetric one.

We notice that there is another similar experiment for a junction between Pb and an iron pnictide $Ba_{1-x}K_xFe_2As_2$ with $x = 0.29$ and $x = 0.49$, where symmetric critical currents have been observed [78]. It is possible that in order to see the TRSB state, and thus the asymmetric critical currents, the hole doping rate is to be tuned to the overdoping regime, according to a recent theoretical work [43].

To summarize, in superconductors with three or more bands, time-reversal symmetry may be broken in the presence of repulsive interband couplings, characterized by nontrivial phase differences among condensates. Due to the broken time-reversal symmetry, asymmetric critical currents appear in a Josephson junction between a single-band and a multi-band superconductor. Subharmonic Shapiro steps become more prominent since the tunneling currents carried by different bands may cancel each other, which reduces the sizes of integer Shapiro steps.

Chapter 3

Fractional Flux Plateau in Magnetization Curve of Multi-Component Superconductor Loop

Vortex with 2π phase winding is a hallmark of macroscopic quantum state such as superfluidity and superconductivity [1, 19, 79, 80]. In superconductors, a vortex is accompanied by a quantum of magnetic flux $\Phi_0 = hc/2e$ in a closed path with zero supercurrent. Since the quantization of magnetic flux is intimately related to the phase winding, superconductivity gap functions carrying intrinsic phase variation induced by unconventional pairing symmetry should leave unique consequences on the response to external magnetic field. By now several interesting examples are available. A tricrystal ring of cuprate superconductor $YBa_2Cu_3O_{7-\delta}$ was observed to carry a half flux quanta $\Phi_0/2$, which is the signature for d-wave pairing symmetry [59]. In a ring-shaped setup composed by Nb and $NdFeAsO_{0.88}F_{0.12}$, flux jumps in odd-number multiple of half flux quanta were observed [81–83], which provides a support to the S_{+-} pairing symmetry for iron-pnictide superconductors [30, 52, 84–89]. Half-valued fluxoid jumps in magnetization curve of a thin annular coil made of Sr_2RuO_4 were reported being consistent with the p-wave pairing symmetry [90].

In the previous chapter we have found that in a Josephson junction between a conventional single-component superconductor and a multi-component superconductor in TRSB state, the critical current should be asymmetric with respect to the current direction as the consequence of broken TRS [91]. As a matter of fact, unequal critical currents in opposite current directions were observed experimentally in a Josephson junction between PbIn and $BaFe_{1.8}Co_{0.2}As_2$ [74]. Therefore, the TRSB state may have been realized already in iron-based superconductors, which is consistent with a microscopic analysis where band structures and strongly correlated effects are taken into account [43]. To cross check this novel superconducting phenomenon becomes an important issue.

In the present chapter, we address a new phase-sensitive property of the TRSB superconducting state. As schematically shown in Fig. 3.1, we consider a loop of multi-component superconductor where the two halves are occupied by two TRSB states carrying on opposite chiralities, accompanied by two domain walls associated with inter-component phase kinks. We reveal explicitly that fractional flux plateaus appear in magnetization curve associated with free-energy minima, where the domain walls accommodate phase kinks among different

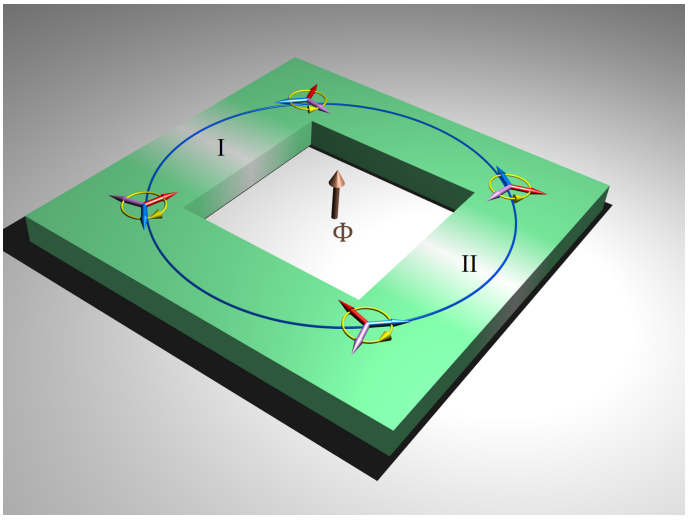

FIGURE 3.1: Schematic setup with a loop of time-reversal-symmetry-broken (TRSB) superconductor, where the two halves are occupied by the two degenerate states with opposite chiralities. The three arrows denote the phases of order parameters and the yellow circle indicates the chirality referring to the mutual phases red → blue → purple among three condensates. Between the two halves of the loop there are two domain wall I and II accommodating inter-component phase kinks.

components leading to 2π phase winding along the loop only in one or two of the three condensates. While the heights of fractional flux plateaus depend on material parameters and temperature, they form pairs with heights related by the flux quantum Φ_0, which is a unique signature of TRSB superconducting state and can be used to confirm the state itself [92]. In a more general point of view this provides a novel chance to explore relative phase difference, phase kink and soliton in ubiquitous multi-component superconductivity.

3.1 Fractional Flux in Superconductor Loop

In order to reveal the essence of physics we first consider an isotropic TRSB state which is generated by three equivalent condensates with equal mutual repulsion. For simplicity all order parameters are taken as s-wave from now on. The two states in the loop are given by $\Psi = \{\psi_1, \psi_2, \psi_3\} = |\psi|\{1, e^{i2\pi/3}, e^{i4\pi/3}\}$ and Ψ^* with opposite chiralities (see Fig. 3.1). Across each of the two domain walls between the left and right halves of the superconductor loop, there is a phase kink where inter-component phase difference between two of the three order parameters shrinks to zero and reopens in the opposite way continuously, resulting a sign reversal in the phase difference at the two sides of domain (see Fig. 2). We notice that phase kinks are gauge-invariant objects, which inevitably appear at the interface between two bulks of TRSB states with opposite chiralities.

When the two domain walls accommodate the phase kink between the same two condensates, such as that between condensate 1 and 2 defined as D_{12} in Fig. 3.2(a), the phase rotation integrated in a counterclockwise manner (indicated by L in Fig. 3.2) over the two domain walls cancel each other, resulting in the same phase winding in all the three condensates. In this case, the flux trapped in the loop is an integer multiple of flux quantum Φ_0 when the loop is thick enough to fully screen the magnetic field.

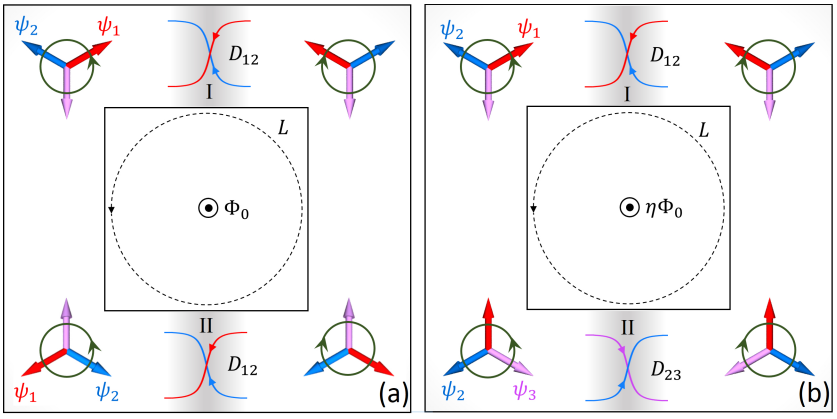

FIGURE 3.2: Illustration of relation between the phase kinks at domain wall I and II and the flux trapped in the superconductor loop: (a) phase kinks between a same pair of components which can only trap integer multiples of flux quantum; (b) phase kinks between two different pairs of components which can trap fractional flux ($0 < \eta < 1$). Colored curves at the domain walls refer to the phase variations in corresponding condensates, and D_{ij} is for the gauge-invariant phase kink between condensate i and j. The dashed circle denotes the direction for counting phase winding in the loop.

The situation differs when the two domain walls accommodate different phase kinks, such as D_{12} and D_{23} in domain wall I and II respectively shown in Fig. 3.2(b). By inspection one sees that ψ_2 rotates $4\pi/3$ anticlockwise over the two domain walls, while ψ_1 and ψ_3 rotate $-2\pi/3$. When the external magnetic field provides the additional phase rotation of $2\pi/3$ in all condensates, a state with 2π phase winding in ψ_2 and 0 in both ψ_1 and ψ_3 is stabilized. This yields a fractional flux quanta $\Phi_0/3$ in the loop. The state with a fractional flux trapped in this loop is expected to be stable in a certain range of external magnetic field, which leads to a fractional flux plateau in magnetization curve shown schematically in Fig. 3.3.

The above discussion can be elucidated by the integration of magnetic flux over the superconducting loop using GL formalism where the supercurrent is given by [17, 50]

$$\mathbf{J} = \sum_{j=1,2,3} \frac{2e}{m_j} |\psi_j|^2 \hbar \left(\nabla \varphi_j - \frac{2\pi}{\Phi_0} \mathbf{A} \right), \tag{3.1}$$

with m_j and φ_j the effective mass and phase of component-j. For a thick loop, supercurrent is zero deep inside the superconductor. In this case the magnetic flux trapped in the loop is given by the line integration of phase differences as can be seen from Eq. (3.1)

$$\begin{aligned} \Phi &= \frac{\Phi_0}{2\pi} \left[\oint_C \frac{p_1 \nabla\varphi_1 + p_2 \nabla\varphi_2 + p_3 \nabla\varphi_3}{p_1 + p_2 + p_3} dl \right] \\ &= \frac{\Phi_0}{2\pi} \left[\oint_C \nabla\varphi_1 dl + \int_{\mathrm{DW}} \frac{p_2 \nabla\varphi_{12} + p_3 \nabla\varphi_{13}}{p_1 + p_2 + p_3} dl \right], \end{aligned} \tag{3.2}$$

with $p_j = |\psi_j|^2/m_j$ and $\varphi_{ij} = \varphi_j - \varphi_i$ for $i, j = 1, 2, 3$, where *"C"* is a closed path along the loop with zero supercurrent everywhere (see Fig. 1), and the "DW" denotes domain-wall regimes (grey parts in Fig. 2) with phase kinks. In the second line, we divide the integrand into two terms, indicating two contributions to the total magnetic flux. The first contribution should be an integer multiple of 2π due to the single-valued wave function in the loop. The integrand in the second contribution is nonzero only on domain walls. This contribution is

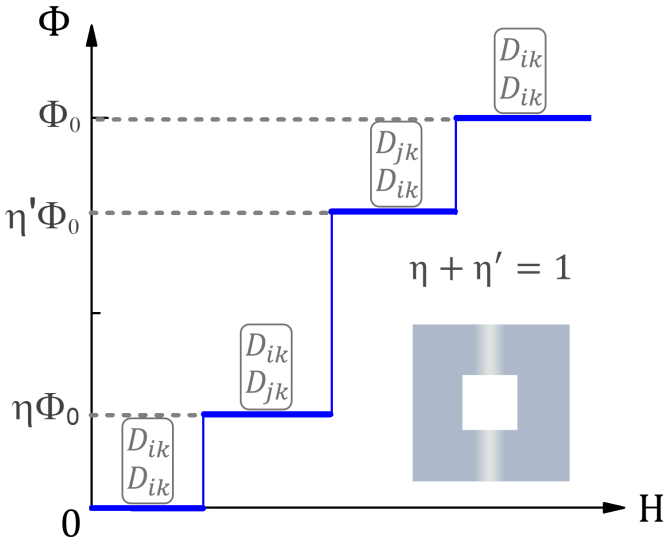

FIGURE 3.3: Schematic magnetization curve with fractional flux plateaus displayed together with gauge-invariant phase kinks denoted by [D_{ik}/D_{jk}] in the order of domain wall I and II.

nonzero when two different phase kinks are realized at domain wall I and II, with the value depending also on the quantities p_j.

Presuming the same length of domain walls I and II, the two configurations [D_{ik}/D_{jk}] and [D_{jk}/D_{ik}] at the domain walls [I/II] take the same free energy. However, integrating phase differences for these two configurations along the closed path in the anticlockwise way (see Fig. 3.2) results in opposite fractional values of 2π in the second term in Eq. (3.2). Therefore, these two configurations give two fractional fluxes Φ_1 and Φ_2 related by the flux quantum Φ_0. Fractional flux plateaus with corresponding configurations of phase kinks are schematically shown in Fig. 3.3.

3.2 TDGL Approach

Here we adopt GL formalism to check the thermodynamic stability of states carrying fractional fluxes. The GL free-energy functional of a three-band superconductor with Josephson-like inter-component couplings is given by [41, 50]

$$\begin{aligned} F &= \sum_{j=1,2,3}\left[\alpha_j\left|\psi_j\right|^2+\frac{\beta_j}{2}\left|\psi_j\right|^4+\frac{\hbar^2}{2m_j}\left|\left(\frac{\nabla}{i}-\frac{2\pi}{\Phi_0}\mathbf{A}\right)\psi_j\right|^2\right] \\ &\quad -\sum_{j,k=1,2,3;j<k}\gamma_{jk}\left(\psi_j^*\psi_k+c.c.\right)+\frac{1}{8\pi}\left(\nabla\times\mathbf{A}\right)^2, \end{aligned} \tag{3.3}$$

where α_j is a temperature-dependent coefficient which is negative when $T < T_{cj}$ and positive when $T > T_{cj}$, with T_{cj} the critical point of the superconducting component-j before considering intercomponent couplings, and γ_{jk} is an intercomponent coupling taken as constant for simplicity. For $\gamma_{12}\gamma_{13}\gamma_{23} < 0$, a TRSB superconducting state appears when the coefficients in Eq. (5.1) satisfy conditions revealed in a previous work [41]. To

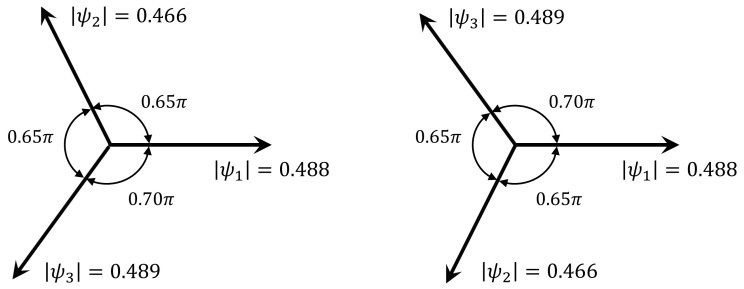

FIGURE 3.4: Amplitudes and phases of order parameters in two TRSB states with parameters $\alpha'_1 = 0.012, \alpha'_2 = 0.013$, $\alpha'_3 = 0.011$, $\gamma'_{12} = \gamma'_{23} = -0.24$, $\gamma'_{13} = -0.25$, $m'_1 = m'_3 = 1$, $m'_2 = 1.1$, $\beta'_1 = \beta'_2 = \beta'_3 = 1$ and $\kappa_1 = 1.5$. See text for definitions of the dimensionless GL parameters.

be specific, we put $\gamma_{12}, \gamma_{13}, \gamma_{23} < 0$, namely all repulsive Josephson-like couplings, since it is easy to see that other TRSB states can be generated from this case by simple gauge transformation.

We adopt dimensionless quantities given by [93]

$$\begin{gathered}\mathbf{x} = \lambda_1(0)\mathbf{x}',\ \mathbf{A} = \lambda_1(0)H_{tc1}(0)\sqrt{2}\mathbf{A}',\ \mathbf{J} = \frac{2e\hbar\psi_{10}^2(0)}{m_1\xi_1(0)}\mathbf{J}', \\ \psi_j = \psi_{10}(0)\psi'_j,\ \alpha_j = -\alpha_1(0)\alpha'_j, \beta_j = \beta_1\beta'_j,\ \gamma_{jk} = -\alpha_1(0)\gamma'_{jk}, \\ m_j = m_1 m_j',\ \kappa_1 = \lambda_1(0)/\xi_1(0),\ F = G_0 F'\end{gathered} \tag{3.4}$$

with $\psi_{10}^2(0) = -\alpha_1(0)/\beta_1$, $\lambda_1(0) = \sqrt{m_1c^2/[4\pi\psi_{10}^2(0)(2e)^2]}$, $\xi_1(0) = \sqrt{-\hbar^2/[2m_1\alpha_1(0)]}$, $H_{tc1} = \sqrt{-4\pi\alpha_1(0)\psi_{10}^2(0)}$ and $G_0 = H_{tc1}^2(0)/4\pi$. In the dimensionless units, the GL free energy is rewritten as

$$F' = \sum_{j=1,2,3}\left[\alpha'_j\left|\psi'_j\right|^2 + \frac{\beta'_j}{2}\left|\psi'_j\right|^4 + \frac{1}{m_{j'}}\left|\left(\frac{1}{i\kappa_1}\nabla - \mathbf{A}'\right)\psi'_j\right|^2\right] - \sum_{j,k=1,2,3;j<k}\gamma'_{jk}\left(\psi_j^{*\prime}\psi'_k + c.c.\right) + \left(\nabla\times\mathbf{A}'\right)^2. \tag{3.5}$$

The system can be described by the following TDGL equations in the zero-electric potential gauge [24]

$$\frac{\partial\psi'_j}{\partial t} = -\alpha'_j\psi'_j - \beta'_j|\psi'_j|^2\psi'_j - \frac{1}{m_{j'}}\left(\frac{1}{i\kappa_1}\nabla - \mathbf{A}'\right)^2\psi'_j + \sum_{k=1,2,3;k\neq j}\gamma'_{jk}\psi'_k \tag{3.6}$$

with $j = 1, 2, 3$ and

$$\sigma\frac{\partial\mathbf{A}'}{\partial t} = \sum_{j=1,2,3}\frac{1}{m'_j}|\psi'_j|^2\left(\frac{1}{i\kappa_1}\nabla\varphi'_j - \mathbf{A}'\right) - \nabla\times\nabla\times\mathbf{A}' \tag{3.7}$$

with σ the coefficient of normal conductivity. At equilibrium the left-hand sides of Eqs. (3.6) and (3.7) are zero, which gives the GL equations. By solving three GL equations in Eq. (3.6) with $\mathbf{A}' = 0$, we obtain the amplitudes and phases of the condensates at zero magnetic field [41].

In the present multi-component superconducting system, the critical point T_c is higher than T_{cj} for $j = 1, 2, 3$. In order to make sure that the GL formalism is valid for investigating the thermodynamics properties of the coupled system, we choose temperature satisfying $T_{cj} < T \lesssim T_c$, where α'_j are positive and small. In Fig. 3.4

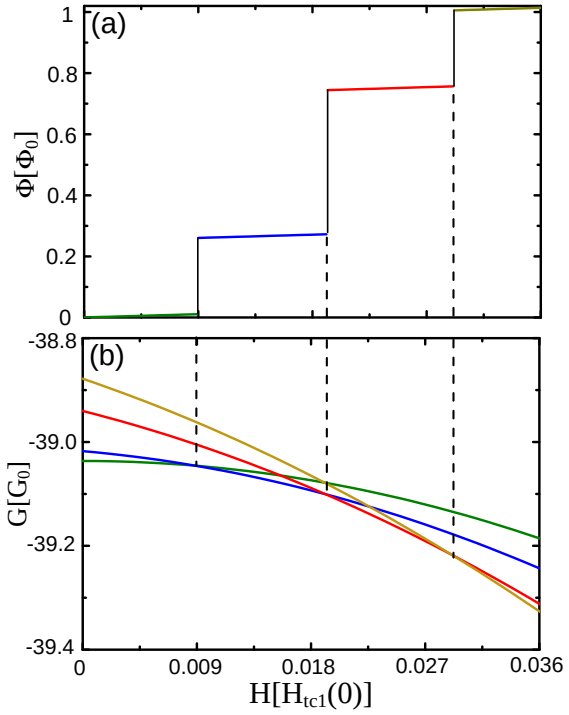

FIGURE 3.5: (a) Magnetization curve of thermodynamically stable state and (b) Gibbs free energies of several competing states in the superconductor loop shown in Fig. 1 upon sweeping external magnetic field. Parameters are the same as Fig. 3.4. The superconductor loop is of square shape with outer frame of $24\lambda_1(0)$ and inner frame of $8\lambda_1(0)$.

we display the two TRSB states with opposite chiralities, which are used for the following study on the magnetization process.

We take a square loop with external dimension $24\lambda_1(0) \times 24\lambda_1(0)$ and the wall thickness $8\lambda_1(0)$ to investigate the magnetic response. From Eq. (3.1) we obtain the the penetration length $\lambda^2 = (\sum_j |\psi'_j|^2/m'_j)^{-1}\lambda_1^2(0)$ in the dimensionless form. For the states given in Fig. 3.4, $\lambda = 1.22\lambda_1(0)$ is much smaller than the thickness of loop wall. Therefore, one can take the closed path "C" as the middle line of the superconducting loop where supercurrent is negligibly small (see Appendix). At the edge of superconductor, we presume that no supercurrent flows out of the superconductor, and the **B** field at the external edge of superconductor loop is fixed to the value of applied magnetic field.

The magnetization curve derived from TDGL equations (3.6) and (3.7) is shown in Fig. 3.5, where fractional flux plateaus corresponding to states with free-energy minima are obtained. When the magnetic field is small, there is no flux penetrating into the loop. As the magnetic field increases to $H/H_{tc1}(0) = 0.009$, the stable state takes a *fractional flux* $\Phi_1 = 0.26\Phi_0$. This state remains stable till the magnetic field $H/H_{tc1}(0) = 0.019$, yielding a plateau in the magnetization curve. As the magnetic field increases further, there appears another state with fractional flux $\Phi_2 = 0.74\Phi_0$ in the regime $0.019 \leq H/H_{tc1}(0) \leq 0.029$. We can see that both Φ_1 and Φ_2 deviate from $\Phi_0/3$ and $2\Phi_0/3$, because of the three inequivalent condensates in the system. Nevertheless, it is clear that the relation $\Phi_1 + \Phi_2 = \Phi_0$ is satisfied as revealed in Sec. 3.1. For even larger magnetic field, the stable state permits one flux quantum Φ_0 inside the loop. Note that the magnetic fields for the fractional flux

plateaus are very small as compared with the typical field $H_{tc1}(0)$ and thus there is no vortex inside the body of superconductor.

We check the phase kinks at the two domain walls I and II and the phase windings along the loop in the three condensates at the fractional flux plateaus. At $\Phi_1 = 0.26\Phi_0$, phase kink D_{12} and D_{23} are realized at region I and II respectively, and ψ_2 rotates 2π along the loop leaving ψ_1 and ψ_3 unwinding. At $\Phi_1 = 0.74\Phi_0$, the phase kinks D_{12} and D_{23} are at domain wall II and I, opposite to the case of $\Phi_1 = 0.26\Phi_0$, and ψ_1 and ψ_3 rotate 2π with ψ_2 unwinding. At integer flux quanta $\Phi = 0$ and $\Phi = \Phi_0$, the phase kink is D_{12} at both domain wall I and II. All these are in accordance with the discussion in Sec. 3.1. In general, there are at most six fractional flux plateaus between the integer flux quanta 0 and Φ_0. For GL parameters given in Fig. 3.4 we can only see two plateaus in Fig. 3.5(a) because the free energies of domain walls satisfy $F(D_{12}) \lesssim F(D_{23}) < F(D_{13})$ such that only the phase-kink pair D_{12} and D_{23} is stabilized.

3.3 Temperature Dependence

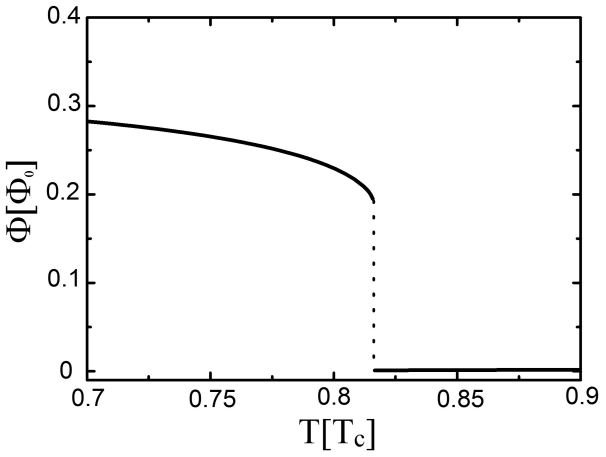

FIGURE 3.6: Temperature dependence of trapped flux in superconductor loop. Parameters are the same as the Fig. 3.4 except for the changing α_j with temperature.

The amplitudes and inter-component phase differences of order parameters change with temperature, leading to variation in stable domain-wall structures. As a result, both height and width of fractional flux plateau should change as temperature is swept. It is also possible that a phase kink becomes unstable and changes to another one at a critical temperature, leading to a jump of flux since different pairs of phase kinks correspond to different fluxes.

Here we give a typical example of temperature dependence of trapped flux with our numerical results shown in Fig. 3.6. For simplicity, we consider the linear temperature dependence of α_j with $\alpha_j = \alpha_j(0)(1 - T/T_{cj})$ where $\alpha_j(0) < 0$ and $T_{c1} = T_{c2} = T_{c3}$. At the initial state at $T = 0.7T_c$, the stable fractional flux is $0.29\Phi_0$ with phase kink D_{12} at domain wall I and D_{13} at domain wall II. As temperature increases, the value of the fractional flux changes thereupon. At $T \approx 0.82T_c$, D_{13} becomes unstable and changes to D_{12}, and simultaneously a flux jump takes place.

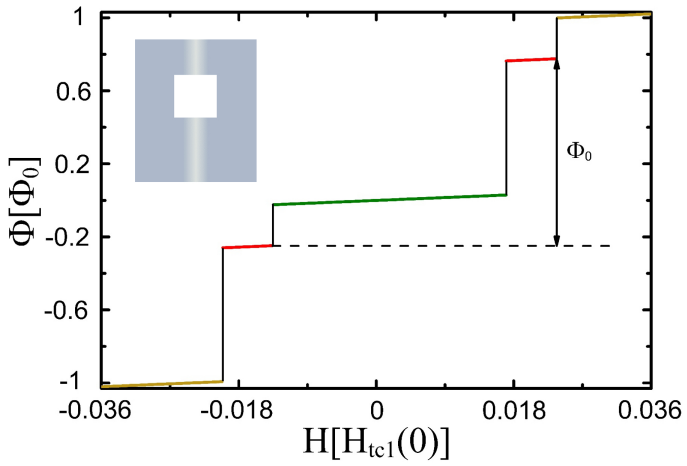

FIGURE 3.7: Magnetization curve with two fractional flux plateaus for an asymmetric superconductor loop, where the width of side including domain II is enlarged to $12\lambda_1(0)$ from that given in Fig. 3.5. The parameters are the same as Fig. 3.4 except for $\alpha_1' = 0.025$, $\alpha_2' = 0.028$ and $\alpha_3' = 0.022$.

3.4 Asymmetric Superconductor Loop

Up to this point, the superconductor loop is presumed to have the same width at domain wall I and II, which guarantees the degeneracy of domain-wall energy between phase-kink pairs [D_{ik}/D_{jk}] and [D_{jk}/D_{ik}]. In this case, it is easy to see that the magnetization curve in Fig. 3.3 should be symmetric with respect to the direction of magnetic field. In general, the two widths can be different. In the latter case [D_{ik}/D_{jk}] may be unstable even though [D_{jk}/D_{ik}] is stable associated with free-energy minimum. As shown in Fig. 3.7 for an asymmetric superconducting loop, the fractional flux plateau at $\Phi = 0.74\Phi_0$ remains stable for $0.017 \leq H/H_{tc1}(0) \leq 0.023$, while that at $\Phi = 0.26\Phi_0$ disappears in contrast to Fig. 3.5, since they are associated with different phase-kink configurations at domain wall I and II. It is worth noticing that even in this asymmetric loop the plateau at $\Phi = -0.26\Phi_0$ is still stable for $-0.020 \leq H/H_{tc1}(0) \leq -0.014$, since it is associated with the same phase-kink configuration with that at $\Phi = 0.74\Phi_0$ and a difference of flux quantum Φ_0 coming from the first term in Eq. (3.2). In this asymmetric loop, the magnetization curve is asymmetric with respect the direction of magnetic field as in Fig. 3.7. The property that fractional flux plateaus in positive and negative magnetic fields are paired with the difference of flux quantum Φ_0 is robust, and can be taken as a crosscheck for fractional flux plateaus originated from the TRSB state.

3.5 Discussions and Conclusions

In the present chapter we study the case that the left and right halves of the superconductor loop take the two TRSB states with opposite chiralities. This situation can be realized in experiments by cooling the whole system from temperature above T_c with laser heat pulse irradiated on region I and II [94]. The two halves condensate independently and by chance arrive at the different TRSB superconducting states, leading to the two domain walls at region I and II after releasing the irradiation. In order to check the stability of this configuration, we estimate the free energy of the whole system in terms of TDGL approach. As shown in Fig. 3.8, the state

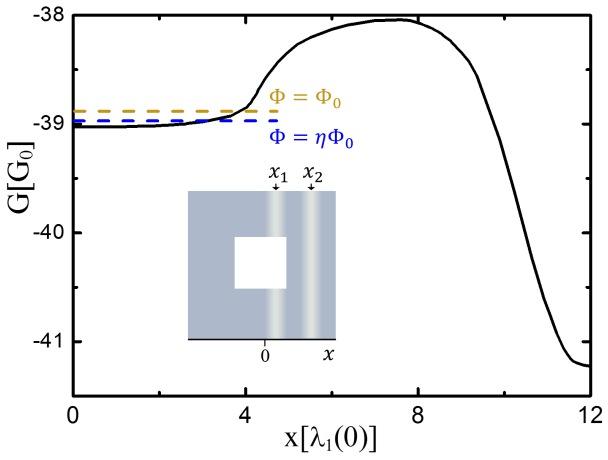

FIGURE 3.8: Gibbs free energy for the system in Fig. 1 with two halves occupied by the two TRSB states with opposite chiralities as a function of the location of domain walls x defined in the inset. Parameters and sample size are the same as Fig. 3.5.

with two domain walls locating at the middle of the top and bottom sides of the loop corresponds to a free-energy minimum. The domain walls once generated should be stable since moving them outside the loop is prohibited by a large free-energy barrier which is produced by an elongated, single domain wall during the process of domain-wall relocating (see that at x_2 in the inset of Fig. 3.8). The stability of the present setup against relocating one of the two domain walls along the loop can be provided by widening the left and right arms of the loop. The increase in free energy in states with fractional fluxes and integer flux quanta upon application of external magnetic field is smaller by one order of magnitude than the free-energy barrier as seen in Fig. 3.8, which justifies the discussion on fractional flux plateaus in the present work.

At this point we notice that the free-energy barrier in Fig. 3.8 generated by the two TRSB states at the two halves

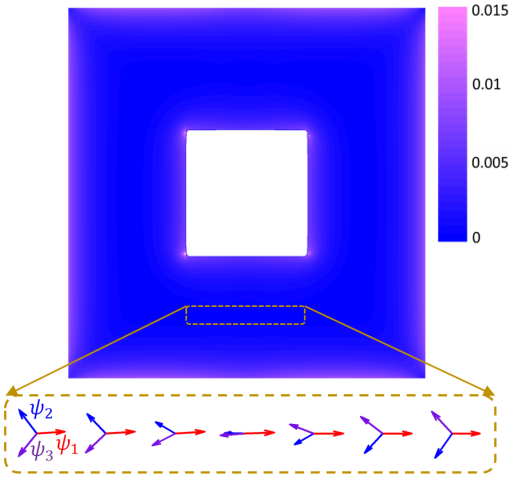

FIGURE 3.9: Distribution of supercurrent density $\mathbf{J}'$ in the superconductor loop for the fractional flux plateau of $\Phi = 0.26\Phi_0$ in Fig. 5, and that of order parameters on domain wall II. The directions and lengths of arrows refer to phases and amplitudes of order parameters, where $|\psi_2|$ and $|\psi_3|$ are suppressed to 0.63 and 0.77 of the bulk values while $|\psi_1|$ remains almost unchanged.

of superconductor loop is crucially important for the thermodynamic stability of fractional flux plateaus. From Eq. (3.2) one might think that a two-component superconductor or a three-component one with preserved TRS can also accommodate fractional fluxes. However, in these cases there is no free-energy barrier like that in Fig. 3.8, and states with fractional fluxes are unstable.

An example of the distribution of supercurrent density in the superconductor loop and order parameters on domain walls is shown in Fig. 3.9, where the superconductivity survives in all components and the Meissner effect screens the magnetic field and thus the total supercurrent to zero. The important feature here is that, although the supercurrents in individual components are not zero due to the phase shifts, they flow in the opposite directions and cancel each other, leading to zero total supercurrent. The situation of a domain wall as discussed in the present work is quite different from a vortex, where the phase winding induces a divergent kinetic energy, which requests the total suppression of amplitude of the superconducting order parameter at the vortex core.

Half-valued fluxoid jumps in magnetization curve was reported in a small multi-component superconducting sample comparable with penetration length[90]. This results in no full screening of magnetic field, and thus the magnetization curve exhibits finite slope for any external magnetic field. Namely, there is no fractional flux plateau in their system. In previous studies on vortex states of TRSB superconductor it was discussed that vortex cores of different condensates can deviate from each other in space [47, 57, 95–97]. However, without a closed path along which supercurrent is zero everywhere, there is no fractional flux plateau in magnetization curve.

To summarize, we have studied the magnetic response of a loop of three-component superconductor with two degenerate time-reversal symmetry broken states at two halves. When the two domain walls between the two halves accommodate different inter-component phase kinks, fractional flux plateaus appear in the magnetization curve which form pairs related to each other by the flux quantum. These properties are expected to be helpful for detecting experimentally the time-reversal symmetry broken superconducting state which can be realized in iron-pnictide superconductors. In a general point of view, this endeavour provides a novel chance to explore relative phase difference, phase kink and soliton in ubiquitous multi-component superconductivity.

Chapter 4

Dissociation of Vortices in Multi-Component Superconductors

In a type II superconductor, magnetic field penetrates into sample in terms of vortices associated with tiny magnetic fluxes. In single-band case, a vortex, namely a 2π phase rotation of the superconducting order parameter, carries quantized magnetic flux Φ_0. Multi-band superconductors are different because multiple condensates simultaneously couple to a common gauge field, and a vortex associated with 2π phase rotation in one condensate only carries a fraction flux as shown in the previous chapter. When interband phase differences are locked to each other due to strong couplings, phase rotation along a closed path is the same for different condensates. Therefore, vortices in different bands overlap in space, which makes the vortex in an individual component difficultly observed. The situation is different when a phase separation exists between the two time-reversal symmetry broken (TRSB) superconducting states with opposite chiralities in a sample. On domain walls [41, 42, 57, 98], interband phase difference develops a phase kink as shown in Fig. 4.1, resulting in different winding numbers in different components in presence of external magnetic field and thus dissociation of vortices in different components. In the present work we consider a constriction junction where such a domain wall is stabilized due to the small size of junction.

4.1 Model

In the present work, we study superconductors with external magnetic field where the order parameters are inhomogeneous. A direct minimization of GL free energy is difficult in this case. We use the same TDGL approach we introduced in the previous chapter.

As an icon we mainly focus here on the isotropic case ($\alpha_1 = \alpha_2 = \alpha_3 \equiv \alpha, \beta_1 = \beta_2 = \beta_3 \equiv \beta, m_1 = m_2 = m_3 \equiv m, \gamma_{12} = \gamma_{13} = \gamma_{23} \equiv \gamma < 0$), where the dimensionless GL free energy function is given by

$$F' = \sum_{j=1,2,3} \left[\alpha' \left|\psi'_j\right|^2 + \frac{1}{2}\left|\psi'_j\right|^4 + \frac{1}{m'}\left| \left(\frac{1}{i\kappa_1}\nabla - \mathbf{A}' \right) \psi'_j \right|^2 \right] - \sum_{j,k=1,2,3;j<k} \gamma' \left(\psi_j^{*\prime} \psi'_k + c.c. \right) + (\nabla \times \mathbf{A}')^2 \qquad (4.1)$$

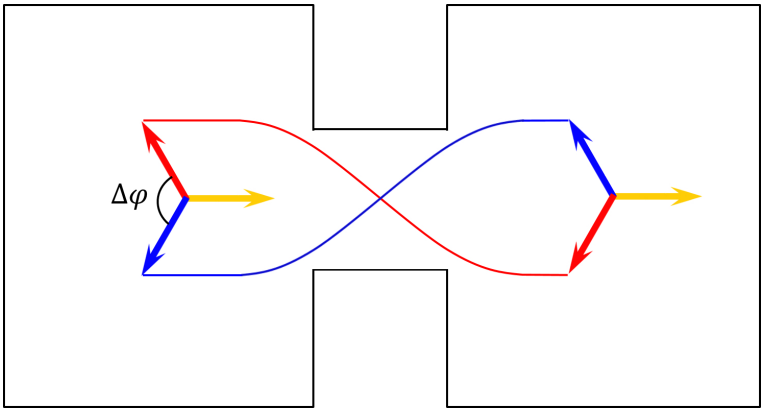

FIGURE 4.1: Schematics of constriction junction between two bulks with distinct TRSB states. A domain wall forms on the constriction where phase difference between red and blue order parameters $\Delta\varphi$ closes and opens again.

by using the dimensionless units in Eq. (3.4). T_c is determined by $\alpha(T_c) + \gamma = 0$. The degenerate TRSB states are $\hat{\Psi} = |\psi|(1, e^{i2\pi/3}, e^{i4\pi/3})$ and $\hat{\Psi}^* = |\psi|(1, e^{-i2\pi/3}, e^{-i4\pi/3})$ where $|\psi| = \sqrt{-\alpha - \gamma}$ for $T < T_c$. In a TDGL simulation, the sample is discretized into a grid of meshes. The mesh size should be carefully selected because a too small size increases the simulation time, which may cause insufficient relaxation, and large sizes may give artificial results. Here, we carefully select the mesh size as $\Delta x = \Delta y = 0.1\lambda_1(0)$ when parameters are $\alpha = 0.2, \gamma = -0.3$ and $\kappa_1 = 4$. We confirmed that further decreasing the mesh size does not change the results.

4.2 Dissociated Vortices on Constriction

Here we consider a structure of two bulks connected by a constriction as shown in Fig. 4.1. The size of constriction is adjusted to be comparable with the coherence length. We focus on the case with distinct TRSB states ($\hat{\Psi}$ and $\hat{\Psi}^*$) in the two bulks, and thus a domain wall forms on the constriction where configuration of three order parameters deforms from the rigid $2\pi/3$ structure. For example, phase difference between blue and red order parameters closes once and opens again, which forms a phase kink as shown in Fig. 4.1.

A laser heat pulse can be used to realize this situation in experiments [94]. At temperature above T_c, we irradiate the heat pulse on the constriction. When we cool the sample below T_c, the two bulks transform to superconducting states with distinct TRSB states by chance. We then switch off the heat pulse. Superconductivity recovers on the constriction and a domain wall forms. After that we apply the magnetic field to bring vortices into the superconductor.

In simulations, two bulks are put at TRSB states with opposite chiralities as the initial condition of TDGL equations. The self-consistent evolution drives the system to a stable state with a domain wall on the constriction. Then we switch on the external magnetic field H, and the system evolves again with flux penetrating into the sample from the boundaries and forming vortices inside. A typical vortex configuration near the constriction is shown in Fig. 4.2 for the final stable state. It is interesting to find that on the constriction only ψ_2 has a 2π phase winding but ψ_1 and ψ_3 do not, as seen in Fig. 4.2(a).

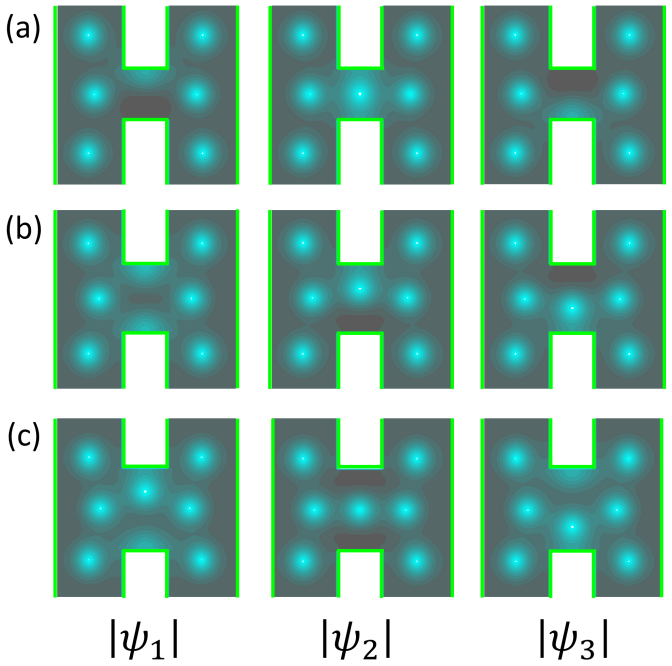

FIGURE 4.2: Simulation results of stable vortex distribution in three components in presence of domain wall on constriction. All panels are contour figures of amplitudes of three order parameters where red, blue and yellow in Fig. 4.1 correspond to component-1, 2 and 3 respectively. Area in panel is 10×10 which is a part of a larger sample with boundaries shown by green lines. Width of constriction in (a), (b) and (c) is 2.6, 3.6 and 4.4. Parameters are $\alpha' = 0.2$, $H' = 0.25$, $\gamma' = -0.3$ and $\kappa_1 = 4.0$.

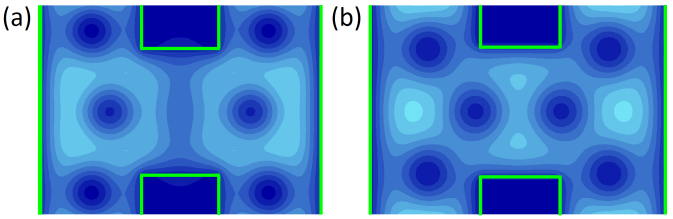

FIGURE 4.3: Magnetic field distribution on constriction when two bulks are at (a) two distinct TRSB states (b) an identical TRSB state. Parameters are the same as Fig. 4.2. Area in panel is 10×7 which is a part of a large sample with boundaries shown by green lines. Width of constriction is the same as Fig. 2(c).

We then increase the width of constriction, vortices in component-1 and component-3 start to penetrate the constriction as shown in Figs. 4.2(b) and (c). We can see that vortex cores in different components do not overlap on the constriction, in contrast to those outside the constriction area. When vortices in all components overlap, all order parameters at the core are zero which allow strong magnetic field penetration. While on the constriction, only one order parameter is zero at vortex core, and thus the penetrated field is weak due to the screening from the other two components. These dissociated vortices form a ribbon-like distribution of magnetic field as shown in Fig. 4.3(a) and Fig. 4.4. In a symmetric sample, the vortex configuration should be symmetric as seen in Fig. 4.4(a). When the constriction shifts from center as shown in Fig. 4.4(b), the ribbon becomes asymmetric as well. This is different from a previous work [95], where irregular ribbon structures were obtained despite of symmetric sample. When the two bulks at the two sides of constriction take a same TRSB state, there is only integer vortices as shown in Fig. 4.3(b).

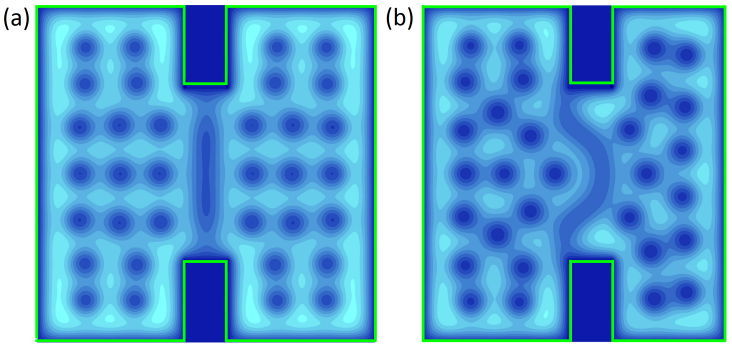

FIGURE 4.4: Magnetic field distribution in presence of dissociated vortices for different sample shapes. Parameter are the same as Fig. 4.2. The sample size is 20×20 for (a) and 18×20 for (b) with boundaries shown by green lines. Width of the constriction is 10.

4.3 Discussions and Conclusions

The dissociation of vortices in different components discussed in this chapter are based on the structure of domain walls in TRSB states. Therefore, the creation and stability of the domain wall are important. In the present chapter, we use a controllable method: create a domain wall with laser heat pulse and stabilize the domain wall by shrinking the its size. In this way, the domain wall can be stable as long as the section of constriction is much smaller than the bulk.

To summarize, in superconductors with three or more components, a stable domain wall forms on a small junction between two time-reversal symmetry broken states with opposite chiralities. Under external magnetic field, vortices in different components dissociate from each other on the junction, where magnetic field distribution exhibits ribbon-like structures. This is a clear manifestation of time-reversal symmetry broken superconducting states in multi-component superconductors.

Chapter 5

First-Order Phase Transition associated with Vortex Penetration in Two-Component Superconductors

Superconductors are classified into type-I and type-II depending on their response to applied magnetic fields [19]. When applied fields are small, superconductors of both types expel magnetic field completely which is known as the Meissner effect. For larger fields, Type-I superconductors still accommodate the Meissner state (uniform superconducting state) until a sudden break down of superconductivity at thermodynamic critical field H_{tc} through a first-order phase transition. However in type-II superconductors, superconducting state is broken little by little starting from H_{c1} ($H_{c1} < H_{tc}$) where a single vortex with a normal core begins to penetrate. Vortex number increases under larger applied fields until the complete suppression of superconductivity at H_n ($H_n > H_{tc}$). The phase transition are continuous at both H_{c1} and H_n.

Due to the evidence of two superconducting gaps found in V[99], Nb-doped $SrTiO_3$[100] and MgB_2 [27, 101], the magnetic responses of two-band superconductors attract a lot of attentions. Coherence length in individual components, penetration length and the conventional interface have been adopted to discuss the vortex states in two-component superconductors [93, 102–105].

In this chapter we will renew the study with the help of one-dimensional variations of order parameters and magnetic induction with two boundaries at normal state under thermodynamic critical field H_{tc}. In a certain regime of parameters, we find a confined superconducting phase where the superconductivity grows to a state different from the bulk state and the magnetic field is not screened to zero. Correspondingly, we find a first-order phase transition between the Meissner and vortex state.

5.1 Two-Component Ginzburg-Landau Theory

Here we adopt Ginzburg-Landau (GL) theory to study the two-component superconductivity. The free-energy density functional is given by [50]

$$\begin{aligned} F &= \sum_{j=1,2}\left[\alpha_j\left|\psi_j\right|^2+\tfrac{\beta_j}{2}\left|\psi_j\right|^4+\tfrac{\hbar^2}{2m_j^*}\left|\left(\tfrac{\nabla}{i}-\tfrac{2\pi}{\Phi_0}\mathbf{A}\right)\psi_j\right|^2\right] \\ &\quad -\gamma\left(\psi_1^*\psi_2+c.c.\right)+\tfrac{1}{8\pi}\left(\nabla\times\mathbf{A}\right)^2, \end{aligned} \tag{5.1}$$

where α_j is a temperature-dependent coefficient which is negative when $T < T_{cj}$ and positive when $T > T_{cj}$, where T_{cj} is the critical temperature of the superconducting component-j in absence of inter-component coupling, and γ is the coefficient of inter-component coupling taken as constant for simplicity. By variating F with respect to variations in ψ_j^* and $\mathbf{A}$, we obtain the GL equations

$$\alpha_j\psi_j+\beta_j|\psi_j|^2\psi_j+\frac{1}{2m_j}\left(\frac{\hbar}{i}\nabla-\frac{2e}{c}\mathbf{A}\right)^2\psi_j-\gamma\psi_k=0 \tag{5.2}$$

with $j,k=1,2$ but $j\neq k$ and

$$\frac{c}{4\pi}\nabla\times\nabla\times\mathbf{A}=\sum_{j=1,2}\frac{2e\hbar}{m_j}|\psi_j|^2\left(\nabla\varphi_j-\frac{2\pi}{\Phi_0}\mathbf{A}\right). \tag{5.3}$$

Now we consider the temperature very close to the critical temperature T_c and obtain the solutions approximated to the first of $(1-T/T_c)$. The superconducting order parameters in bulk ψ_{sj} follow the linear GL equations

$$\begin{bmatrix} \alpha_1 & -\gamma \\ -\gamma & \alpha_2 \end{bmatrix}\begin{bmatrix} \psi_{s1} \\ \psi_{s2} \end{bmatrix}=0 \tag{5.4}$$

or in a vector form $\mathbf{Q}\cdot\mathbf{\Psi}=\mathbf{0}$ with coupling matrix $\mathbf{Q}$. T_c is given by the highest temperature where the determinant of $\mathbf{Q}$ becomes zero; i.e.,

$$\alpha_1(T_c)\alpha_2(T_c)-\gamma^2=0. \tag{5.5}$$

It is easy to see that both α_j are positive close to T_c and ratio between order parameters is

$$\frac{\psi_{s1}}{\psi_{s2}}\approx\frac{\gamma}{\alpha_1(T_c)}=\frac{\alpha_2(T_c)}{\gamma}. \tag{5.6}$$

By combining Eq. (5.6) with the full GL equations

$$\begin{bmatrix} \alpha_1+\beta_1\psi_{s1}^2 & -\gamma \\ -\gamma & \alpha_2+\beta_2\psi_{s2}^2 \end{bmatrix}\begin{bmatrix} \psi_{s1} \\ \psi_{s2} \end{bmatrix}=0, \tag{5.7}$$

we obtain the bulk value of order parameters

$$\psi_{s1}^2=\frac{1}{\alpha_1}\left(\frac{\beta_1}{\alpha_1^2}+\frac{\beta_2}{\alpha_2^2}\right)^{-1}\left(1-\frac{\alpha_1\alpha_2}{\gamma^2}\right) \tag{5.8}$$

and

$$\psi_{s2}^2 = \frac{1}{\alpha_2}\left(\frac{\beta_1}{\alpha_1^2} + \frac{\beta_2}{\alpha_2^2}\right)^{-1}\left(1 - \frac{\alpha_1\alpha_2}{\gamma^2}\right), \tag{5.9}$$

from which the thermodynamic critical field H_{tc} is given by

$$H_{tc} = \sqrt{4\pi\left(\frac{\beta_1}{\alpha_1^2} + \frac{\beta_2}{\alpha_2^2}\right)^{-1}}\left(1 - \frac{\alpha_1\alpha_2}{\gamma^2}\right). \tag{5.10}$$

From Eq. (5.3), we obtain the penetration length

$$\lambda^2 = \frac{c^2}{16\pi e^2}\left[\left(\frac{1}{m_1\alpha_1} + \frac{1}{m_2\alpha_2}\right)\left(1 - \frac{\alpha_1\alpha_2}{\gamma^2}\right)\right]^{-1}\left(\frac{\beta_1}{\alpha_1^2} + \frac{\beta_2}{\alpha_2^2}\right) \tag{5.11}$$

which becomes divergent at T_c.

Next we explore the coherence length by considering a small disturbance of order parameter ψ_j from the bulk value ψ_{sj} without magnetic field in presence. We set $\psi_j = \psi_{sj} + \delta_j$, where $\delta_j \ll \psi_{sj}$. From Eq. (5.2), we obtain

$$\alpha_j\delta_j + 3\beta_j|\psi_{sj}|^2\delta_j - \frac{\hbar^2}{2m_j}\nabla^2\delta_j - \gamma\delta_k = 0. \tag{5.12}$$

For exponentially decaying disturbance $\delta_j = A_j\exp(-\sqrt{2}x/\xi)$, we have

$$\begin{bmatrix} \alpha_1 + 3\beta_1\psi_{s1}^2 - \frac{\hbar^2\xi^{-2}}{m_1} & -\gamma \\ -\gamma & \alpha_2 + 3\beta_2\psi_{s2}^2 - \frac{\hbar^2\xi^{-2}}{m_2} \end{bmatrix}\begin{bmatrix} A_1 \\ A_2 \end{bmatrix} = 0. \tag{5.13}$$

The coherence length ξ is determined by the zero determinant of the above matrix. Although there are two solutions, we found that only one coherence length is divergent close to T_c and it is given by

$$\xi^{-2} = \frac{2}{\hbar^2}\left(\frac{1}{m_1\alpha_1} + \frac{1}{m_2\alpha_2}\right)^{-1}\left(1 - \frac{\alpha_1\alpha_2}{\gamma^2}\right). \tag{5.14}$$

Now let us study the nucleation field in a bulk sample in the presence of magnetic field B along the z axis. B is uniform and equals to applied magnetic field H. A conventional gauge is $A_y = Hx$. Because order parameters are very small at nucleation field, we adopt the linear GL equations

$$\alpha_j\psi_j + \frac{1}{2m_j}\left(\frac{\hbar}{i}\nabla - \frac{2e}{c}Hx\right)^2\psi_j - \gamma\psi_k = 0. \tag{5.15}$$

We look for a solution in the form $\psi_j = e^{ik_y y}e^{ik_z z}f_j(x)$. Nucleation field H_n is obtained at $k_y = k_z = 0$, and thus we have

$$\left[-\nabla_x^2 + \left(\frac{2\pi H_n}{\Phi_0}\right)^2 x^2\right]f_j + \frac{2m_j}{\hbar^2}\left(\alpha_j f_j - \gamma f_k\right) = 0. \tag{5.16}$$

Based on the lowest level Landau solution with $f_j = b_j \exp\left(-\frac{1}{2}\frac{2\pi H_n}{\Phi_0}x^2\right)$, we obtain

$$\begin{bmatrix} \alpha_1 + \frac{1}{m_1}\frac{\pi\hbar^2 H_n}{\Phi_0} & -\gamma \\ -\gamma & \alpha_2 + \frac{1}{m_2}\frac{\pi\hbar^2 H_n}{\Phi_0} \end{bmatrix} \begin{bmatrix} b_1 \\ b_2 \end{bmatrix} = 0. \tag{5.17}$$

For nonzero solution of order parameters, the determinant of the above matrix is required to be zero, which gives the nucleation field

$$H_n = \frac{\Phi_0}{\pi\hbar^2}\frac{1-\alpha_1\alpha_2/\gamma^2}{1/m_1\alpha_2 + 1/m_2\alpha_2}, \tag{5.18}$$

and the ratio between amplitudes of two order parameters

$$\frac{b_1}{b_2} = \frac{\gamma}{\alpha_1}. \tag{5.19}$$

5.2 Superconductivity under Magnetic Fields

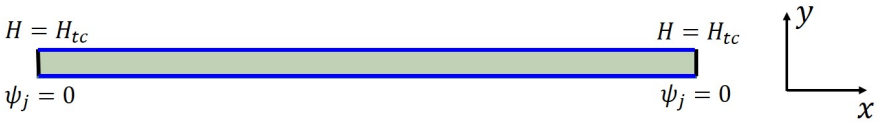

FIGURE 5.1: An infinitely large superconductor with variations of superconducting order parameters and magnetic induction along x-axis, with two boundaries taken as the normal state under the thermodynamic field H_{tc}.

Now we consider an infinitely large two-dimensional superconductor as shown in Fig. (5.1), where the superconductivity is uniform along the y-axis but varies along the x-axis, and thus we are solving a one-dimensional problem. The boundaries at x-axis are chosen at the normal state under H_{tc} because this state has the same Gibbs free energy with the bulk state without magnetic field.

This one-dimensional problem is useful in discussing the magnetic response in single-component superconductors. When superconductivity grows to the bulk state with complete suppression of the magnetic field, a negative interface energy and thus a type-II superconductivity are suggested. On the other hand, when superconductivity cannot grow at all, a positive interface energy and thus a type-I superconductivity are suggested.

We adopt this model on the two-component superconductors and hope to find something unconventional. We use the two-component TDGL approach where the GL free energy functional is given by

$$F' = \sum_{j=1,2}\left[\alpha'_j\left|\psi'_j\right|^2 + \frac{\beta'_j}{2}\left|\psi'_j\right|^4 + \frac{1}{m_{j'}}\left|\left(\frac{1}{i\kappa_1}\nabla - \mathbf{A}'\right)\psi'_j\right|^2\right] - \gamma'\psi^{*\prime}_j\psi'_k + (\nabla\times\mathbf{A}')^2. \tag{5.20}$$

with all quantities defined in dimensionless units provided in Eq. (3.4).

We obtain a new superconducting state where the distributions of superconducting order parameters and magnetic fields are shown in Fig. 5.2(a) and (b). In Fig. 5.2(a) order parameters grow to $\psi_{s'j}$ in the center of the system, which is smaller than the bulk order parameter ψ_{sj}, and then decrease in a symmetric way to zero.

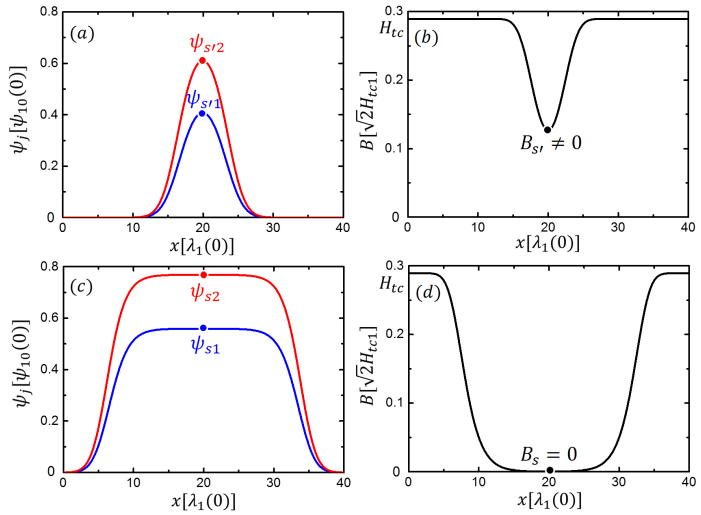

FIGURE 5.2: Distribution of (a) order parameters and (b) magnetic fields in the sample shown in Fig. 5.1. The parameters for (a) and (b) are $\alpha_1' = \alpha_2' = 0.1$, $\beta_1' = 1$, $\beta_2' = 0.2$, $m_1' = 1$, $m_2' = 6$, $\gamma' = 0.3$, $\kappa_1 = 0.71$, and for (c) and (d) are the same except for $\kappa_1 = 0.8$.

Since the superconductivity only appear in a confined region, we name it "confined superconducting phase". Correspondingly, the magnetic field decreases to $B_{s'} \neq 0$ at the center and then increases back to H_{tc}. When the length of the sample increases, the confined superconducting state remains unchanged. We find

$$\frac{\psi_{s'1}}{\psi_{s'2}} \neq \frac{\psi_{s1}}{\psi_{s2}}, \tag{5.21}$$

which indicates $(\psi_{s'1}, \psi_{s'2})$ is a different state from (ψ_{s1}, ψ_{s2}).

solution is for two-component system, which however behaves similarly to conventional single component ones.

For comparison we draw Fig 5.2(c) and (d) which is the solution for two-component system, which however behaves similarly to conventional single-component ones: the order parameters grow from the boundaries and reach the bulk values in the interior, where terraces of bulk order parameter form. When the length of sample increases, the order parameters still extends to the boundaries and the terrace becomes longer. Here we use the name "extended superconducting phase" to distinguish it from the confined superconducting phase.

5.3 Parameter Dependence

Now we continuously change the parameter κ_1 and obtain the excess free energy η of the stable state as

$$\eta = \int_0^{2L} \left(F - \frac{H_{tc} B}{4\pi} + \frac{H_{tc}^2}{8\pi} \right) dx \tag{5.22}$$

where $x = 0$ and $x = 2L$ are the coordinate of the left and right side of the sample. The result is shown in Fig. 5.3, where there are three regions of κ_1 associated with different stable states, divided by κ_1^* and κ_1^{**}. We have $\kappa_1^* \approx 0.68$ and $\kappa_2^{**} \approx 0.725$ for the parameters given in Fig. 5.2.

For $\kappa_1 < \kappa_1^*$, the stable state is normal state with $\eta = 0$, which is due to $H_n < H_{tc}$. At $\kappa_1 = \kappa_1^*$, we have $H_c = H_{tc}$. For $\kappa_1^* < \kappa_1 < \kappa_1^{**}$, the confined superconducting phase appears. As κ_1 is increased to κ_1^{**}, the peak values of order parameters approach the bulk value. At $\kappa_1 = \kappa_1^{**}$, the confined and extended superconducting phases have the same free energy, and for $\kappa_1 > \kappa_1^{**}$, the extended superconducting phase is always obtained.

5.4 Phase Diagram

From the information of interface between superconducting and normal state, we can analyze the vortex states under applied magnetic field and the associated phase transitions.

For $\kappa < \kappa_1^*$, we have $H_n = H_{tc}$ and thus a typical Type-I superconductivity is obtained. Superconductivity collapse from the Meissner state (uniform superconducting state) to normal state associated with a magnetization jump, which indicates a first-order phase transition at H_{tc}, as shown in the phase diagram Fig. 5.4(a).

The region $\kappa_1 > \kappa_1^{**}$ is also conventional because the superconducting order parameters grow to bulk order parameter from the normal state under H_{tc}, which indicates a typical type-II superconductor. Therefore, we still have the continuous phase transition at vortex penetration field H_{c1} and nucleation field H_n as shown in Fig. 5.4(c).

The nontrivial region with novel physics is $\kappa_1^* < \kappa_1 < \kappa_2^{**}$, where the confined superconducting phase is stable. This indicates that upon penetration vortices form vortex lattice which the lattice constant as the width of the confined superconducting region. Between two vortex cores the superconductivity recovers to a state different from the bulk superconducting state and the magnetic field is not suppressed to zero. Therefore, we have simultaneous entry of many vortices together to form a tight vortex lattice in the whole sample at the threshold

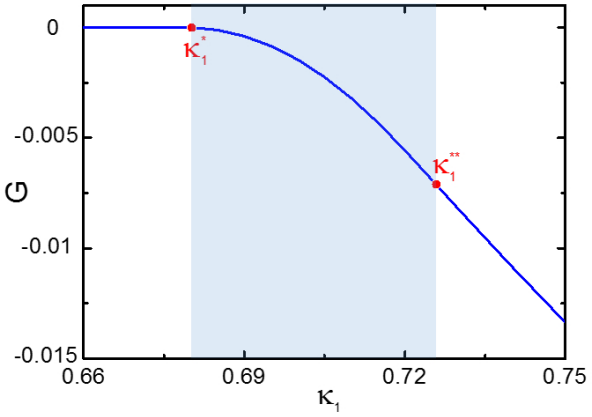

FIGURE 5.3: κ_1 dependence of excess free energy of two-component superconductor in Fig. (5.1). The parameters except κ_1 are the same with Fig. 5.2.

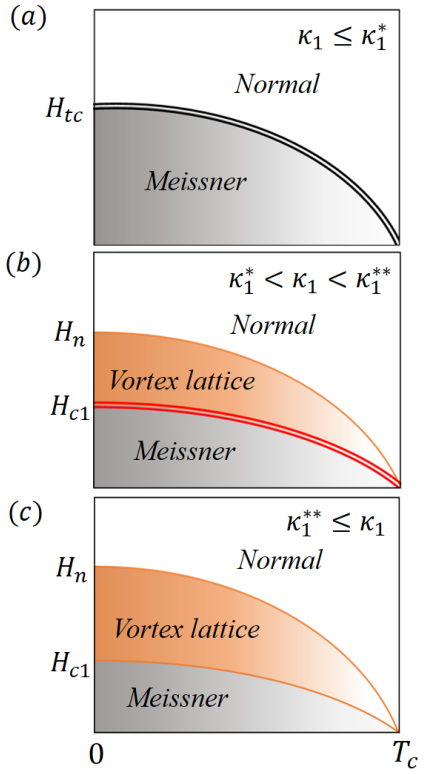

FIGURE 5.4: H-T phase diagram for two-component superconductors. Three diagrams correspond to three regions of κ_1 in Fig. 5.3. The double and single line represent first-order and continuous phase transition.

field H_{c1}, leading to a large magnetization jump which indicates a first-order phase transition. The phase diagram of this novel case is shown in Fig. 1.13(b).

5.5 Discussions and Conclusions

In single-component superconductors, we have $\kappa_1^* = \kappa_1^{**} = 1/\sqrt{2}$ which dichotomizes the superconductors to type-I and type-II superconductor. Therefore, the first-order phase transition associated with the vortex penetration is a unique phenomenon in multi-component superconductors. Here we introduced a new method to study the superconductivity under magnetic field by considering the grown superconductivity from the normal state under H_{tc}. This method is useless in single-component superconductors because the superconductivity only grows to the bulk state and the magnetic field screened to zero, which is equivalent to the study of interface between bulk superconducting state and the normal state. However, in multi-component superconductors, this method gives the novel confined superconducting phase.

Our theory is different the discussion of vortex penetration when symbolic $\xi_1 < \sqrt{2}\lambda < \xi_2$ is considered [102, 106], where ξ_1 and ξ_2 indicate the coherence length of two components in absence of the intercomponent coupling. The use of ξ_1 and ξ_2 constrains the study at temperature smaller than the critical temperature of each component, which implied the ignorance of intercomponent couplings. Here we study the system at temperature above T_{c1} and T_{c2} with effect of intercomponent couplings considered.

To summarize, in this chapter we have studied the magnetic response of a two-component superconductor by exploring the one-dimensional variations of order parameters and magnetic induction with two boundaries at the normal state under H_{tc} for convenience. In a certain regime of parameters, we find a confined superconducting phase where superconductivity grows to a state different from the bulk state and the magnetic field is not suppressed to zero, which has no counterpart in single-component superconductors. For superconductors in this parameter regime, upon penetration many vortices enter together to form a tight vortex lattice, which leads to a first-order phase transition.

Chapter 6

Conclusions

In superconductors with three or more bands, time-reversal symmetry may be broken in the presence of repulsive interband couplings, resulting in a pair of degenerate states characterized by opposite chiralities. In this thesis, I have mainly studied the novel phenomena in three-component superconductors with broken time-reversal symmetry.

I have considered a Josephson junction between a three-band superconductor with broken TRS and a single-band superconductor. Phenomena such as asymmetric critical currents, subharmonic Shapiro steps and symmetric Fraunhhofer patterns are revealed theoretically. It is intriguing to notice that asymmetric critical currents have been observed in a hybrid junction between a single-band superconductor PbIn and an iron-based superconductor $BaFe_{2-x}Co_xAs_2$. The difference between two critical currents is well beyond the experimental precision. In the light of our theoretical work, TRSB states have already been realized in iron-based superconductors.

To cross check the time-reversal symmetry broken state, I have explored the magnetic response a loop of such superconductor with two halves occupied by the two states with opposite chiralities. Fractional flux plateaus are found in magnetization curve associated with free-energy minima, where the two domain walls between the two halves of loop accommodate different inter-component phase kinks leading to finite winding numbers around the loop only in a part of all condensates. Fractional flux plateaus form pairs related by the flux quantum $\Phi_0 = hc/2e$, although they individually take arbitrary values depending on material parameters and temperature. This phenomenon is a clear evidence of time-reversal symmetry broken superconductivity, and in a general point of view it provides a novel chance to explore relative phase difference, phase kink and soliton in ubiquitous multi-component superconductivity such as that in iron pnicitides.

When prepared carefully there is a stable domain wall on a constriction which connects two bulks in states with opposite chiralities. Under certain external magnetic fields, vortices in different components dissociate with each other, resulting in a ribbon shape distribution of magnetic field at the position of the domain wall.

In addition to superconductors with three or more components, novel phenomena are also available in two-component superconductors. We have studied the magnetic response of two-component superconductors. In a certain regime of parameters, we find a confined superconducting phase where superconductivity grows to a state different from the bulk state and the magnetic field is not suppressed to zero, which has no counterpart

in single-component superconductors. For superconductors in this parameter regime, upon penetration many vortices enter together to form a tight vortex lattice, which leads to a first-order phase transition.

Bibliography

[1] F. London. Superfluids. *John Wiley & Sons, Inc., New York*, 1950.

[2] J. Bardeen, L. N. Cooper, and J. R. Schrieffer. Theory of superconductivity. *Phys. Rev.*, 108:1175, 1957. URL http://journals.aps.org/pr/abstract/10.1103/PhysRev.108.1175.

[3] B. S. Deaver and W. M. Fairbank. Experimental evidence for quantized flux in superconducting cylinders. *Phys. Rev. Lett.*, 7:43, 1961. URL http://dx.doi.org/10.1103/PhysRevLett.7.43.

[4] R. Doll and W. Näbauer. Experimental proof of magnetic flux quantization in a superconducting ring. *Phys. Rev. Lett.*, 7:51, 1961. URL http://dx.doi.org/10.1103/PhysRevLett.7.51.

[5] B. D. Josephson. Possible new effects in superconductive tunneling. *Physics Letters*, 1:251, 1962. URL http://www.sciencedirect.com/science/article/pii/0031916362913690#.

[6] P. W. Anderson and J. M. Rowell. Probable observation of the josephson superconducting tunneling effect. *Phys. Rev. Lett.*, 10:230, 1963. URL http://prl.aps.org/abstract/PRL/v10/i6/p230_1.

[7] I. K. Yanson, V. M. Svistunov, and I. M. Dmitrenko. Experimental observation of the tunneling effect for cooper pairs with the emission of photons. *Sov. Phys. JETP*, 21:650, 1965. URL http://www.jetp.ac.ru/cgi-bin/e/index/e/21/3/p650?a=list.

[8] K. K. Likharev. Superconducting weak links. *Rev. Mod. Phys.*, 51:101, 1979. URL http://rmp.aps.org/abstract/RMP/v51/i1/p101_1.

[9] R. P. Feynman, R. B.Leighton, , and M. Sands. The feynman lectures on physics, vol iii, quantum mechanics. *Addison-Wesley Publishing Company, Inc.*, 1965.

[10] W. H. Parker, D. N. Langenberg, A. Denenstein, and B. N. Taylor. Determination of $e/\hbar$, using macroscopic quantum phase coherence in superconductors. i. experiment. *Phys. Rev.*, 177:639, 1969. URL http://journals.aps.org/pr/abstract/10.1103/PhysRev.177.639.

[11] W. S. Corak, B. B. Goodman, C. B. Satterthwaite, and A. Wexler. Exponential temperature dependence of the electronic specific heat of superconducting vanadium. *Phys. Rev.*, 96:1442, 1954. URL http://journals.aps.org/pr/abstract/10.1103/PhysRev.96.1442.2.

[12] M. A. Biondi, A. T. Forrester, M. P. Garfunkel, and C. B. Satterthwaite. Experimental evidence for an energy gap in superconductors. *Rev. Mod. Phys.*, 30:1109, 1958. URL http://journals.aps.org/rmp/abstract/10.1103/RevModPhys.30.1109.

[13] E. Maxwell. Isotope effect in the superconductivity of mercury. *Phys. Rev.*, 78:477, 1950. URL http://journals.aps.org/pr/abstract/10.1103/PhysRev.78.477.

[14] C. A. Reynolds, B. Serin, W. H. Wright, and L. B. Nesbitt. Superconductivity of isotopes of mercury. *Phys. Rev.*, 78:487, 1950. URL http://dx.doi.org/10.1103/PhysRev.78.487.

[15] H. Fröhlich. Theory of the superconducting state. i. the ground state at the absolute zero of temperature. *Phys. Rev.*, 79:845, 1950. URL http://journals.aps.org/pr/abstract/10.1103/PhysRev.79.845.

[16] L. N. Cooper. Bound electron pairs in a degenerate fermi gas. *Phys. Rev.*, 104:1189, 1956. URL http://journals.aps.org/pr/abstract/10.1103/PhysRev.104.1189.

[17] M. Tinkham. Introduction to superconductivity. *McGraw-Hill, Inc., New York*, 1996.

[18] V. L. Ginzburg and L. D. Landau. On the theory of superconductivity. *zh. Eksp. Teor. Fiz.*, 20:1064, 1950.

[19] A. A. Abrikosov. On the magnetic properties of superconductors of the second group. *zh. Eksp. Teor. Fiz.*, 32:1442, 1957. URL http://www.mn.uio.no/fysikk/english/research/groups/amks/superconductivity/vortex/1957.html.

[20] L. P. Gor'kov. On the magnetic properties of superconductors of the second group. *Sov. Phys. JETP*, 36:1364, 1959. URL http://www.w2agz.com/Library/Classic%20Papers%20in%20Superconductivity/.

[21] P. G. De Gennes. Superconductivity of metals and alloys. *Westview Press*, 1999.

[22] D. Saint-James, G. Sarma, and E. J. Thomas. Type ii superconductivity. *Pergamon Press*, 1969.

[23] L. P. Gor'kov and G. M. Eliashberg. Generalization of the ginzburg-landau equations for non-stationary problems in the case of alloys with paramagnetic impurities. *zh. Eksp. Teor. Fiz.*, 54: 612, 1968. URL http://public.magnet.fsu.edu/Gorkov/Sov.%20Phys.%20%20JETP,%2027,%20328%20(1968).pdf.

[24] W. D. Gropp, H. G. Kaper, G. K. Leaf, D. M. Levine, M. Palumbo, and V. M. Vinokur. Numerical simulation of vortes dynamics in type-ii superconductors. *J. Comput. Phys.*, 123:254, 1996. URL http://www.sciencedirect.com/science/article/pii/S0021999196900224.

[25] H. Suhl, B. T. Matthias, and L. R. Walker. Bardeen-cooper-schrieffer theory of superconductivity in the case of overlapping bands. *Phys. Rev. Lett.*, 3:552, 1959. URL http://prl.aps.org/abstract/PRL/v3/i12/p552_1.

[26] J. Kondo. Superconductivity in transition metals. *Prog. Theor. Phys.*, 29:1, 1963. URL http://ptp.ipap.jp/link?PTP/29/1/.

[27] J. Nagamatsu, N. Nakagawa, T. Muranaka, Y. Zenitani, and J. Akimitsu. Superconductivity at 39 k in magnesium diboride. *Nature*, 410:63, 2001. URL http://www.nature.com/nature/journal/v410/n6824/full/410063a0.html.

[28] C. Buzea and T. Yamashita. Review of the superconduting properties of MgB_2. *Supercond. Sci. Technol.*, 14:R115, 2001. URL http://iopscience.iop.org/0953-2048/14/11/201.

[29] Y. Kamihara, T. Watanabe, M. Hirano, and H. Hosono. Iron-based layered superconductor $La[O_{1-x}F_x]FeAs$ ($x = 0.05 - 0.12$) with $t_c = 26k$. *Nature*, 130:3269, 2008. URL http://pubs.acs.org/doi/abs/10.1021/ja800073m.

[30] K. Ishida, Y. Nakai, and H. Hosono. To what extent iron-pnictide new superconductors have been clarified: A progress report. *J. Phys. Soc. Jpn.*, 78:062001, 2009. URL http://jpsj.ipap.jp/link?JPSJ/78/062001/.

[31] H. Kontani amd S. Onari. Orbital-fluctuation-mediated superconductivity in iron pnictides: Analysis of the five-orbital hubbard-holstein model. *Phys. Rev. Lett.*, 104:157001, 2010. URL http://prl.aps.org/abstract/PRL/v104/i15/e157001.

[32] H. Ding, P. Richard, K. Nakayam, K. Sugawara, T. Arakane, Y. Sekiba, A. Takayama, S. Souma, T̃. Sata, T. Takahashi, Z. Wang, X. Dai, Z. Fang, G. F. Chen, J. L. Luo, and N. L. Wang. Observation of fermi-surface-dependent nodeless superconducting gaps in $Ba_{0.6}K_{0.4}Fe_2As_2$. *EPL*, 83:47001, 2008. URL http://iopscience.iop.org/0295-5075/83/4/47001.

[33] K. Nakayama, T. Sato, P. Richard, Y. M. Xu, Y. Sekiba, S. Souma, G. F. Chen, J. L. Luo, N. L. Wang, H. Ding, and T. Takahashi. Observation of fermi-surface-dependent nodeless superconducting gaps in $Ba_{0.6}K_{0.4}Fe_2As_2$. *Europhys. Lett.*, 85:67002, 2009. URL http://iopscience.iop.org/0295-5075/85/6/67002/.

[34] V. Cvetkovic and Z. Tesanovic. Valley density-wave and multiband superconductivity in iron-based pnictide superconductors. *Phys. Rev. B*, 80:024512, 2009. URL http://prb.aps.org/abstract/PRB/v80/i2/e024512.

[35] I. Eremin and A. V. Chubukov. Magnetic degeneracy and hidden metallicity of the spin-density-wave state in ferropnictides. *Phys. Rev. B*, 81:024511, 2010. URL http://prb.aps.org/abstract/PRB/v81/i2/e024511.

[36] D. F. Agterberg, V. Barzykin, and L. P. Gorkov. Conventional mechanisms for exotic superconductivity. *Phys. Rev. B*, 60:14868, 1999. URL http://prb.aps.org/abstract/PRB/v60/i21/p14868_1.

[37] V. Stanev and Z. Tesanovic. Three-band superconductivity and the order parameter that breaks time-reversal symmetry. *Phys. Rev. B*, 81:134522, 2010. URL http://prb.aps.org/abstract/PRB/v81/i13/e134522.

[38] Y. Tanaka and T. Yanagisawa. Chiral ground state in three-band superconductors. *J. Phys. Soc. Japan*, 79:114706, 2010. URL http://jpsj.ipap.jp/link?JPSJ/79/114706/.

[39] R. G. Dias and A. M. Marques. Frustrated multiband superconductivity. *Supercond. Sci. Technol.*, 24:085009, 2011. URL http://iopscience.iop.org/article/10.1088/0953-2048/24/8/085009/meta;jsessionid=90C85B092C232B6C3BBDF45E16E10621.c4.iopscience.cld.iop.org.

[40] T. Yanagisawa, Y. Takana, I. Hase, and K. Yamaji. Vortices and chirality in multi-band superconductors. *J. Phys. Soc. Jpn.*, 81:024712, 2012. URL http://jpsj.ipap.jp/link?JPSJ/81/024712/.

[41] X. Hu and Z. Wang. Stability and josephson effect of time-reversal-symmetry-broken multicomponent superconductivity induced by frustrated intercomponent coupling. *Phys. Rev. B*, 85:064516, 2012. URL http://prb.aps.org/abstract/PRB/v85/i6/e064516.

[42] S. Z. Lin and X. Hu. Massless leggett mode in three-band superconductors with time-reversal-symmetry breaking. *Phys. Rev. Lett.*, 108:177005, 2012. URL http://prl.aps.org/abstract/PRL/v108/i17/e177005.

[43] S. Maiti and A. V. Chubukov. $s + is$ state with broken time-reversal symmetry in fe-based superconductors. *Phys. Rev. B*, 87:144511, 2013. URL http://journals.aps.org/prb/abstract/10.1103/PhysRevB.87.144511.

[44] B. J. Wilson and M. P. Das. Time-reversal-symmetry-broken state in the bcs formalism for a multi-band superconductor. *J. Phys.: Condens. Matter*, 25:425702, 2013. URL http://iopscience.iop.org/article/10.1088/0953-8984/25/42/425702#metrics.

[45] N. V. Orlova, A. A. Shanenko, M. V. Milosevic, and F. M. Peeters. Ginzburg-landau theory for multiband superconductors: Microscopic derivation. *Phys. Rev. B*, 87:134510, 2013. URL http://journals.aps.org/prb/abstract/10.1103/PhysRevB.87.134510.

[46] M. Marciani, L. Fanfarillo, C. Castellani, and L. Benfatto. Leggett modes in iron-based superconductors as a probe of time-reversal symmetry breaking. *Phys. Rev. B*, 88:214508, 2013. URL http://journals.aps.org/prb/abstract/10.1103/PhysRevB.88.214508.

[47] Y. Takahashi, Z. Huang, and X. Hu. *hct* phase diagram of multi-component superconductors with frustrated inter-component couplings. *J. Phys. Soc. Jpn.*, 83:034701, 2014. URL http://journals.jps.jp/doi/abs/10.7566/JPSJ.83.034701.

[48] A. Hinojosa, R. M. Fernandes, and A. V. Chubukov. Time-reversal symmetry breaking superconductivity in the coexistence phase with magnetism in Fe pnictides. *Phys. Rev. Lett.*, 113:167001, 2014. URL http://journals.aps.org/prl/abstract/10.1103/PhysRevLett.113.167001.

[49] Y. Tanaka. Multicomponent superconductivity based on multiband superconductors. *Supercond. Sci. Technol.*, 28:034002, 2015. URL http://m.iopscience.iop.org/article/10.1088/0953-2048/28/3/034002;jsessionid=FD9F8A32487FA56C98ADC6151A34F684.c4.iopscience.cld.iop.org#metrics.

[50] A. Gurevich. Limits of the upper critical field in dirty two-gap superconductors. *Physica C*, 456:160, 2007. URL http://www.sciencedirect.com/science/article/pii/S0921453407000111.

[51] H. Kontani amd S. Onari. Orbital-fluctuation-mediated superconductivity in iron pnictides: Analysis of the five-orbital hubbard-holstein model. *Phys. Rev. Lett.*, 104:157001, 2010. URL http://prl.aps.org/abstract/PRL/v104/i15/e157001.

[52] I. I. Mazin, D. J. Singh, M. D. Johannes, and M. H. Du. Unconventional superconductivity with a sign reversal in the order parameter of $LaFeAs[O_{1-x}F_x]$. *Phys. Rev. Lett.*, 101:057003, 2008. URL http://journals.aps.org/prl/abstract/10.1103/PhysRevLett.101.057003.

[53] J. Paglione and R. L. Greene. High-temperature superconductivity in iron-based materials. *Nature Phys.*, 6:645, 2010. URL http://www.nature.com/nphys/journal/v6/n9/full/nphys1759.html.

[54] K. Okazaki, Y. Ota, Y. Kotani, Y. Ishida, T. Shimojima, T. Kiss, S. Watanabe, C. T. Chen, C. H. Lee, H. Eisaki, T. Saito, H. Fukazawa, Y. Kohori, K. Hashimoto, T. Shibauchi, Y. Matsuda, H. Ikeda, H. Miyahara, R. Arita, A. Chainani, and S. Shin. Octet-line node structure of superconducting order parameter in KFe_2As_2. *Science*, 337:1314, 2012. URL http://www.sciencemag.org/content/337/6100/1314.

[55] S. Maiti, M. M. Korshunov, and A. V. Chubukov. Gap symmetry in KFe_2As_2 and the $\cos 4\theta$ gap component in lifeas. *Phys. Rev. B*, 85:014511, 2012. URL http://journals.aps.org/prb/abstract/10.1103/PhysRevB.85.014511.

[56] M. Sigrist, D. B. Bailey, and R. B. Laughlin. Fractional vortices as evidence of time-reversal symmetry breaking in high-temperature superconductors. *Phys. Rev. Lett.*, 74:3249, 1995. URL http://prl.aps.org/abstract/PRL/v74/i16/p3249_1.

[57] J. Garaud, J. Carlstrom, and E. Babaev. Topological solitons in three-band superconductors with broken time reversal symmetry. *Phys. Rev. Lett.*, 107:197001, 2011. URL http://prl.aps.org/abstract/PRL/v107/i19/e197001.

[58] M. Sigrist. Time-reversal symmetry breaking states in high-temperature superconductors. *Prog. Theor. Phys.*, 99:6, 1998. URL http://ptp.oxfordjournals.org/content/99/6/899.

[59] C. C. Tsuei and J. R. Kirtley. Pairing symmetry in cuprate superconductors. *Rev. Mod. Phys.*, 72:969, 2000. URL http://journals.aps.org/rmp/abstract/10.1103/RevModPhys.72.969.

[60] T. K. Ng and N. Nagaosa. Broken time-reversal symmetry in josephson junction involving two-band superconductors. *Europhys. Lett.*, 87:17003, 2009. URL http://iopscience.iop.org/0295-5075/87/1/17003.

[61] V. Stanev. Model of collective modes in three-band superconductors with repulsive interband interactions. *Phys. Rev. B*, 85:174520, 2012. URL http://journals.aps.org/prb/abstract/10.1103/PhysRevB.85.174520.

[62] M. Silaev and E. Babaev. Unusual mechanism of vortex viscosity generated by mixed normal modes in superconductors with broken time reversal symmetry. *Phys. Rev. B*, 88:220504, 2013. URL http://journals.aps.org/prb/abstract/10.1103/PhysRevB.88.220504.

[63] A. F. Andreev. Thermol conductivity of the intermediate state of superconductors. ii. *Sov. Phys. JETP*, 19:1228, 1964. URL http://www.jetp.ac.ru/cgi-bin/dn/e_020_06_1490.pdf.

[64] G. E. Blonder, M. Tinkham, and T. M. Klapwijk. Transition from metallic to tunneling regimes in superconducting microconstrictions: Excess current, charge imbalance, and supercurrent conversion. *Phys. Rev. B*, 25:4515, 1982. URL http://journals.aps.org/prb/abstract/10.1103/PhysRevB.25.4515.

[65] I. O. Kulik. Macroscopic quantization and the proximity effect in s-n-s junctions. *Sov. Phys. JETP*, 30:944, 1970. URL http://www.jetp.ac.ru/cgi-bin/e/index/e/30/5/p944?a=list.

[66] I. B. Sperstad, J. Linder, and A. Sudb∅. Quantum transport in ballistic $s\pm$-wave superconductors with interband coupling: Conductance spectra, crossed andreev reflection, and josephson current. *Phys. Rev. B*, 80:144507, 2009. URL http://journals.aps.org/prb/abstract/10.1103/PhysRevB.80.144507.

[67] C. W. J. Beenakker. Universal limit of critical-current fluctuations in mesoscopic josephson junctions. *Phys. Rev. Lett.*, 67:3836, 1991. URL http://journals.aps.org/prl/abstract/10.1103/PhysRevLett.67.3836.

[68] A. A. Golubov, M. M. Kupriyanov, and E. ll'ichev. The current-phase relation in josephson junctions. *Rev. Mod. Phys.*, 76:411, 2004. URL http://journals.aps.org/rmp/abstract/10.1103/RevModPhys.76.411.

[69] L. N. Bulaevskii, V. V. Kuzii, A. A. Kuzi, and A. A. Sobyanin. Superconducting system with weak coupling to the current in the ground state. *JETP Lett.*, 25:290, 1977. URL http://adsabs.harvard.edu/abs/1977JETPL..25..290B.

[70] A. Buzdin and A. E. Koshelev. Periodic alternating 0-and π-junction structures as realization of φ-josephson junctions. *Phys. Rev. B*, 67:220504, 2003. URL http://journals.aps.org/prb/abstract/10.1103/PhysRevB.67.220504.

[71] L. F. Chang and P. F. Bagwell. Ballistic josephson-current flow through an asymmetric superconductorcnormal-metalcsuperconductor junction. *Phys. Rev. B*, 49:15853, 1994. URL http://journals.aps.org/prb/abstract/10.1103/PhysRevB.49.15853.

[72] S. Shapiro. Josephson currents in superconducting tunneling: The effect of microwaves and other observations. *Phys. Rev. Lett.*, 11:80, 1963. URL http://journals.aps.org/prl/abstract/10.1103/PhysRevLett.11.80.

[73] Y. Tanaka. Josephson effect between s wave and $d_x^2 - y^2$ wave superconductors. *Phys. Rev. Lett.*, 72:3871, 1994. URL http://journals.aps.org/prl/abstract/10.1103/PhysRevLett.72.3871.

[74] S. Schmidt, S. Doring, F. Schmidl, V. Grosse, and P. Seidel. $BaFe_{1.8}Co_{0.2}As_2$ thin film hybrid josephson junctions. *Appl. Phys. Lett.*, 97:172504, 2010. URL http://journals.aps.org/rmp/abstract/10.1103/RevModPhys.76.411.

[75] S. Doring, S. Schmidt, F. Schmidl, V. Tympel, S. Haindl, F. Kurth, K. Iida, I. Monch, B. Holzapfel, and P. Seidel. Edge-type josephson junctions with co-doped ba-122 thin films. *Supercond. Sci. Technol.*, 25:084020, 2012. URL http://iopscience.iop.org/article/10.1088/0953-2048/25/8/084020/meta.

[76] G. R. Berdiyorov, M. V. Milosevic, L. Covaci, and F. M. Peeters. Rectification by an imprinted phase in a josephson junction. *Phys. Rev. Lett.*, 107:177008, 2011. URL http://journals.aps.org/prl/abstract/10.1103/PhysRevLett.107.177008.

[77] T. Golod, A. Rydh, and V. M. Krasnov. Detection of the phase shift from a single abrikosov vortex. *Phys. Rev. Lett.*, 104:227003, 2010. URL http://journals.aps.org/prl/abstract/10.1103/PhysRevLett.104.227003.

[78] X. H. Zhang, Y. S. Oh, Y. Liu, L. Q. Yan, K. H. Kim, R. L. Greene, and I. Takeuchi. Observation of the josephson effect in $Pb/Ba_{1-x}K_xFe_2As_2$ single crystal junctions. *Phys. Rev. Lett.*, 102:147002, 2009. URL http://journals.aps.org/prl/abstract/10.1103/PhysRevLett.104.227003.

[79] L. Onsager. Magnetic flux through a superconducting ring. *Phys. Rev. Lett.*, 7:50, 1961. URL http://journals.aps.org/prl/abstract/10.1103/PhysRevLett.7.50.

[80] N. Byers and C. N. Yang. Theoretical considerations concerning quantized magnetic flux in superconducting cylinders. *Phys. Rev. Lett.*, 7:46, 1961. URL http://journals.aps.org/prl/abstract/10.1103/PhysRevLett.7.46.

[81] C. T. Chen, C. C. Tsuei, M. B. Ketchen, Z. A. Ren, and Z. X. Zhao. Integer and half-integer flux-quantum transitions in a niobiumciron pnictide loop. *Nature Phys.*, 6:260, 2010. URL http://www.nature.com/nphys/journal/v6/n4/abs/nphys1531.html.

[82] W. Q. Chen, F. Ma, Z. Y. Liu, and F. C. Zhang. π junction to probe antiphase s-wave pairing in iron pnictide superconductors. *Phys. Rev. Lett.*, 103:207001, 2009. URL http://journals.aps.org/prl/abstract/10.1103/PhysRevLett.103.207001.

[83] D. Parker and I. I. Mazin. Possible phase-sensitive tests of pairing symmetry in pnictide superconductors. *Phys. Rev. Lett.*, 102:227007, 2009. URL http://journals.aps.org/prl/abstract/10.1103/PhysRevLett.102.227007.

[84] K. Kuroki, S. Onari, R. Arita, H. Usui, Y. Tanaka, H. Kontani, and H. Aoki. Unconventional pairing originating from the disconnected fermi surfaces of superconducting $LaFeAs[O_{1-x}F_x]$. *Phys. Rev. Lett.*, 101:087004, 2008. URL http://journals.aps.org/prl/abstract/10.1103/PhysRevLett.101.087004.

[85] W. Q. Chen, K. Y. Yang, Y. Zhou, and F. C. Zhang. Strong coupling theory for superconducting iron pnictides. *Phys. Rev. Lett.*, 102:047006, 2008. URL http://journals.aps.org/prl/abstract/10.1103/PhysRevLett.102.047006.

[86] S. Graser, T. A. Maier, P. J. Hirschfeld, and D. J. Scalpino. Near-degeneracy of several pairing channels in multiorbital models for the fe pnictides. *New J. Phys.*, 11:025016, 2009. URL http://iopscience.iop.org/article/10.1088/1367-2630/11/2/025016/meta.

[87] F. Wang, H. Zhai, Y. Ran, A. Vishwanath, and D. H. Lee. Functional renormalization-group study of the pairing symmetry and pairing mechanism of the feas-based high-temperature superconductor. *Phys. Rev. Lett.*, 102:047005, 2009. URL http://journals.aps.org/prl/abstract/10.1103/PhysRevLett.102.047005.

[88] K. Seo, B. A. Bernevig, and J. Hu. Pairing symmetry in a two-orbital exchange coupling model of oxypnictides. *Phys. Rev. Lett.*, 101:206404, 2008. URL http://journals.aps.org/prl/abstract/10.1103/PhysRevLett.101.206404.

[89] P. C. Dai, J. P. Hu, and E. Dagotto. Magnetism and its microscopic origin in iron-based high-temperature superconductors. *Nature Phys.*, 8:709, 2012. URL http://www.nature.com/nphys/journal/v8/n10/full/nphys2438.html.

[90] J. Jang, D. G. Ferguson, V. Vakaryuk, R. Budakian, S. B. Chung, P. M. Goldbart, and Y. Maeno. Observation of half-height magnetization steps in sr2ruo4. *Science*, 331:186, 2011. URL http://www.sciencemag.org/content/331/6014/186.short.

[91] Z. Huang and X. Hu. Josephson effects in three-band superconductors with broken time-reversal symmetry. *Appl. Phys. Lett.*, 104:162602, 2014. URL http://scitation.aip.org/content/aip/journal/apl/104/16/10.1063/1.4872261.

[92] Z. Huang and X. Hu. Fractional flux plateau in magnetization curve of multi-component superconductor loop. *Phys. Rev. B*, 92:214516, 2015. URL http://journals.aps.org/prb/abstract/10.1103/PhysRevB.92.214516.

[93] S. Z. Lin and X. Hu. Vortex states and the phase diagram of a multiple-component ginzburg-landau theory with competing repulsive and attractive vortex interactions. *Phys. Rev. B*, 84:214505, 2011. URL http://prb.aps.org/abstract/PRB/v84/i21/e214505.

[94] J. Tate, B. Cabrera, S. B. Felch, and J. T. Anderson. Precise determination of the cooper-pair mass. *Phys. Rev. Lett.*, 62:845, 1989. URL http://journals.aps.org/prl/abstract/10.1103/PhysRevLett.62.845.

[95] J. Garaud and E. Babaev. Domain walls and their experimental signatures in $s + is$ superconductors. *Phys. Rev. Lett.*, 112:017003, 2014. URL http://journals.aps.org/prl/abstract/10.1103/PhysRevLett.112.017003.

[96] S. Gillis, J. Jaykka, and M. V. Milosevic. Vortex states in mesoscopic three-band superconductors. *Phys. Rev. B.*, 89:024512, 2014. URL http://journals.aps.org/prb/abstract/10.1103/PhysRevB.89.024512.

[97] Z. Huang and X. Hu. Vortices with fractional flux quanta in multi-band superconductors. *J. Supercond. Nov. Magn. in press*, 2015. URL http://link.springer.com/article/10.1007%2Fs10948-015-3309-x.

[98] M. Sigrist and D. F. Agterberg. The role of domain walls on the vortex creep dynamics in unconventional superconductors. *Prog. Theor. Phys.*, 102:965, 1999. URL http://ptp.oxfordjournals.org/content/102/5/965.abstract.

[99] L. Y. L. Shen, N. M. Senozan, and N. E. Phillips. Evidence for two energy gaps in high-purity superconducting nb, ta, and v. *Phys. Rev. Lett.*, 14:1025, 1965. URL http://journals.aps.org/prl/abstract/10.1103/PhysRevLett.14.1025.

[100] G. Binnig, A. Baratoff, H. E. Hoenig, and J. G. Bednorz. Two-band superconductivity in Nb-doped $SrTiO_3$. *Phys. Rev. Lett.*, 45:1352, 1980. URL http://journals.aps.org/prl/abstract/10.1103/PhysRevLett.45.1352.

[101] S. Souma, Y. Machida, T. Sato, T. Takahashi, H. Matsui, S.-C. Wang, H. Ding, A. Kaminski, J. C. Campuzano, S. Sasaki, and K. Kadowaki. The origin of multiple superconducting gaps in MgB_2. *Nature (London)*, 423:65, 2003. URL http://www.nature.com/nature/journal/v423/n6935/abs/nature01619.html.

[102] E. Babaev and M. Speight. Semi-meissner state and neither type-i nor type-ii superconductivity in multicomponent superconductors. *Phys. Rev. B*, 72:180502, 2005. URL http://journals.aps.org/prb/abstract/10.1103/PhysRevB.72.180502.

[103] J. Geyer, R. M. Fernandes, V. G. Kogan, and J. Schmalian. Interface energy of two-band superconductors. *Phys. Rev. B*, 82:104521, 2010. URL http://journals.aps.org/prb/abstract/10.1103/PhysRevB.82.104521.

[104] A. A. Shanenko, M. V. Milosevic, and F. M. Peeters. Extended ginzburg-landau formalism for two-band superconductors. *Phys. Rev. Lett.*, 106:047005, 2011. URL http://journals.aps.org/prl/abstract/10.1103/PhysRevLett.106.047005.

[105] L. Komendova, M. V. Milosevic, A. A. Shanenko, and F. M. Peeters. Different length scales for order parameters in two-gap superconductors: Extended ginzburg-landau theory. *Phys. Rev. B*, 84:064522, 2011. URL http://journals.aps.org/prb/abstract/10.1103/PhysRevB.84.064522.

[106] Victor Moshchalkov, Mariela Menghini, T. Nishio, Q. H. Chen, A.V. Silhanek, V. H. Dao, L. F. Chibotaru, N. D. Zhigadlo, and J. Karpinski. Type-1.5 superconductivity. *Phys. Rev. Lett.*, 102:117001, 2009. URL http://journals.aps.org/prl/abstract/10.1103/PhysRevLett.102.117001.

Publication list:

(1) Zhao Huang and Xiao Hu, "Josephson Effects in Three-Band Superconductors with Broken Time-Reversal Symmetry", *Applied Physics Letters*, vol. 104, 162602 (2014).

(2) Zhao Huang and Xiao Hu, "Fractional Flux Plateau in Magnetization Curve of Multi-Component Superconductor Loop", *Physical Review B*, 92, 214516 (2015).

(3) Zhao Huang and Xiao Hu, "Vortices with Fractional Flux Quanta in Multi-Band superconductors", *Journal of Superconductivity and Novel Magnetism*, (doi: doi: 10.1007/s10948-015-3309-x).

(4) Yuki Takahashi, Zhao Huang and Xiao Hu, "H-T Phase Diagram of Multi-Component Superconductors with Frustrated Inter-Component Couplings", *Journal of the Physical Society of Japan*, vol. 83, 034701 (2014).

(5) Yuki Takahashi, Zhao Huang and Xiao Hu, "Unconventional Vortex State in Multicomponent Superconductors with Time-Reversal Symmetry Breaking", *Physica C*, vol. 493, 82 (2013)